Dynamics and entanglement of exotic quantum liquids

Thomas Veness
Wadham College
University of Oxford

A thesis submitted for the degree of
Doctor of Philosophy in Theoretical Physics
Trinity Term 2017

Dynamics and entanglement of exotic quantum liquids

Thomas Veness

Wadham College, University of Oxford

A thesis submitted for the degree of *Doctor of Philosophy in Theoretical Physics*

Trinity Term 2017

Abstract

This thesis focuses on the one-dimensional Hubbard model, considering both dynamical response functions and also particular entanglement measures of highly excited eigenstates.

In Chapter 2 we discuss how to describe the optical conductivity at finite energy scales. In order to calculate the dynamical response of this interacting system, it is necessary to go beyond the conventional Luttinger liquid picture. Using mobile impurity models and integrability we make quantitative predictions which can be compared with numerics.

In Chapter 3, we investigate the existence of the so-called "quantum disentangled liquid" (QDL) in the same system. The diagnostic for the QDL involves understanding the bipartite entanglement entropy of highly excited eigenstates. Here we use results from integrability and strong-coupling expansions to argue that such a state of matter is realised in the Hubbard chain in a specific sense.

Acknowledgements

I unreservedly thank Professor Fabian Essler for his guidance over the past $4-\epsilon$ years. His keen physical insight and formidable technical ability have been immensely valuable in supporting and challenging me and my understanding of the field. He is patient, generous, and caring; I could not have asked for more in a supervisor.

I also want to thank the other faculty for guiding me, most notably Professor Steve Simon for broadening my understanding of physics, and Professor John Chalker for his sage advice and kind words.

I have been extremely fortunate to share my time in Oxford with a uniquely friendly and talented set of individuals who have taught me so much, including Adam Nahum, Curt von Keyserlingk, Neil Robinson, Dima Kovrizhin, and Yuri van Nieuwkerk. Further thanks are also due to those who have had the peculiar misfortune of sharing an office with me: Bruno Bertini, Richard Fern, Stefan Groha, Fenner Harper, and the long-suffering Dillon Liu.

Deep thanks to Benjamin Yadin, who is still excited to discuss physics with me after eight years, and has been a reliable and genuine friend throughout our undergraduate and graduate studies.

My time in Oxford has also been enriched by sharing special moments of quiet reflection in the mountains. I am especially grateful to Tim Crothers, Andy Howell, and Matt Titterington for sharing those with me.

I am indebted to my parents and sister for always being available for support and encouragement in all that I do.

Finally, Anna Sonley has been unerringly kind, patient, and thoughtful; for this, and for everything else, thank you.

Contents

Chapter 1

Introduction

Spurred by the success of quantum mechanics in the early 20th century, theoretical physicists turned to study many-body problems in earnest. Studying an enormous number of degrees of freedom has a price: even ostensibly simple many-body quantum systems are capable of collective behaviours which are qualitatively distinct from the "fundamental" ingredients of the system. This is simultaneously the root of the difficulty in studying quantum many-body systems, and also the source of the fascinating variety of behaviour identified in both theory and experiment. An attempt to understand these complex behaviours throws the limitations of reductionism into sharp relief[1] and instead guided theorists to embrace the idea that *more is different*[2].

When considering interacting systems of electrons, the basic components are the same for insulators, metals, superconductors, quantum hall fluids, topological insulators, magnets and much more, yet the resulting materials do not obviously betray their common origin. Indeed, the vast range of phenomena observed in today's condensed matter laboratories may leave the graduate student feeling hopelessly overwhelmed at the prospect of understanding even basic materials without resorting to numerical methods directly simulating systems with a huge number of tunable parameters.

It is perhaps to great surprise (and solace) that despite this apparent complexity there are 'simple' theoretical models which not only qualitatively reproduce real-world behaviour, but can also offer a precise quantitative understanding in appropriate regimes. The historical perspective on studying such models is that they are simple enough to make meaningful statements, but not so simple that they fail to capture

the "important physics". In many cases this can be understood more precisely in terms of the renormalisation group (RG)[3]. The philosophy here is to integrate out high-energy degrees of freedom in order to flow to an effective low-energy theory. In this picture, the long-distance physics of a simple model which we can understand and an intractable complicated model may flow to the same RG fixed point. The RG is an astonishingly powerful theoretical tool when our model is at a critical point[4] or in a particular scaling limit. In these cases the RG explains why simple models can impressively describe the behaviour of ostensibly more complicated systems.

To be more concrete, the model to which we devote most of this thesis is precisely one of these simplifications. In order to try to understand electrons hopping on a lattice and interacting via Coloumb interactions, we introduce the one-band Hubbard model, defined by the Hamiltonian

$$H = -t \sum_{\langle ij \rangle, \sigma} c^\dagger_{i,\sigma} c_{j,\sigma} + U \sum_i n_{i,\uparrow} n_{i,\downarrow}, \tag{1.1}$$

where the sum $\langle ij \rangle$ is over nearest neighbours on some bipartite lattice, $t > 0$ is the hopping strength, and $U > 0$ is the repulsive on-site interaction. We have two species of fermions with spin $\sigma = \uparrow, \downarrow$, represented by fermionic operators satisfying the canonical anticommutation relations $\{c_{i,\sigma}, c_{j,\sigma'}\} = 0$, $\{c_{i,\sigma}, c^\dagger_{j,\sigma'}\} = \delta_{i,j}\delta_{\sigma,\sigma'}$, and $n_{i,\sigma} = c^\dagger_{i,\sigma} c_{i,\sigma}$. Introduced by J. Hubbard [5], this is essentially the simplest model of interacting electrons on a lattice that one could imagine, where only the bare essence of the Coulomb interaction has been left intact. With $U = 0$, the electrons are free and form two bands in momentum-space, describing a conductor when not completely filled, and a band insulator otherwise.

At half-filling, the Hubbard model is capable of displaying Mott-insulating behaviour i.e. it can undergo a phase transition from a metal to an insulator which is driven by electron-electron interactions as opposed to being insulating purely due to Pauli exclusion. This can be understood intuitively: at $U = 0$, free fermions manifestly describe a metallic ground state. For $U/t \to \infty$, any particle-hole excitation must create a doubly-occupied site and therefore incur a penalty $\sim U$, indicating

that the system is insulating in nature. Deep in the Mott insulating phase the Fermi surface is completely absent.

The Hubbard model also allows us to understand the origin of magnetic materials as a result of Coulomb interactions[6] and exchange statistics of the underlying electrons. As will be discussed in Chapter 3, at half-filling and large repulsive interactions perturbation theory shows us that the effective low-energy description is given, at leading order in t/U, by the antiferromagnetic spin-$\frac{1}{2}$ Heisenberg model[7]

$$H = \frac{4t^2}{U} \sum_{\langle ij \rangle} \mathbf{S}_i \cdot \mathbf{S}_j + \cdots , \tag{1.2}$$

where the sum is over nearest-neighbour sites i, j. This model is particularly noteworthy as it admits an exact solution in one spatial dimension[8], and has been the subject of intense theoretical study. Higher order terms can be kept in this strong-coupling expansion, corresponding to longer-range ring-exchange terms, and are suppressed by further powers of t/U.

1.1 Quasi-one-dimensional systems

Whilst samples in the laboratory are conventionally three-dimensional, this does not preclude one-dimensional physics from being observable in particular regimes. In such a scenario we can meaningfully talk about quasi-one-dimensional systems. For the sake of illustration, we can consider coupled spin chains comprising spin-S representations of SU(2), forming a three-dimensional crystal with an intra-chain coupling $J_\parallel$, and inter-chain couplings $J_\perp \ll J_\parallel$ i.e.

$$H = J_\parallel \sum_{i,j} \left[\mathbf{S}_{i,j} \cdot \mathbf{S}_{i+1,j} \right] + J_\perp \sum_{i,\langle j,k \rangle} \left[\mathbf{S}_{i,j} \cdot \mathbf{S}_{i,k} \right] , \tag{1.3}$$

where the sum is over sites i within a chain labelled by j, and over chains k adjacent to j, denoted by $\langle j, k \rangle$. At extremely low energies, we will probe the system on the longest length scales and we expect the system to be dominated by three-dimensional physics. However, if we probe the system on some energy scale ω such that $J_\perp \ll \omega \sim J_\parallel$, then we expect to have one-dimensional behaviour, where the three-dimensional

physics can be accounted for perturbatively. On intermediate energy scales we will observe some crossover regime between the one-dimensional and three-dimensional physics. This "dimensional crossover" can be understood in terms of the RG flow of inter-chain couplings[9].

In the past decade or so, experimental advances in cold atomic systems have made it possible to realise one-dimensional physics in a purer sense than that above[10, 11]. These systems are sufficiently isolated that the time-evolution of the system is accurately described by unitary dynamics. Some experiments have such fine control over system parameters that they can even be used to directly address difficult theoretical questions e.g. the stability of certain novel states of matter for numbers of particles far beyond what is accessible via numerical techniques such as exact diagonalisation [12, 13].

One-dimensional systems exhibit stark differences to their higher-dimensional counterparts: the Mermin-Wagner theorem[14] shows that in 1D isotropic spin-S Heisenberg models, there can be no ferromagnet or antiferromagnetic order at finite temperature. More general comments by Hohenberg[15] lead one to the conclusion that one-dimensional systems with local interactions cannot break continuous symmetries at finite temperature. Fluctuations in one-dimensional systems are sufficiently strong to melt what we might expect to be an ordered phase and we cannot construct a consistent mean field theory. This means that the ground state of one-dimensional systems are often in a liquid-like state i.e. there are quantum fluctuations on all length scales. We say that a state possesses long-range order[16] if there exist local operators $\mathcal{O}_i$ and $\mathcal{O}_j$ acting on sites i and j respectively, such that

$$\lim_{|i-j|\to\infty} \langle \mathcal{O}_i \mathcal{O}_j \rangle \neq 0. \tag{1.4}$$

It may be that we find a scenario with power-law decay i.e. $\langle \mathcal{O}_i \mathcal{O}_j \rangle \sim |i-j|^{-\alpha}$, where there are fluctuations on all length scales. This scenario is known as *quasi-long-range order*, and is often the "closest we can get" to long-range order in 1D. Understanding the asymptotic (i.e. long-distance) behaviour of quantities such as (1.4) is crucial for describing many experimental results in condensed matter systems.

1.1.0.1 Measurement of quantum systems

Quantum mechanics is fundamentally a theory which describes the outcome of measurements on some system[17]; and the rôle of experiment in both the validation of theory and spurring new understanding and directions in research is difficult to overstate. We therefore focus here on a few correlation functions which are experimentally pertinent. As the theorist is best poised make statements about long-distance properties of systems, one often considers the asymptotic form of correlation functions of local quantities. The joy of universality means that analytic results for correlations functions from specific tractable models have a bearing on much more complicated models within which calculation is formidable, impossible or both.

We therefore introduce a few common *response functions*; these quantitatively describe the response of quantum systems to experimental probes, and there is a long history of attempting to calculate these in interacting quantum systems[18]. A commonly considered response function in electronic systems is the spectral function, defined by

$$A(k,\omega) = -\frac{1}{\pi}\mathrm{Re}\int_0^\infty \mathrm{d}t e^{i\omega t}\sum_l e^{-ikla_0}\langle GS|\{c_{j+l}(t), c_j^\dagger(0)\}|GS\rangle, \tag{1.5}$$

where a_0 is the lattice spacing, gives information about the single-particle content of a system, as well as being directly accessible via angle-resolved photo-emission spectroscopy experiments[18]. Such measurements on quasi-one-dimensional organic conductors (TTF-TCNQ) have been interpreted in terms of the spectral function for the one-dimensional Hubbard model[19, 20].

One may also consider the density structure factor (DSF), which is defined by

$$S(q,\omega) = \int \mathrm{d}x \int \mathrm{d}t e^{i(\omega t - qx)}\langle \rho(x,t)\rho(0,0)\rangle, \tag{1.6}$$

where $\rho(x,t)$ is the Heisenberg-picture operator corresponding to the density at position x i.e. $\rho(x) = c^\dagger(x)c(x)$. The DSF can be understood as the linear response to an external field coupling to the density ρ, and is crucial to understanding Coulomb drag experiments in quantum wires[21–24]. We will consider the behaviour of the DSF as

a case study of the Luttinger liquid and its failures as an effective field theory for one-dimensional spinless fermionic systems in certain regimes. Analytical calculation of response functions is generally a very difficult problem in interacting problems.

We devote Chapter 2 to considering the optical conductivity in the Hubbard chain. The optical conductivity describes the linear response of a system upon the application of an electric field, which couples to the charge degrees of freedom. The optical conductivity in the Hubbard model at half-filling has been studied both analytically and numerically[25]. In this case there is a field-theoretical limit where results can be understood in terms of the Sine-Gordon model, a massive integrable theory which lies outside of the scope of this thesis. We consider the optical conductivity away from this particular limit.

1.2 Integrability

One-dimensional models are particularly peculiar in the sense that some of them admit exact solutions. The name is perhaps slightly misleading: there is much left unknown about exactly solvable models. The exact solution essentially offers a tremendous reduction in the complexity of finding eigenstates of the system. Instead of having to diagonalise an exponentially large matrix (in the system size L), one can instead solve $\mathcal{O}(L)$ algebraic equations. As is often the case, the reason behind this reduction in complexity is intimately related to symmetry. Entire volumes have been published with regard to the solution and study of integrable systems, and we therefore refer the reader to these for a comprehensive account [26–30]. Although a precise definition of quantum integrability is currently not agreed upon[31], one of the most important features is the existence of an extensive number of local conserved quantities. This is common to all of the integrable systems with which we will concern ourselves. This large symmetry allows us to greatly simplify the task of finding e.g. energy eigenvalues of the particular Hamiltonian. In the case of the Heisenberg model, a priori one needs to find an eigenvalue of a $2^L \times 2^L$ matrix. Yet the exact solution via coordinate Bethe Ansatz reduces this to solving $\mathcal{O}(L)$ algebraic

equations. This is an enormous reduction of complexity, but still leaves many of the properties of the system opaque due to the implicit nature of the solution.

Nature is not integrable: integrable models are extremely fine-tuned, and generic perturbations violate integrability. Deviations from integrability can cause significant changes in properties of the system: eigenvalues level statistics can change from Poisson to Wigner-Dyson[32] and long-time relaxational behaviour may be described by different statistical ensembles[33]. However, if we "weakly" break integrability, the decay of quasiparticles can be parametrically slow[34] and many properties appear the same within the given experimental resolution. In the problems we study, we will generally avoid pursuing the extremely interesting question of what happens when integrability is broken.

1.3 Luttinger liquids and bosonisation

In condensed matter physics, we are often interested in using effective models to describe the long-wavelength behaviour of many-body systems. This behaviour is important both due to its experimental relevance, and also as this is where universal features are manifest. At criticality or in the scaling regime the renormalisation group allows us to understand that various characteristics of the system are insensitive to fine-tuning of microscopic parameters of our model.

In three-dimensional systems, we are familiar with the notion of the Fermi liquid[35, 36]. In the free-fermionic model, our ground state is a filled Fermi sea and the free elections define infinitely long-lived particle excitations on top of this. Upon the addition of repulsive interactions the picture remains qualitatively similar: adding a bare electron on top of the Fermi sea is no longer an eigenstate of the system. The quasiparticle excitations are a "dressed" version of the bare electron with a finite lifetime.

The state corresponding to the quasiparticle excitation must match in some basic ways with the non-interacting eigenstates: it must be a superposition with the correct charge and momentum. The overlap between the appropriate free excitation and the

quasi-particle, called the *quasiparticle residue*, is finite. Indeed, there is still a notion of the Fermi surface in the interacting picture, and the lifetime of the quasiparticles diverges as we approach the Fermi surface, as the quasiparticles become an ever-better approximation to the free excitations. The Fermi liquid therefore leads us to a universal description of a huge range of electronic systems in three dimensions.

One might hope that there is still a notion akin to the Fermi liquid in lower dimensions, but for interacting spinful Fermions in one dimension the picture is fundamentally different. The generic existence of spin-charge separation demonstrates that the quasiparticle excitations of the Landau Fermi liquid are inappropriate for trying to understand one-dimensional systems: the excitations of the one-dimensional system are *not* continuously related to the electrons of the non-interacting system, even for arbitrarily weak perturbations.

In order to understand the picture that emerges in one-dimensional liquids we turn to bosonisation[37–44]. In one dimension and at low energies, certain interacting models of fermions can be mapped onto a non-interacting model of one-dimensional bosons. The crucial assumption in this identification is the linearisation of the fermionic dispersion relations. Following the arguments of Haldane, non-linearities are formally irrelevant but will see how more recent results highlight that they are nonetheless important for various quantities of interest.

We introduce the idea of bosonisation in the simplest possible way, where a particularly constructive approach can be found in Ref. [44]. Consider the one-dimensional free fermionic Hamiltonian

$$H = -t \sum_j \left(c_j^\dagger c_{j+1} + c_{j+1}^\dagger c_j \right) + \mu \sum_j c_j^\dagger c_j, \tag{1.7}$$

which is trivially diagonalised for periodic boundary conditions by going to momentum space i.e.

$$c(k_n) = \frac{1}{\sqrt{L}} \sum_{j=0}^{L-1} e^{ik_n j a_0} c_j, \qquad k_n = \frac{2\pi n}{L a_0}, \tag{1.8}$$

$$H = \sum_k c^\dagger(k) c(k) \left[\mu - 2t \cos k a_0 \right]. \tag{1.9}$$

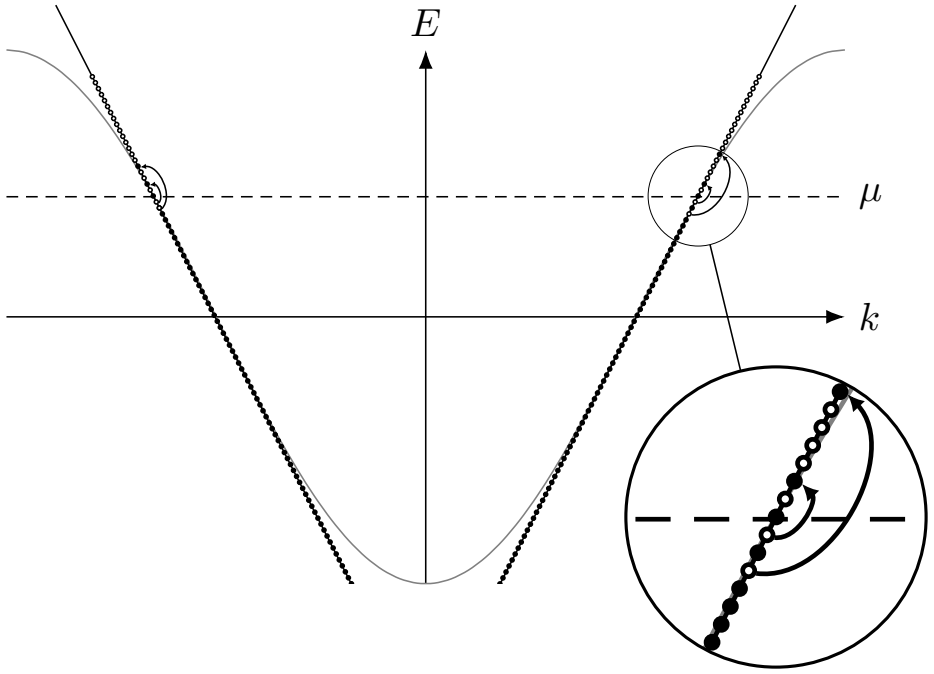

Figure 1.1: Linearised spectrum for a low-lying excited state in the tight-binding chain of (1.7). The curved arrows indicate particle-hole excitations on top of the filled Fermi sea.

The ground state of this Hamiltonian is given by a Fermi sea where we have filled up to momentum k_F i.e.

$$\begin{aligned} |GS\rangle &= \prod_{|k|<k_F} c^\dagger(k)|0\rangle, \\ \cos k_F a_0 &= \frac{\mu}{2t}. \end{aligned} \tag{1.10}$$

The low-energy excitations above the ground state correspond to particle-hole excitations about the Fermi sea. If we wish to describe low-energy properties of the system, we can approximate this by two linear dispersion relations centred on the Fermi points, giving us an effective Hamiltonian of the form

$$H_{\text{eff}} \sim \sum_k c^\dagger_{k,R} c_{k,R} v_F(k - k_F) - \sum_k c^\dagger_{k,L} c_{k,L}(k + k_F). \tag{1.11}$$

This is graphically shown in Fig. 1.1. The canonical partition function for this system, where we have subtracted the ground-state energy is given by

$$Z_{\text{canonical}} = \left[\sum_{n=0}^{\infty} z^n P(n)\right]^2, \tag{1.12}$$

where $z = e^{-\beta v_F \frac{2\pi}{La_0}}$ and $P(n)$ is the partition of the integer n. The linearisation has introduced an enormous degeneracy as the energy of a branch is completely specified by its total momentum. It is simple to verify that the generating function of the partitions of the integers satisfies [45]

$$\sum_{n=0}^{\infty} z^n P(n) = \prod_{n=1}^{\infty} \frac{1}{1-z^n}, \tag{1.13}$$

which, as all energies are positive i.e. $0 < z < 1$ allows us to cast

$$Z_{\text{canonical}} = \left[\prod_{n=1}^{\infty} \left(1 + z^n + z^{2n} + \cdots \right) \right]^2. \tag{1.14}$$

This is very suggestive of a bosonic representation of the same system i.e.

$$H_{\text{bosonic}} = \frac{2\pi v_F}{La_0} \sum_{n>0} n \left(b_n^\dagger b_n + b_{-n}^\dagger b_{-n} \right), \tag{1.15}$$

which will, by construction, reproduce the correct partition function. These bosonic modes are precisely the particle-hole excitations. The bosonisation identities take this further and, more than just an equivalence of the partition functions, it is possible to actually establish an equality of *operators* on the Hilbert space[44]. If we split off the modes at the right and left Fermi points, we can write the fermionic annihilation operator as

$$c_j \sim \sqrt{a_0} \left(R(x) e^{ik_F x} + L(x) e^{-ik_F x} \right), \qquad x = ja_0 \tag{1.16}$$

where $R(x)$ and $L(x)$ are slowly-varying fermionic modes about the right and left Fermi points respectively. The bosonisation identities[44] establish that there is a precise mapping between fermionic fields and bosonic fields

$$R(x) = \frac{\eta}{\sqrt{2\pi a_0}} e^{-i\sqrt{4\pi}\varphi_R(x)}, \qquad L(x) = \frac{\bar{\eta}}{\sqrt{2\pi a_0}} e^{i\sqrt{4\pi}\varphi_L(x)}, \tag{1.17}$$

where the bosonic fields satisfy the commutation relations

$$[\varphi_R(x), \varphi_R(x')] = \frac{i}{4} \text{sign}(x - x') = -[\varphi_L(x), \varphi_L(x')]. \tag{1.18}$$

The factors η and $\bar{\eta}$ are so-called Klein factors and enforce anti-commutation relations between $L(x)$ and $R(x)$ by obeying the algebra $\{\eta, \bar{\eta}\} = 0$, $\eta^2 = \bar{\eta}^2 = 1$. The bosonic

fields $\varphi_R(x)$ and $\varphi_L(x)$ admit the mode expansion in terms of bosonic modes β_n, satisfying $[\beta_n, \beta_m^\dagger] = \delta_{n,m}$, given by

$$\begin{aligned}\varphi_R(vt-x) &= Q + \frac{P}{2L}(vt-x) + \sum_{n>0} \frac{1}{\sqrt{4\pi n}} \left[\beta_n e^{ik_n(x-vt)} + \beta_n^\dagger e^{-ik_n(x-vt)}\right], \\ \varphi_L(vt+x) &= \bar{Q} + \frac{\bar{P}}{2L}(vt+x) + \sum_{n>0} \frac{1}{\sqrt{4\pi n}} \left[\beta_{-n} e^{-ik_n(x+vt)} + \beta_{-n}^\dagger e^{ik_n(x+vt)}\right],\end{aligned} \tag{1.19}$$

where $[Q, P] = i = [\bar{Q}, \bar{P}]$. In terms of the bosonic fields, we can write the effective low-energy Hamiltonian, retaining only the most relevant terms, as

$$\mathcal{H}_{\text{eff}} = \frac{v_F}{2} \int \mathrm{d}x \, \left[(\partial_x \Phi)^2 + (\partial_x \Theta)^2\right], \tag{1.20}$$

where $\Phi = \varphi_L + \varphi_R$, $\Theta = \varphi_R - \varphi_L$. It is a simple exercise to verify that the mode expansion allows one to calculate free fermionic correlation functions using the bosonisation identity (1.17).

The point of all of this is that the free-fermionic theory can be expressed in terms of a bosonic theory and the correlation functions of the fermionic theory can be expressed as correlations of bosonic fields. The utility lies in the fact that the truth of these statements extends even beyond the free regime, and this is the notion behind the picture of the Luttinger liquid as a universal description of the low-energy physics of one-dimensional critical systems[46]. Interactions that would be quartic in the fermionic degrees of freedom are *quadratic* in the bosonic degrees of freedom, meaning that the effective Hamiltonian is, remarkably, still simple to diagonalise in terms of the bosonic modes! We will see later that by bosonising additional interaction terms, we can perturbatively identify parameters in the Luttinger liquid Hamiltonian which simply act to renormalise couplings in the free theory i.e.

$$\mathcal{H}_{LL} = \frac{v}{2} \int \mathrm{d}x \, \left[\frac{1}{K} (\partial_x \Phi)^2 + K (\partial_x \Theta)^2\right]. \tag{1.21}$$

For stronger interactions, if still in the gapless Luttinger liquid phase, we can fix v and K by comparing the finite-size spectra for exactly solvable models. This technique will generalise as a way to fix parameters for calculations beyond the simple linear Luttinger liquid regime.

The calculation of simple correlation functions now reduces to a textbook exercise. Among other things, we can see that there is no Migdal discontinuity for the Luttinger liquid, which is crucial in developing the Landau Fermi liquid[47], and demonstrates the different nature of the one-dimensional case.

1.4 Non-linear Luttinger liquids and mobile impurity models

The Luttinger liquid allows us to say a lot about the low-energy physics of interacting models due to the linearisation of the spectrum. This simplicity is also the root of many problems in the Luttinger liquid. Haldane showed that curvature of the fermionic dispersion relation does not alter the leading asymptotic behaviour of the *equal-time* fermionic propagator $G(x, 0)$[46, 48].

In Landau's Fermi liquid picture, we start from non-interacting particles with an infinite lifetime. Upon the addition of interactions, we can calculate the self-energy via perturbation theory. The excitations of the original picture acquire a finite lifetime perturbatively: the single-particle Greens function broadens from having a sharp delta-function peak to having some finite width. One is therefore tempted to proceed analogously in one dimension, including interactions perturbatively. If we consider the DSF, the curvature of non-interacting fermions has drastic consequences in the perturbation theory: a generic density-density interaction leads to logarithmic divergences at the threshold energy[49] at leading order in the perturbation expansion. Conventionally, the appearance of such divergences is cured by resummation of some subsequence of diagrams to all orders in perturbation theory. This is a difficult task in general, and it is worthwhile to consider the kinematics of the situation, as we will see in Section 1.4.1. In short, a deep hole producing a divergence due to particles scattering near the Fermi surface, is essentially the same physics as the Fermi edge singularity[41, 50–52], except here the impurity is not static. This does not destroy the singularity, and following this techniques through gives a precise understanding of the singular behaviour at the threshold.

In the Luttinger liquid theory the curvature term is formally irrelevant, corresponding to an interaction between the bosonic modes. One may therefore attempt to include the curvature terms perturbatively in the free bosonic picture[53]. This is plagued with singularities at the mass shell $\omega = vq$ due to the highly degenerate nature of all bosonic states with the same momentum, which is a direct consequence of the linear dispersion. Far away from the mass shell, this can be understood in perturbation theory[54], but near the threshold this is not applicable. At a finite energy scale formally irrelevant terms have *not flowed to zero* and therefore have a finite coupling which gives rise to infrared singularities in perturbation theory near the threshold.

We therefore wish to understand the behaviour of one-dimensional quantum liquids beyond the linear regime. We know from exactly solvable models and perturbation theory of non-interacting fermions that spin-charge separate continues to exist even in the presence of curvature, but understanding the interacting problem with curvature within perturbation theory is extremely difficult. Whilst the linear Luttinger liquid is tremendously useful for describing static properties of a huge number of one-dimensional systems, it fails to make sensible predictions for dynamical quantities that are difficult to account for in perturbation theory. Indeed, in the XXZ model, the linear Luttinger liquid fails to correctly predict transverse spin structure factors in the non-interacting limit[55, 56].

1.4.1 Resolution

In this section, we will follow the treatment of Ref. [56] to understand explicitly how the mobile impurity model arises in the simplest scenario. To be concrete, we introduce the interacting fermionic model

$$H = -t\sum_{j=1}^{L}\left(c_j^\dagger c_{j+1} + c_{j+1}^\dagger c_j\right) + t\Delta\sum_{j=1}^{L} :n_j::n_{j+1}:, \tag{1.22}$$

where the colons indicate normal-ordering of the operators i.e. $:n_j := n_j - \langle GS|n_j|GS\rangle$, and we take periodic boundary conditions i.e. $c_{L+1} = c_1$. We are considering the case

of spinless fermions: this benefits from the constructive nature of the solution, which is less forthcoming in the case of spinful fermions. We consider this at some filling where the non-interacting ground state is defined by Fermi momentum k_F.

We wish to understand the DSF of (1.6) for spinless fermions in one dimension, which we reiterate is defined by

$$S(q,\omega) = \int \mathrm{d}x \int \mathrm{d}t e^{i(\omega t - qx)} \langle c^\dagger(x,t) c(x,t) c^\dagger(0,0) c(0,0) \rangle. \tag{1.23}$$

We first consider free fermions ($\Delta = 0$) and the case of half-filling i.e the ground state is a filled Fermi sea up to the Fermi momentum $k_F = \frac{\pi}{2}$. In this case, it follows from an elementary calculation that the DSF is given by[57]

$$S(q > 0, \omega > 0) = \frac{\theta(\omega - 2\sin q)\theta(4\sin q/2 - \omega)}{\sqrt{(4\sin q/2)^2 - \omega^2}}, \tag{1.24}$$

that is, for slices of fixed momentum q, the DSF has finite support at the lower edge of which is a step and at the upper edge there is a power-law singularity (square root), and the power does *not* depend on the momentum. The form of the DSF is shown in Fig. 1.2.

The existence of a threshold is a consequence of the topology of the Fermi surface in one dimension. Having only two points means that for a large range of momenta we cannot connect the Fermi points, unlike in two dimensions where for any wavevector $\mathbf{q}$ such that $|\mathbf{q}| < 2k_F$, we can always construct particle-hole excitations with arbitrarily small energy, as shown in Fig. 1.3. Although the free-fermionic picture is simple, we note that the kinematics of excitations at the lower threshold are of a remarkably simple nature, and this will remain true in the interacting picture. The lower threshold in the non-interacting picture is made up of one deep hole that traces the dispersion from k_F through to $-k_F$ and has a particle excitation at the Fermi surface[1] Upon adding interactions the picture does change, but some of the highlighted aspects remain the same. A threshold still exists, but we will find that the behaviour at the threshold depends on the momentum in a non-trivial way.

[1]Due to the particle-hole symmetric nature of the filling we have considered, we must also take the case of the high-energy particle and the low-energy hole.

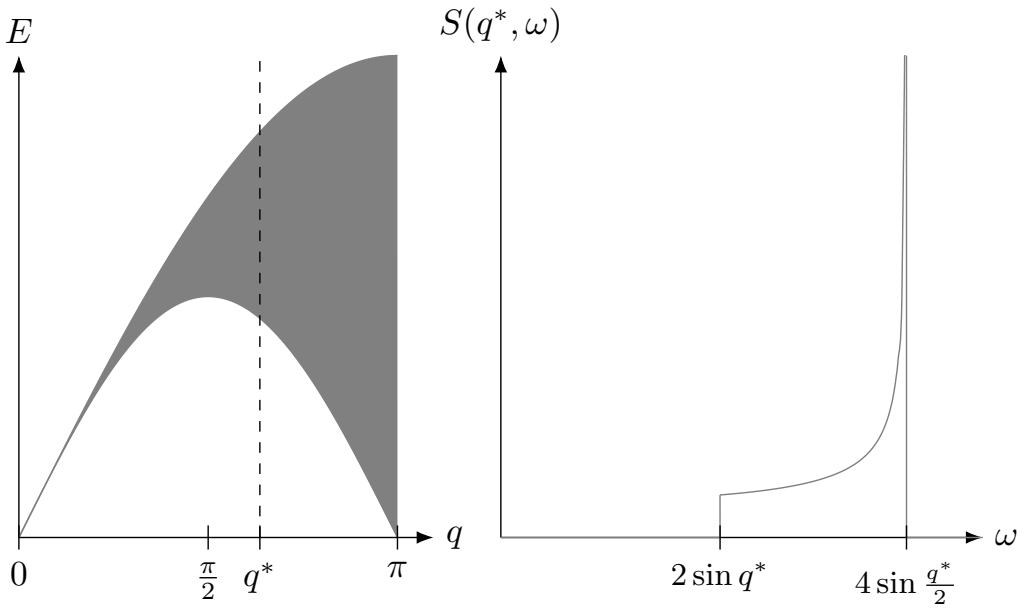

Figure 1.2: Plot of the DSF for the tight-binding chain found in (1.24). The shaded region in the left figure indicates the region of support of the DSF. The right figure shows the form of the DSF for a cut at fixed momentum q^*. Singular behaviour can be observed at the thresholds, both of which will be modified by interactions.

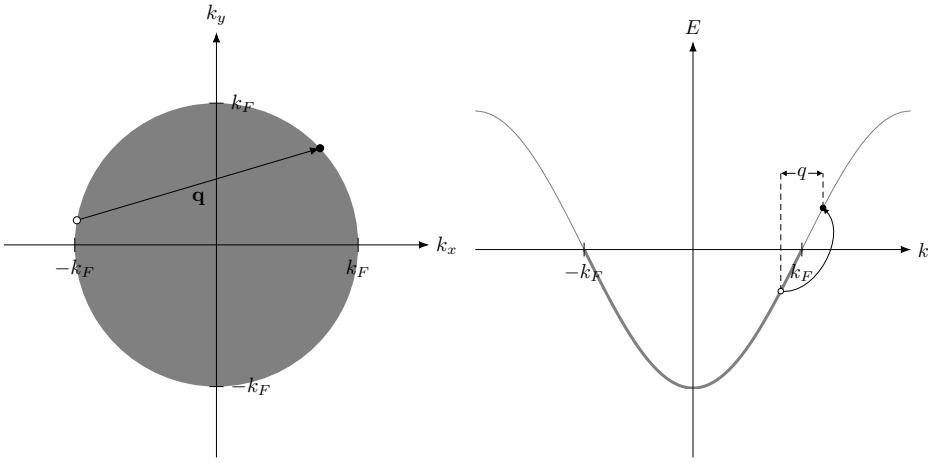

Figure 1.3: Creating a low-energy particle-hole excitation with momentum $|\mathbf{q}| \leq 2k_F$ in the 2D free fermion theory compared with a particle-hole excitation with momentum q in the 1D free fermion theory.

If we consider the spectral representation of the DSF, we have

$$S(q,\omega) = (2\pi)^2 \sum_n \left| \langle n | \sum_k c^\dagger(P_n + k) c(k) | GS \rangle \right|^2 \delta(\omega - E_n) \delta(q - P_n), \tag{1.25}$$

where we have resolved over a complete set of energy eigenstates $|n\rangle$ with energy E_n and momentum P_n. The constraints on the eigenstates $|n\rangle$ appearing in the sum are two-fold: firstly, we can only make particle-hole excitations, as the Hamiltonian still commutes with total fermion number. Second, momentum is still a good quantum number, and hence we are only considering particle-hole excitations with a particular net momentum.

For zero interaction, the excited states contributing near the threshold consist of a single high-energy fermionic excitation and a hole at the Fermi surface. Upon the addition of interactions, we can think of this as being dressed by particle-hole excitations. These must be particle-hole excitations, due to the number-conserving nature of the Hamiltonian. Indeed, the kinematics at the threshold are of the same sort as the non-interacting case: we have a "deep hole" contributing an $\mathcal{O}(1)$ term to the energy, and then a superposition of particle-hole excitations on top of this which contribute $\mathcal{O}(L^{-1})$ terms to the energy. These kinematics motivate the decomposition of the Fermionic field, in analogy to the low-energy case, as

$$c_j \to \sqrt{a_0} \left[e^{ik_F x} R(x) + e^{-ik_F x} L(x) + e^{i(k_F - q)kx} d(x) \right]. \tag{1.26}$$

Here q is the momentum at which we wish to resolve the DSF (1.25). This allows us to identify the pertinent component of the density operator with

$$\rho(x) \sim e^{-iqx} R^\dagger(x) d(x) + \text{h.c.}, \tag{1.27}$$

which will determine the correlation function we wish to evaluate in the field theory. Using the operator identification (1.26), we can write the low-energy limit of the free Hamiltonian in the form

$$H_{\text{free}} = iv_F \int \mathrm{d}x \left[L^\dagger(x) \partial_x L(x) - R^\dagger(x) \partial_x R(x) \right] + \int \mathrm{d}x \, d^\dagger(x) \left[\varepsilon_0(k) - iu_0(k) \partial_x \right] d(x), \tag{1.28}$$

where $v_F = 2t \sin k_F$ and we have set $a_0 = 1$ for notational simplicity. For the impurity piece, we have $\varepsilon_0 = -2t \cos k$, $u_0 = 2t \sin k$.

In such a case bosonisation is not necessary in order to understand the results, and the DSF is easily shown to reproduce the step function onset at the appropriate energy. Far away from the threshold this method fails to capture the correct behaviour because the kinematics are *not* the same and the decomposition of (1.26) is inapplicable. Note that in this case we find the same power-law behaviour as in the Luttinger liquid, and the threshold is determined correctly by the dispersion relation of the impurity. We will see that the addition of interactions leads to a change in the singular behaviour at the threshold.

We now go beyond the free picture and consider small but non-zero Δ: we insert the decomposition of the Fermi field into our Hamiltonian and bosonise the low-energy modes at the Fermi points, this leads us to the mobile impurity model (MIM). The free part remains the same as in the standard bosonisation case and when we include the interaction piece the full Hamiltonian can be written as

$$\begin{aligned} H = &\frac{v}{2} \int \mathrm{d}x \left[\frac{1}{K} \left(\partial_x \Phi\right)^2 + K \left(\partial_x \Theta\right)^2 \right] \\ &+ \int \mathrm{d}x \, d^\dagger(x) \left(\epsilon - iu\partial_x\right) d(x) \\ &+ \int \mathrm{d}x \, d^\dagger(x) d(x) \left[\kappa_L \partial_x \varphi_L + \kappa_R \partial_x \varphi_R\right] \end{aligned} \tag{1.29}$$

where we have neglected irrelevant terms and the renormalisation of the chemical potential. At leading order in Δ, we can identify

$$\begin{aligned} K &= 1 - \frac{\Delta}{\pi} \sin(k_F), & v &= \left(1 + \frac{\Delta}{\pi} \sin(k_F)\right) v_F, \\ \varepsilon &= \varepsilon_0 \left(1 + \frac{\Delta}{\pi} \sin k_F\right), & u &= u_0 \left(1 - \frac{\Delta}{\pi} \sin k_F\right), \\ \kappa_L &= -\frac{4\Delta}{\sqrt{\pi}} \sin^2 \frac{k + k_F}{2}, & \kappa_R &= -\frac{4\Delta}{\sqrt{\pi}} \sin^2 \frac{k - k_F}{2}. \end{aligned} \tag{1.30}$$

We can see that the Hamiltonian we have written down in (1.29) includes low-energy modes, the impurity corresponding to the deep hole and a coupling between them. For small interactions, we perturbatively control what the coupling constants are in the

MIM. Away from small interactions, this picture is expected to still hold, but must be considered phenomenological: alternative methods must be used to fix the coupling constants. Within this effective model, correlation functions can be calculated, and this is achieved via diagonalisation of this model in precisely the same manner as used in the X-ray edge singularity problem [52, 58]. This corresponds to a unitary transformation which can be understood as changing the boundary conditions of the Luttinger Liquid's bosonic fields when they pass the mobile impurity, defined by the operator

$$U = e^{-i\int_{-\infty}^{\infty} \mathrm{d}x[\gamma_R\varphi_R(x)+\gamma_L\varphi_L(x)]d^\dagger(x)d(x)}, \tag{1.31}$$

which we use to transform the relevant terms in the Hamiltonian as

$$\begin{aligned}
\varphi_R^\circ(x) &= U\varphi_R U^\dagger = \varphi_R - \frac{\gamma_R}{4}\int \mathrm{d}x' \mathrm{sign}(x-x')d^\dagger(x')d(x'),\\
\varphi_L^\circ(x) &= U\varphi_L U^\dagger = \varphi_L + \frac{\gamma_L}{4}\int \mathrm{d}x' \mathrm{sign}(x-x')d^\dagger(x')d(x'),\\
\widetilde{d}(x) &= UdU^\dagger = d(x)e^{i(\gamma_R\varphi_R+\gamma_L\varphi_L)}e^{-\frac{i}{8}(\gamma_R^2-\gamma_L^2)\int \mathrm{d}x' \mathrm{sign}(x-x')d^\dagger(x')d(x')}.
\end{aligned} \tag{1.32}$$

This allows us to decouple the low-energy and impurity degrees of freedom by taking

$$\begin{pmatrix}\kappa_R\\ \kappa_L\end{pmatrix} = \begin{pmatrix} u-\frac{v}{2}\left(K+\frac{1}{K}\right) & \frac{v}{2}\left(K-\frac{1}{K}\right)\\ -\frac{v}{2}\left(K-\frac{1}{K}\right) & -u-\frac{v}{2}\left(K+\frac{1}{K}\right)\end{pmatrix}\begin{pmatrix}\gamma_R\\ \gamma_L\end{pmatrix}. \tag{1.33}$$

Combining these leaves us with the free Hamiltonian consisting of the sum of a low-energy piece and an impurity piece, with renormalised impurity energy

$$\begin{aligned}
H = &\frac{v}{2}\int \mathrm{d}x \left[\frac{1}{K}\left(\partial_x\Phi^\circ\right)^2 + K\left(\partial_x\Theta^\circ\right)^2\right]\\
&+\int \mathrm{d}x\, \widetilde{d}^\dagger(x)\left(\widetilde{\varepsilon} - i\widetilde{u}\partial_x\right)\widetilde{d}(x) + \dots\ ,
\end{aligned} \tag{1.34}$$

where $\widetilde{\varepsilon} = \varepsilon + \frac{u}{4}\left(\gamma_R^2-\gamma_L^2\right) + \frac{v}{2}\left[\frac{1}{K}\left(\frac{\gamma_R-\gamma_L}{2}\right)^2 + K\left(\frac{\gamma_R+\gamma_L}{2}\right)^2\right] + \frac{1}{2}\left(\kappa_R\gamma_R - \kappa_L\gamma_L\right)$ and $\widetilde{u} = u$. Projection of the fermionic operators onto the effective degrees of freedom is straightforward in this problem. Writing the density-density correlator in terms of the bosonised degrees of freedom as in (1.27), employing the unitary transformation allows us to calculate the onset at the threshold as a standard exercise in bosonisation,

yielding

$$
\begin{aligned}
S^{\text{thresh}}(q,\omega) &\sim \theta(\omega-\omega_L(q))\left(\omega-\omega_L(q)\right)^{\nu}, \\
\nu &= \frac{1}{2}\left[K\left(\frac{1}{2}-\frac{\gamma_R+\gamma_L}{\sqrt{4\pi}}\right)^2+\frac{1}{K}\left(1-\frac{\gamma_R-\gamma_L}{\sqrt{4\pi}}\right)^2\right]-1 \\
&\approx -\frac{8\Delta}{\pi}\frac{\sin^2\left(\frac{q}{2}\right)}{v_F-u_0}+\mathcal{O}(\Delta^2),
\end{aligned}
\tag{1.35}
$$

This threshold singularity has been validated in numerical studies[56]. Here we considered the perturbative regime where Δ is small. In this case, we identified everything to leading order in Δ. In principle one can continue to consider higher orders in Δ by projecting operators onto the low-energy subspace[2] . However, from the Bethe Ansatz, we know that the gapless phase extends for all $|\Delta| < 1$, and we can use a different scheme to identify the coupling constants. Here we outline the principle that will allow us to calculate threshold exponents in generic Bethe Ansatz solvable models.

The diagonal form of the transformed Hamiltonian allows us to write down the finite-size excitation spectrum by using the mode expansion, leading to the so-called "shifted conformal spectrum", as the terms look very similar to that of the usual conformal field theory, given by

$$
\begin{aligned}
E = e_{GS}L+\varepsilon(k)+\frac{2\pi v}{L}\Bigg[&\frac{1}{K}\left(q_R+q_L+\frac{\gamma_R-\gamma_L}{2}\right)^2+K\left(q_R-q_L+\frac{\gamma_R+\gamma_L}{2}\right)^2 \\
&+\sum_{l=1}^{\infty} l(M_l^+ + M_l^-)\Bigg],
\end{aligned}
\tag{1.36}
$$

with q_R, q_L, M_l^+, M_l^- integers, corresponding to excitations at the right/left Fermi points and particle-hole excitations around the right/left Fermi points respectively. Due to the boundary-changing operator U, the boundary conditions of our conformal fields now depend on the details of the mobile impurity sector. All of our unknown coupling constants appear either implicitly or explicitly in the finite-size energy spectrum. In the case of an integrable model, we can actually calculate the finite-size

[2] Indeed, in calculating the impurity propagator, we assumed that the impurity was long-lived, and this is true in the case the integrable model which we chose. In the general case, we expect a finite lifetime of the impurity to broaden the singularity[49].

energy spectrum *in the presence* of the high-energy excitation. The high-energy excitation determining the threshold corresponds to one of the elementary excitations in the exact solution of the XXZ model. This then allows us to fix all of the parameters and obtain exact results for the asymptotic form of correlation functions, and this is the method we will use in Chapter 2.

Whilst we have only examined the case for spinless fermions, one might hope that the phenomenology will be reproduced in the case of spinful fermions. In this case, the Luttinger Liquid picture necessarily becomes more complicated: as mentioned before, the spin and charge degrees of freedom acquire different velocities upon the addition of even small interactions. The natural way to generalise this to the spin/charge case is to employ refermionisation to consider the strongly interacting spin/charge fermions, covered in Ref. [59]. The idea is then to tune the interactions between the spin/charge fermions to a non-interacting point, called the Luther-Emery point. From here we can then follow a similar perturbative construction to recover MIM physics in spinful systems.

1.5 The Hubbard Chain

A few details of the Hubbard chain have been outlined, but now with greater context we can say more. The motivation for writing it down was simply to capture the physics of a system of spinful electrons with repulsive interactions by considering the tight-binding chain with on-site repulsion. In higher dimensions, the Hubbard model has been the focus of an astonishing amount of theoretical effort to understand the phase diagram and correlation functions via approximate techniques.

However, with pioneering work on integrability and the Bethe Ansatz in the mid-20th century[8, 60, 61], it came to be understood that the 1D Hubbard model admits an exact solution. This allows us to make precise statements: the exact phase diagram in 1D is known as a function of filling, magnetisation and the strength of the interaction U. Notably, the Hubbard chain is a Mott insulator at half-filling for *all* $U > 0$, undergoing a quantum phase transition at $U = 0$[26].

1.5.1 Exact solution of the Hubbard model

While we will not provide a thorough derivation of the exact solution, which can be found in Ref. [26], we will recapitulate the most important aspects. The Bethe Ansatz was introduced in the context of the spin-$\frac{1}{2}$ isotropic Heisenberg model in one dimension[8]. In the ferromagnetic phase, the ground state (with maximal S^z) is given by the fully polarised state of spins i.e. $|GS\rangle = |\uparrow \cdots \uparrow\rangle$. Translational invariance leads us to construct one-particle states of the form $|k\rangle = \frac{1}{\sqrt{L}} \sum_{j=1}^{L} e^{ikj} \sigma_j^x |GS\rangle$. Imposing periodic boundary conditions, this yields the quantisation condition $k = \frac{2\pi n}{L}$ for integer n such that $0 \leq n < L$. At its most basic level, the Bethe Ansatz is a clever generalisation of this plane-wave single spin-flip excitation to multi-particle states. Using this ansatz, periodic boundary conditions lead to a more complicated set of quantisation conditions: one finds a set of algebraic equations for the quasi-momenta [8, 29, 30], and every solution of these algebraic equations implicitly yields an eigenstate. The main complication lies in the fact that, in contrast to the non-interacting case, the quantisation conditions for each individual quasi-momentum depend on all of the other quasi-momenta.

For spinless fermions (or equivalently spin-$\frac{1}{2}$ models which may be mapped onto spinless fermions), the Bethe Ansatz in the form outlined above may be sufficient to identify all of the eigenstates of the model. The Hubbard model, being comprised of two species of fermions, is more complicated than this: it took until 1967 for Yang to make a crucial contribution to so-called nested problems[60]. By using the Bethe Ansatz, solving the eigenvalue problem for the Hubbard model is reduced to a separate eigenvalue problem. This second eigenvalue problem can be solved by a further application of the Bethe Ansatz in a generalised form. This highly non-trivial work then permitted the exact solution of the one-dimensional Hubbard model, which quickly followed[61]. The eigenstates of the one-dimensional Hubbard model with periodic boundary conditions on a system of length L with N electrons, M of which

are spin down, can be understood in terms of solutions of the Lieb-Wu equations[61]

$$\begin{aligned} e^{ik_jL} &= \prod_{\ell=1}^{M} \frac{\lambda_\ell - \sin k_j - iu}{\lambda_\ell - \sin k_j + iu}, \qquad j = 1, \ldots, N, \\ \prod_{j=1}^{N} \frac{\lambda_\ell - \sin k_j - iu}{\lambda_\ell - \sin k_j + iu} &= \prod_{\substack{m=1 \\ m\neq\ell}}^{M} \frac{\lambda_\ell - \lambda_m - 2iu}{\lambda_\ell - \lambda_m + 2iu}, \qquad \ell = 1, \ldots, M \ , \end{aligned} \tag{1.37}$$

where $u = \frac{U}{4t}$. These equations are to be solved for the rapidities $\{k_j\}$, $\{\lambda_\ell\}$. In terms of these rapidities, due to the nested nature of the problem, the eigenstates of the Hubbard model are quite complicated, but we present them for completeness. A particular wavefunction is specified by

$$|\Psi_{M,N}\rangle = \sum_{1\leq x_k\leq L} \psi_{\sigma_1,\ldots,\sigma_N}(x_1, \ldots, x_N) \prod_{j=1}^{N} c^\dagger_{x_j,\sigma_j}|0\rangle \ . \tag{1.38}$$

The functions ψ depend specifically on the ordering of the x_i. We therefore choose a specific permutation Q of the N elements such that $1 \leq x_{Q_1} \leq \ldots \leq x_{Q_N} \leq L$. In the sector Q, the wavefunction is given by[62]

$$\psi_{\sigma_1,\ldots,\sigma_N}(x_1, \ldots, x_N) = \sum_{P\in S_N} \mathrm{sign}(PQ) e^{i\sum_{j=1}^{N} k_{P_j} x_{Q_j}} \varphi(y_1, \ldots, y_M|P), \tag{1.39}$$

where $\sigma_1, \ldots, \sigma_M = -1$, $\sigma_{M+1}, \ldots, \sigma_N = 1$, and the amplitudes $\varphi(y_1, \ldots, y_M|P)$ are given by

$$\varphi(y_1, \ldots, y_M|P) = \sum_{\pi\in S_M} A_\pi \prod_{l=1}^{M} F_P(\lambda_{\pi_l}, y_l). \tag{1.40}$$

The numbers $y_1, \ldots, y_M$ are defined to be the positions of the down spins in the sequence $\sigma_{Q_1}, \ldots, \sigma_{Q_N}$ in increasing order i.e. $1 \leq y_1 < y_2 < \ldots < y_M \leq N$. For fixed permutations $P \in S_N$, $\pi \in S_M$

$$\begin{aligned} F_P(\lambda_j, y) &= \left(\prod_{i=1}^{y-1} \frac{\sin(k_{P_i}) - \lambda_j + iu}{\sin(k_{P_i}) - \lambda_j + iu} \right) \left(\frac{1}{\sin(k_{P_i}) - \lambda_j - iu} \right), \\ A_\pi &= \prod_{1\leq l<k\leq M} \left(\frac{\lambda_{\pi_l} - \lambda_{\pi_k} + u}{\lambda_{\pi_l} - \lambda_{\pi_k}} \right). \end{aligned} \tag{1.41}$$

We refer the reader to Ref. [26] for a complete derivation and discussion of the wavefunctions. The form of the wavefunctions is not particularly illuminating; they consist

of a sum over all permutations of the N rapidities k_j, and so the wavefunction contains $N!$ terms with non-trivial weights in the sum. In terms of direct evaluation of correlation functions, this large number of terms makes exact calculations in the Hubbard model extremely difficult for generic quantities. We note that there do exist techniques for evaluating form factors for particular local operators in integrable models such as the XXZ model, however generalisations to the Hubbard model or other nested models are less well understood. A small number of quantities are simple in terms of these rapidities. For example, the energy of a state is given in units of t by

$$E = -2\sum_{j=1}^{N} \cos k_j + u(L - 2N), \tag{1.42}$$

where $u = U/4t$. This is similar to the free fermionic case except that now the k_j can be complex and are more difficult to solve for.

1.5.2 String hypothesis

The solution of the Lieb-Wu equations (1.37) for complex $\{k_j\}$ and $\{\lambda_\ell\}$ is generally a very difficult task. The real solutions are very important, as these characterise the ground state and a low-lying states in the gapless phase for $U > 0$. In terms of understanding all of the eigenstates, however, one must consider the complex solutions.

The solutions to the Lieb-Wu equations are self-conjugate[26], and so we can consider negative imaginary part without loss of generality. It was noticed that certain solutions tend to form particularly simple patterns in the complex plane[63]. If one of the momenta k_j has a negative imaginary part, then this must correspond to one of the denominators in the product being exponentially close to a pole.

At the simplest level, this forces a relationship between two complex conjugate ks and one Λ which lies on the real axis[63]. In more general terms, it is possible to create a string combining $2m$ ks in the complex plane with m Λs to form a 'k-Λ

string' of length $2m$. This arrangement is given by the pattern[26]

$$\begin{aligned}
k^1 &= \pi - \arcsin(\Lambda'^m + miu), \\
k^2 &= \arcsin(\Lambda'^m + (m-2)iu), \\
k^3 &= \pi - k^2, \\
&\vdots \\
k^{2m-2} &= \arcsin(\Lambda'^m - (m-2)iu), \\
k^{2m-1} &= \pi - k^{2m-2}, \\
k^{2m} &= \pi - \arcsin(\Lambda'^m - miu), \\
\Lambda'^{m,j} &= \Lambda'^m + (m-2j+1)iu, \qquad j = 1, \ldots, m.
\end{aligned} \tag{1.43}$$

Physically, the string solutions correspond to bound states of charge and spin excitations, and exponential decay of these states as a function of distance can be explicitly shown for simple cases[26]. Furthermore, there are bound states of spins which correspond to m Λs forming a string in the complex plane, which are referred to as a 'Λ string' of length m. These have a configuration given by a regularly spaced roots about the 'real centre' Λ^m i.e.

$$\Lambda^{m,j} = \Lambda^m + (m-2j+1)iu, \quad j = 1, \ldots, m. \tag{1.44}$$

As in the case of the k-Λ strings, these string solutions are exponentially close (in N) to the actual solutions for large system sizes.

There exist certain proofs of the exactness as $L \to \infty$ in other Bethe Ansatz integrable models [64], and numerical studies have shown that for small system sizes most solutions of the Lieb-Wu equations are accurately described by string solutions[65]. It is possible to take the string hypothesis and re-express the Lieb-Wu equations (1.37) in terms of string solutions alone. This has the advantage that instead of considering solutions of the Lieb-Wu equations, which generally lie in the complex plane, we can now consider a system of equations for the real centres of strings. The so-called "Takahashi equations" are a massaged form of the logarithm of the Lieb-Wu equations. Because of the multi-valued nature of the logarithm, we must choose

integers/half-odd integers to fix a solution. It is possible to show that the string hypothesis allows us, with the SO(4) symmetry of the Hubbard model, to construct 4^L linearly independent eigenstates and therefore the Bethe Ansatz provides a complete set of energy eigenstates of the 1D Hubbard model[66].

As mentioned above: for large system sizes, the eigenstates of the repulsive Hubbard model can be expressed in terms of solutions of the Takahashi equations. These equations are most conveniently expressed in terms of so-called *counting functions*. Introducing a chemical potential μ and magnetic field B in order to tune the filling and magnetisation, we have that in the case of N electrons, M of which are spin-down, these are defined by

$$\begin{aligned}
\frac{2\pi I_j}{L} &= k_j + \frac{1}{L}\sum_{n=1}^{\infty}\sum_{\alpha=1}^{M_n}\theta\left(\frac{\sin k_j - \Lambda_\alpha^n}{nu}\right) + \frac{1}{L}\sum_{n=1}^{\infty}\sum_{\alpha=1}^{M'_n}\theta\left(\frac{\sin k_j - \Lambda'^n_\alpha}{nu}\right), \quad j = 1,\ldots,N-2M', \\
\frac{2\pi J_\alpha^n}{L} &= \frac{1}{L}\sum_{j=1}^{N-2M'}\theta\left(\frac{\Lambda_\alpha^n - \sin k_j}{nu}\right) - \frac{1}{L}\sum_{m=1}^{\infty}\sum_{\beta=1}^{M_m}\Theta_{nm}\left(\frac{\Lambda_\alpha^n - \Lambda_\beta^m}{u}\right), \qquad \alpha = 1,\ldots,M_n, \\
\frac{2\pi J'^n_\alpha}{L} &= -\frac{1}{L}\sum_{j=1}^{N-2M'}\theta\left(\frac{\Lambda'^n_\alpha - \sin k_j}{nu}\right) - \frac{1}{L}\sum_{m=1}^{\infty}\sum_{\beta=1}^{M'_m}\Theta_{nm}\left(\frac{\Lambda'^n_\alpha - \Lambda'^m_\beta}{u}\right) \\
&\quad + 2\mathrm{Re}[\arcsin(\Lambda'^n_\alpha + niu)], \qquad \alpha = 1,\ldots,M'_n,
\end{aligned} \tag{1.45}$$

where $u = U/4t$, $\theta(x) = 2\arctan(x)$,

$$\Theta_{nm}(x) = \begin{cases} \theta\left(\frac{x}{|n-m|}\right) + 2\theta\left(\frac{x}{|n-m|+2}\right) + \cdots + 2\theta\left(\frac{x}{n+m-2}\right) + \theta\left(\frac{x}{n+m}\right), & n \neq m \\ 2\theta\left(\frac{x}{2}\right) + 2\theta\left(\frac{x}{4}\right) + \cdots + 2\theta\left(\frac{x}{2n-2}\right) + \theta\left(\frac{x}{2n}\right), & n = m \end{cases}, \tag{1.46}$$

and

$$M = \sum_{n=1}^{\infty} n(M_n + M'_n), \qquad M' = \sum_{n=1}^{\infty} nM'_n. \tag{1.47}$$

The sets $\{I_j\}$, $\{J_\alpha^n\}$, $\{J'^n_\alpha\}$ of integer or half-odd integer numbers correspond to charge scattering states, Λ-strings of length n and k-Λ-strings of length $2n$ respectively. They

specify the particular eigenstate under consideration and obey the "selection rules"

$$
\begin{aligned}
I_j &\in \begin{cases} \mathbb{Z}+\frac{1}{2} & \text{if } \sum_m (M_m + M'_m) \text{ odd} \\ \mathbb{Z} & \text{if } \sum_m (M_m + M'_m) \text{ even} \end{cases}, && -\frac{L}{2} < I_j \leq \frac{L}{2}, \\
J^n_\alpha &\in \begin{cases} \mathbb{Z} & \text{if } N - M_n \text{ odd} \\ \mathbb{Z}+\frac{1}{2} & \text{if } N - M_n \text{ even} \end{cases}, && |J^n_\alpha| \leq \frac{1}{2}(N - 2M' - \sum_{m=1}^{\infty} t_{nm} M_m - 1), \\
J'^n_\alpha &\in \begin{cases} \mathbb{Z} & \text{if } L - N + M'_n \text{ odd} \\ \mathbb{Z}+\frac{1}{2} & \text{if } L - N + M'_n \text{ even} \end{cases}, && |J'^n_\alpha| \leq \frac{1}{2}\left(L - N + 2M' - \sum_{m=1}^{\infty} t_{nm} M'_m - 1\right),
\end{aligned}
\tag{1.48}
$$

where $t_{nm} = 2\min(m,n) - \delta_{mn}$. The energy and momentum, measured in units of $t = 1$, of an eigenstate characterised by the set of roots $\{k_j, \Lambda^n_\alpha, \Lambda'^m_\beta\}$ are given by

$$
E = -\sum_{j=1}^{N-2M'} (2\cos k_j + \mu + 2u + B) + 2BM + 4\sum_{n=1}^{\infty}\sum_{\beta=1}^{M'_n} \mathrm{Re}\sqrt{1 - (\Lambda'^n_\beta + niu)^2} + Lu, \tag{1.49}
$$

$$
P = \left[\sum_{j=1}^{N-2M'} k_j - \sum_{n=1}^{\infty}\sum_{\beta=1}^{M'_n} \left(2\,\mathrm{Re}\arcsin\left(\Lambda'^n_\beta + niu\right) - (n+1)\pi\right)\right] \bmod 2\pi. \tag{1.50}
$$

As mentioned before, deviations from the string solutions are expected to be small for large N, M. Although the Takahashi equations look formidable, the integers associated with the counting functions allow us to determine all of the eigenstates. A choice of the integers fixes a unique solution to the Takahashi equations.

1.5.2.1 Ground state

We consider the case where L is even, the total number of electrons N_{GS} is even and the number of down spins M_{GS} is odd. The ground state is then obtained by choosing the set $\{I_j, J^n_\alpha, J'^m_\beta\}$ to be[26]

$$
I_j = -\frac{N_{GS}}{2} - \frac{1}{2} + j, \qquad j = 1, \ldots, N_{GS}, \tag{1.51}
$$

$$
J^1_\alpha = -\frac{M_{GS}}{2} - \frac{1}{2} + \alpha, \qquad \alpha = 1, \ldots, M_{GS}. \tag{1.52}
$$

This configuration is shown for the example $L = 16$, $N_{GS} = 2M_{GS} = 10$ in Fig. 1.4.

As will become clear in Chapter 2, taking the thermodynamic limit of such a configuration will allow us to understand the Takahashi equations in terms of linear

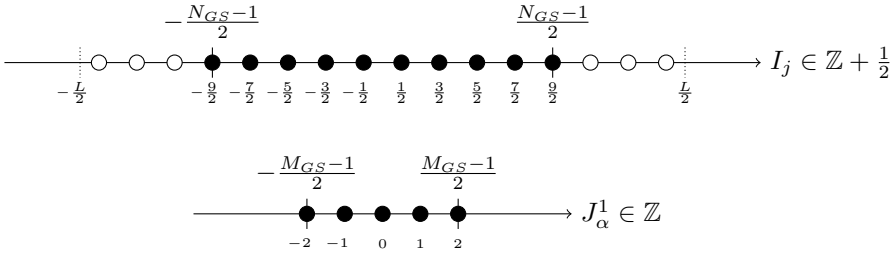

Figure 1.4: Configuration of the integers for the ground state, explicit numbers given are for $L = 16$, $N_{GS} = 10$, $M_{GS} = 5$

integral equations. The finite-size corrections to the energy in the presence of a high-energy excitation (also specified by certain configurations of the integers/half-odd integers) will then allow us to fix parameters in the mobile impurity model. This then permits a non-perturbative prediction for the functional form of threshold singularities.

Whilst being interesting in the context of experimental systems, the Hubbard model is somehow the parent of many other well-studied Hamiltonians in one dimension. In various limits one can obtain the Yang-Gaudin gas, the Heisenberg model, and the sine-Gordon model.

1.5.3 Bosonisation of the Hubbard model

The bosonisation formulae can be generalised to the spinful case. In both cases we wish to describe a low-energy theory in terms of the bosonic modes. Generically, the fermionic operators live at all energies, which includes operators that live outside this low-energy window. One can perturbatively integrate out the high-energy degrees of freedom to project onto a low-energy space of fermionic operators. This will result in higher harmonics of the bosonised fields with non-universal amplitudes for different harmonics[67].

In the spinful case, we introduce bose fields for both the spin up and spin down degrees of freedom $\varphi_{\uparrow/\downarrow}$ and $\bar{\varphi}_{\uparrow/\downarrow}$ corresponding to right- and left-movers respectively. It will turn out to be useful to consider spin $\varphi_s = \varphi_\uparrow - \varphi_\downarrow$ and charge $\varphi_c = \varphi_\uparrow + \varphi_\downarrow$ degrees of freedom. In terms of these, the generalised form of Haldane's bosonisation

identities[46, 48, 59] is

$$c_{j,\sigma} \sim \sqrt{a_0} \sum_{n,m\in\mathbb{Z}} \Gamma^{(\sigma)}_{n,m} A_{n,m} e^{ik_F(1-4n-2m)} e^{-\frac{i}{2}\varphi_c(x)-\frac{i}{2}\sigma\varphi_s(x)} e^{i\frac{2n+m}{2}\Phi_c(x)} e^{-i\sigma\frac{m}{2}\Phi_s(x)}, \quad (1.53)$$

where k_F is the Fermi momentum, $\Gamma^{(\sigma)}_{n,m} = \eta_\sigma(\eta_\sigma\bar{\eta}_\sigma\eta_{\bar{\sigma}}\bar{\eta}_{\bar{\sigma}})^n(\eta_{\bar{\sigma}}\bar{\eta}_\sigma)^m$ are Klein factors, $A_{n,m}$ are non-universal amplitudes, $\Phi_\alpha = \varphi_\alpha + \bar{\varphi}_\alpha$, $\Theta_\alpha = \varphi_\alpha - \bar{\varphi}_\alpha$. The fields satisfy the commutation relations

$$[\Phi_\alpha(x), \Theta_\beta(x')] = 4\pi i\delta_{\alpha,\beta}\mathrm{sign}(x-x'). \quad (1.54)$$

Applying this bosonisation formula to the Hubbard model in the gapless phase (below half-filling) and retaining the most relevant terms allowed by symmetry leads to the spin-charge separated two-component Luttinger liquid, given by[26]

$$H = \sum_{\alpha=c,s} \frac{v_\alpha}{16\pi} \int \mathrm{d}x \left[\frac{1}{K_\alpha} \left(\frac{\partial\Phi_\alpha}{\partial x} \right)^2 + K_\alpha \left(\frac{\partial\Theta_\alpha}{\partial x} \right)^2 \right] + \ldots, \quad (1.55)$$

where the ellipsis signifies RG irrelevant terms. The velocities and Luttinger parameters are equal at $U = 0$, but when the interaction is non-vanishing the charge and spin degrees of freedom acquire separate velocities. This demonstrates clearly how the Fermi liquid fails in one dimension, as the emergent quasiparticles are of a distinct character to those of the electron.

In the spinful case, although the fundamental fermionic degrees of freedom are not a good way of describing the low-energy excitations of the interacting system, as made manifest through charge-spin separation, we *can* define new fermionic operators via the bosonisation formulae, corresponding to fermionic spin and charge excitations. This procedure is known as *refermionisation*, and is also important in the general construction of mobile impurity models[49, 59].

It is important to point out previous contributions to the application of mobile impurity models to the Hubbard model. Ref. [68] considers the true threshold of the spectral function in the Hubbard model, and Ref. [69] goes on to evaluate additional singular contributions to the spectral function for fixed q at higher energies. This arises from excitations which can be identified from the exact solution at higher

energies than the threshold and also give rise to sharp peaks in the spectral function. Understanding the fine structure of the spectral function tells us about the real-time dynamics at late times, which combined with tDMRG data allows the computation of the spectral function at all energies[69].

1.6 Relaxation of quantum many-body systems

It is well understood[35, 70] that the equilibrium properties of a system with Hamiltonian H in contact with a reservoir at inverse temperature β is described by the Gibbs ensemble, defined by the density matrix $\rho = e^{-\beta H}$. It is interesting to ask to what ensemble, if anything, large isolated systems relax, and what the transient behaviour is.

We can understand this relaxational behaviour in the context of the cleanly defined protocol of the *quantum quench*[71]. Here we take a local Hamiltonian with some tunable parameter $H(\Delta_0)$ and initialise the system in its ground state $|\psi_0, \Delta_0\rangle$. At time $t = 0$ we then rapidly change $\Delta_0 \to \Delta$ such that $|\psi_0, \Delta_0\rangle$ is not an eigenstate of $H(\Delta)$. The time evolution is formally is given by

$$|\psi(t)\rangle = e^{-iH(\Delta)t}|\psi_0, \Delta_0\rangle. \tag{1.56}$$

If we consider a local observable[3] $\mathcal{O}$, the task is to evaluate

$$\mathcal{O}_{\text{stat}} = \lim_{t\to\infty}\lim_{L\to\infty}\langle\psi(t)|\mathcal{O}|\psi(t)\rangle, \tag{1.57}$$

if the limit exists. The state $|\psi_0, \Delta_0\rangle$ generically corresponds to a superposition of exponentially many (in L) highly excited eigenstates of $H(\Delta)$. This is a very difficult problem to solve in general, as can be understood by resolving the identity in terms of complete sets of energy eigenstates

$$\mathcal{O}_{\text{stat}} = \lim_{t\to\infty}\lim_{L\to\infty}\sum_{n,m}\langle\psi_0, \Delta_0|\psi_n, \Delta\rangle\langle\psi_m, \Delta|\psi_0, \Delta_0\rangle e^{i(E_n(\Delta)-E_m(\Delta))t}\langle\psi_n, \Delta|\mathcal{O}|\psi_m, \Delta\rangle. \tag{1.58}$$

[3]We consider only local observables, as a quantum many-body system can never relax as a whole. This is simple to see if one considers sums of multiple projectors onto eigenstates, which trivially fail to relax from (1.58), but generically correspond to non-local operators.

This is generally a complicated quantity as the overlaps and form factors do not have a simple known form for most models. Here we focus simply on what the limit is, rather than the richer problem of explicitly evaluating the time evolution of observables.

We expect that if our state has a sufficiently narrow distribution of energies[72] and the energy density is given by

$$e = \lim_{L\to\infty} \frac{1}{L}\langle\psi_0, \Delta_0|H(\Delta)|\psi_0, \Delta_0\rangle, \tag{1.59}$$

that we can describe $\mathcal{O}_{\text{stat}}$ in terms of the microcanonical ensemble

$$\mathcal{O}_{\text{stat}} = \frac{1}{\mathcal{V}} \sum_{|E_n - Le|\leq \delta E} \langle\psi_n, \Delta|\mathcal{O}|\psi_n, \Delta\rangle, \tag{1.60}$$

where the sum is over energy eigenstates $|\psi_n, \Delta\rangle$ of $H(\Delta)$ in the specified energy window. Here, the small energy shell δE will include an exponential number of states in the system size. Up to finite-size corrections, the microcanonical ensemble is equal to the Gibbs ensemble $\rho = e^{-\beta H}$, taken at the inverse temperature β such that

$$\lim_{L\to\infty} \frac{1}{L} \frac{\text{Tr}(e^{-\beta H} H)}{\text{Tr}(e^{-\beta H})} = e. \tag{1.61}$$

The Gibbs ensemble can be understood as maximising entropy subject to the only constraint a generic isolated quantum system has: conservation of energy.

However, the study of isolated systems has led to the identification of other paradigms of relaxation. Integrable systems are an exception to the generic paradigm outlined above. The conservation laws of integrable models severely constrain the evolution and the system retains a memory of far more than just the energy density. In integrable models, we therefore must have additional Lagrange multipliers for *all* of the conserved quantities, leading to the picture of the generalised Gibbs ensemble (GGE)[33, 73–77]. The generalised microcanonical[78] ensemble then corresponds to a sum over states in a narrow shell of energy as well as the other conserved quantities, and is locally equivalent to the GGE.

The other main exception to thermalisation are many-body localised (MBL)[79–82] systems. These are believed to have a complete set of mutually commuting conserved quantities, namely quasi-local Pauli operators[83–85] known as "l-bits". As

well as not relaxing, MBL systems are different to integrable models in the sense that they are not finely tuned.

It is not a priori clear how equations (1.58) and (1.60) should be equal. It is believed that this can be understood via the Eigenstate Thermalisation Hypothesis[72, 87] (ETH). ETH reconciles this by asserting that expectation values of local operators are smooth functions of the energy density. Alternatively, this can be understood as saying that the microcanonical ensemble remains valid in its extreme limit of including only a single eigenstate, as all terms in the sum (1.60) are approximately equal. This picture that all many-body eigenstates of generic local Hamiltonians at finite energy density are created equal naturally leads to the consideration of the properties of individual eigenstates. Whilst generic systems are believed to obey ETH, and integrable systems satisfy a suitably generalised version, MBL systems obviously violate ETH. With this in mind, Ref. [86] introduces the notion of the so-called "quantum disentangled liquid" (QDL). Heuristically, we consider a system of both light and heavy degrees of freedom. We associate these with a mass scale m and M respectively. In the limit of $M/m \to \infty$, the picture is simple: for any particular eigenstate under consideration the heavy particles are literally pinned in place. The heavy particles act as a quenched disorder potential for the light degrees of freedom. We expect there to be a regime where the disorder potential is sufficiently strong that the interacting light degrees of freedom can become many-body localised at finite energy density. The main question posed is whether or not this localisation of the light degrees of freedom 'on' the heavy degrees of freedom at finite energy density can survive when M/m is large but finite. In order to identify this we observe that, in contrast to generic systems, many-body localised eigenstates have area-law bipartite entanglement entropy even at finite energy density.

Considering the entanglement of these eigenstates leads to a precise diagnostic of such QDL behaviour via the entanglement entropy. If the heuristic picture adopted above is correct then we can use the entanglement entropy to clarify the idea further. The notion of 'localisation on the heavy degrees of freedom' is characterised by the

bipartite entanglement entropy after a projective measurement of the heavy degrees of freedom. We are now in a position to define the QDL diagnostic. We say that an eigenstate possesses QDL if: we take a finite energy density eigenstate with volume-law EE and, upon projectively measuring the heavy degrees of freedom, we are left with a state with area-law EE describing the light degrees of freedom.

A simple model in which one might expect to be able to observe such behaviour is the Hubbard model. In $D = 1$ integrability tells us that there is a notion of spin-charge separation at finite energy densities. At half-filling and large U/t, the spinon bandwidth is small, scaling as $\sim t^2/U$, and the charge bandwidth scales as $\sim t$. We therefore consider the spin degrees of freedom as heavy and the charge degrees of freedom as light. This idea has been investigated numerically for small system sizes in Ref. [88], and the results are consistent with the premise.

1.7 This thesis

The non-linear Luttinger liquid, as outlined above, is crucial for describing threshold singularities in one-dimensional quantum liquids, where the Landau Fermi liquid fails to capture even the qualitative physics correctly. Furthermore, the linear Luttinger liquid fails to describe the quantitative singular behaviour at thresholds.

Motivated by the success of mobile impurity calculations, the work of Chapter 2 applies the idea to the scenario of the optical conductivity in the charge-spin separated metallic regime of the one-dimensional Hubbard model. The work presented in Chapter 2 appears in Ref. [89]. Here we use integrability to identify the elementary excitations permitted by symmetry that can contribute at various energy scales, and then apply this to the mobile impurity calculation to both guide our construction of projected operators in the effective model, and in precisely fixing coupling constants to determine the threshold behaviour of dynamical correlation functions. Here there is no "true threshold" as the system is conducting below half-filling, meaning that the optical conductivity has support at all ω. Despite this support at all frequencies, near half-filling there is nonetheless a remnant of the Mott-Hubbard gap: there is

a parametrically large region of low spectral weight which is followed by a significant increase in the value of the optical conductivity. This "threshold" we identify corresponds to the support of a particular bound state excitation of the Hubbard model which we cannot continuously connect to the non-interacting Luther-Emery point as in [59], so here we must rely entirely on the phenomenological picture. The calculation requires various non-trivial steps which are not present in previous non-linear Luttinger liquid calculations. We show that the mobile impurity method is applicable for breaking new ground in a quantitative understanding of complicated response functions in particular models. The predictions of the onset of the optical conductivity compare favourably with data from Ref. [90].

The work presented in Chapter 3 is heavily based on Ref. [91]. Here we attempt to develop the idea that some notion of QDL behaviour can be observed in the Hubbard model. We take two very different approaches to the problem to provide evidence in support of a modified version of the QDL diagnostic. The first approach relies on integrability. We identify an exponential number of eigenstates for which, up to exponential accuracy in U/T at temperature T, the volume-law contribution to the entanglement entropy can be identified as coming solely from the spin sector i.e. the heavy degrees of freedom.

The other approach attempts to deal explicitly with eigenstates. Here we use a strong-coupling expansion to examine the entanglement structure of eigenstates after a measurement of the spin degrees of freedom. We find that in one dimension, within the strong-coupling expansion the leading term has an extremely low entanglement entropy. Furthermore, the structure of this low entanglement persists order-by-order in the expansion and we are led to conclude that only non-perturbative corrections could give rise to a volume-law contribution to the entanglement entropy. As this approach does not rely on integrability, we are able to make some comments on the Hubbard model on higher-dimensional bipartite lattices.

Finally, we close the thesis in Chapter 4 with remarks on what has been covered and what lies ahead.

Chapter 2

Optical conductivity in the Hubbard chain

In this chapter we consider the optical conductivity in the one dimensional Hubbard model in the metallic phase close to half filling. In this regime most of the spectral weight is located at frequencies above an energy scale E_{opt} that tends towards the optical gap in the Mott insulating phase for vanishing doping. Using the Bethe Ansatz we relate E_{opt} to thresholds of particular kinds of excitations in the Hubbard model. We then employ a mobile impurity models to analyze the optical conductivity for frequencies slightly above these thresholds. This entails generalising mobile impurity models to excited states that are not highest weight with regards to the SU(2) symmetries of the Hubbard chain, and that occur at a maximum of the impurity dispersion.

Electron-electron interactions play a crucial rôle in determining the physical response to external probes of various quasi-one-dimensional materials e.g. organic semiconductors[92]. In order to successfully describe the mechanisms and excitations responsible for distinct physical phenomena, it is imperative to have a microscopic model capturing the essence of the physics involved; providing a framework within which realistic physical systems may be interpreted. The one-dimensional Hubbard model[26] offers an excellent theoretical laboratory in which a comprehensive microscopic understanding of the origin of various behaviours can be developed. Here, we consider the Hubbard model with a chemical potential μ and a magnetic field B which

allow us to tune the filling and magnetisation respectively, which for completeness we include as

$$\begin{aligned} H = &-t\sum_{i,\sigma} c^\dagger_{i+1,\sigma}c_{i,\sigma} + c^\dagger_{i,\sigma}c_{i+1,\sigma} + U\sum_i n_{i,\uparrow}n_{i,\downarrow} \\ &- \mu\sum_i (n_{i,\uparrow}+n_{i,\downarrow}) - B\sum_i (n_{i,\uparrow}-n_{i,\downarrow}). \end{aligned} \tag{2.1}$$

As noted in (1.55), the low-energy degrees of freedom in the metallic phase of the Hubbard chain are described [26, 93, 94] by a (perturbed) spin-charge separated Luttinger liquid [40, 41, 46, 48], with Hamiltonian

$$H = \sum_{\alpha=c,s} \frac{v_\alpha}{16\pi}\int \mathrm{d}x\, \left[\frac{1}{K_\alpha}\left(\frac{\partial\Phi_\alpha}{\partial x}\right)^2 + K_\alpha\left(\frac{\partial\Theta_\alpha}{\partial x}\right)^2\right] + \text{irrelevant operators.} \tag{2.2}$$

The parameters K_α, v_α can be calculated for the Hubbard model by solving a system of linear integral equations (see Appendix 2.A). The Bose fields $\Phi_\alpha(x)$ and dual fields $\Theta_\alpha(x)$ obey the commutation relation (1.54). The spectrum of low-lying excitations relative to the ground state for a large but finite system of length L in zero magnetic field is given by [26, 93, 94]

$$\begin{aligned} \Delta E = &\frac{2\pi v_c}{L}\left[\frac{(\Delta N_c)^2}{8K_c} + 2K_c\left(D_c + \frac{D_s}{2}\right)^2 + N_c^+ + N_c^-\right] \\ &+ \frac{2\pi v_s}{L}\left[\frac{\left(\Delta N_s - \frac{\Delta N_c}{2}\right)^2}{2} + \frac{D_s^2}{2} + N_s^+ + N_s^-\right], \end{aligned} \tag{2.3}$$

where ΔN_α, D_α and $N_\alpha^\pm$ are integers or half-odd integers subject to the "selection rules"

$$N_\alpha^\pm \in \mathbb{N}_0, \qquad \Delta N_\alpha \in \mathbb{Z}, \qquad D_c = \frac{\Delta N_c + \Delta N_s}{2} \bmod 1, \qquad D_s = \frac{\Delta N_c}{2} \bmod 1. \tag{2.4}$$

At low energies, correlation functions can be calculated from (2.2) and generically exhibit singularities at the thresholds of the allowed collective spin and charge degrees of freedom, with power-law exponents given in terms of the quantities ΔN_α, D_α, $N_\alpha^\pm$, and K_α. As discussed in Chapter 1, when working at a finite energy scale RG irrelevant terms have a non-zero coupling and may (and in fact generically do) significantly alter the predictions of the unperturbed Luttinger-liquid [54–56, 59, 68, 69, 95–115]. Over the last decade or so a fairly general method for taking into account

the effects of certain irrelevant operators in the vicinities of kinematic thresholds has been developed[49, 116]. The case of spin-charge separated Luttinger liquids has very recently been revisited [59] in order to make it explicitly compatible with exactly known properties of the Hubbard model. The essence of this approach is that, when considering a response function, there are thresholds in the (k, ω)-plane that correspond to particular excitations. In integrable models, these excitations hold privileged positions: they are stable (i.e. have infinite lifetimes) and can be identified in terms of the exact solution. If the kinematics near the threshold are described by a case in which small number of high-energy excitations carry most of the energy (in the precise sense of up to corrections of $\mathcal{O}(L^{-1})$) then the problem becomes analogous to that of the X-ray edge singularity problem for a mobile impurity [117].

In this work we employ mobile impurity methods to study the optical conductivity

$$\sigma_1(\omega) = -\frac{\text{Im } \chi^J(\omega)}{\omega}, \qquad \chi^J(\omega) = -ie^2 \int_0^\infty dt\ e^{i\omega t} \sum_{l=-L/2}^{L/2-1} \langle GS|[J_l(t), J_0(0)]|GS\rangle, \tag{2.5}$$

where J_j is the density of the current operator

$$J_j = -it \sum_\sigma \left[c^\dagger_{j,\sigma} c_{j+1,\sigma} - c^\dagger_{j+1,\sigma} c_{j,\sigma} \right]. \tag{2.6}$$

In the Mott insulating phase of the Hubbard model the optical conductivity has been previously determined [25, 118–121]: $\sigma_1(\omega)$ vanishes inside the optical gap 2Δ, where Δ is the Mott gap. At frequencies $\omega > 2\Delta$ there is a sudden power-law onset $\sigma_1(\omega) \sim \sqrt{\omega - 2\Delta}$. Away from half-filling, the system is a metal and therefore has a finite conductivity for all ω, specifically acquiring a Drude peak[122, 123] at $\omega = 0$. The low-frequency behaviour has been previously studied[124–126] in the framework of Luttinger liquid theory, predicting ω^3 behaviour for $0 < \omega \ll t$. Close to half-filling one expects most of the spectral weight in $\sigma_1(\omega)$ to be located above an energy scale E_{opt} that tends to 2Δ as we approach half-filling. The scale E_{opt} has been previously correctly identified in Ref. [127]. In the same work it was conjectured that the optical conductivity increases in a power-law fashion above E_{opt}

$$\sigma_1(\omega) \sim (\omega - E_{\text{opt}})^\zeta\ \Theta(\omega - E_{\text{opt}})\ , \tag{2.7}$$

where ζ is a real number which can be identified with a quantity that may be calculated from the Bethe Ansatz. As we will see in the following, the mobile impurity approach leads to a more complicated functional form. In the case where power-law behaviour can be observed, we find that ζ has a different formulation in terms of Bethe Ansatz quantities to the predictions of Ref. [127].

The outline of this chapter is as follows. In Sec. 2.1, we consider the spectral representation of the optical conductivity and identify the quantum numbers of the states contributing non-zero spectral weight. In Sec. 2.2 we review the Bethe Ansatz description of the ground state and construct the excited states considered in Sec. 2.1, specifically identifying the thresholds of these continua. In Sec. 2.3 we calculate the threshold/edge behaviour for the associated excitations via the mobile impurity approach, fixing the coupling constants using the Bethe Ansatz to determine the finite-size corrections to the energy in the presence of the high-energy excitation.

2.1 Spectral representation of the current-current correlator

In considering the optical conductivity as defined in (2.5), the basic quantity of interest is

$$\langle GS|J_{j+\ell}(t)J_j(0)|GS\rangle = \sum_n \langle GS|J_{j+\ell}|n\rangle\langle n|J_j|GS\rangle e^{-i(E_n-E_{GS})t}, \tag{2.8}$$

where $\{|n\rangle\}$ constitute a complete set of energy eigenstates. To understand threshold behaviours, we wish to identify the states contributing to this sum. A crucial insight to this end are global continuous symmetries and their relation to the energy eigenstates provided by the exact Bethe Ansatz solution[62, 66, 128–130]. In the case of zero magnetic field and chemical potential, the Hubbard model possesses two independent

SU(2) symmetries[26, 131, 132]:

$$\begin{aligned} S^z &= \frac{1}{2}\sum_{i=1}^{L}(c^\dagger_{i,\uparrow}c_{i,\uparrow} - c^\dagger_{i,\downarrow}c_{i,\downarrow}), \qquad S^+ = \sum_{i=1}^{L} c^\dagger_{i,\uparrow}c_{i,\downarrow}, \qquad S^- = \sum_{i=1}^{L} c^\dagger_{i,\downarrow}c_{i,\uparrow}\ , \\ \eta^z &= \frac{1}{2}\sum_{i=1}^{L}(c^\dagger_{i,\uparrow}c_{i,\uparrow} + c^\dagger_{i,\downarrow}c_{i,\downarrow} - 1), \quad \eta^+ = \sum_{i=1}^{L}(-1)^i c^\dagger_{i,\downarrow}c^\dagger_{i,\uparrow}, \quad \eta^- = \sum_{i=1}^{L}(-1)^i c_{i,\uparrow}c_{i,\downarrow}. \end{aligned} \tag{2.9}$$

The S^α generate the well known spin rotational SU(2) symmetry, while the η^α are known as η-pairing generators. The Bethe Ansatz provides us with the *lowest weight states*[62], which we denote by $|LWS;\mathbf{m}\rangle$. Here $\mathbf{m}$ is a multi-index which labels all distinct regular Bethe Ansatz states in the sense of Ref. [62]. The states are lowest-weight with respect to the two SU(2) algebras in the sense that

$$\eta^-|LWS;\mathbf{m}\rangle = 0 = S^+|LWS;\mathbf{m}\rangle\ . \tag{2.10}$$

Each state $|LWS;\mathbf{m}\rangle$ is defined on a system of length L and has a well-defined number of electrons N and z-component of spin S_z. A complete basis of states is given by $\left\{(\eta^+)^k(S^-)^l|LWS;\mathbf{m}\rangle \mid k=0,\ldots,L-N;\ l=0,\ldots,2S^z\right\}$. For the repulsive Hubbard model below half-filling, the ground state in zero magnetic field and finite chemical potential is a spin singlet and a lowest-weight η-pairing state i.e.

$$S^-|GS\rangle = S^+|GS\rangle = \eta^-|GS\rangle = 0. \tag{2.11}$$

Using the algebra defined in (2.9) it is readily verified that $[\eta^-,[\eta^-,J_j]] = 0$ and therefore for integer $m \geq 0$

$$\langle LWS;\mathbf{n}|(\eta^-)^{m+1}J_j|GS\rangle = \langle LWS;\mathbf{n}|(\eta^-)^m[\eta^-,J_j]|GS\rangle = \delta_{m,0}\langle LWS;\mathbf{n}|[\eta^-,J_j]|GS\rangle. \tag{2.12}$$

This shows that the only states that may have a non-zero overlap with $J_j|GS\rangle$ are lowest weight states $|LWS;\mathbf{m}\rangle$ or η-pairing descendant states of the form $\eta^+|LWS;\mathbf{m}\rangle$, which implies the expansion

$$J_j|GS\rangle = \sum_{\mathbf{m}}\left(a_{\mathbf{m}}|LWS;\mathbf{m}\rangle + b_{\mathbf{m}}\eta^+|LWS;\mathbf{m}\rangle\right), \tag{2.13}$$

where $a_{\mathbf{m}}$, $b_{\mathbf{m}}$ are complex coefficients. Substituting this into (2.8) provides further constraints on the subset of energy eigenstates that may make non-vanishing contributions to the correlator. The subset consists of

1. Lowest-weight states with N_{GS} electrons with $\mathbf{S}^2 = S^z = 0$;

2. States of the form $\eta^+|LWS;\mathbf{m}\rangle$, with $|LWS;\mathbf{m}\rangle$ having $N_{GS}-2$ electrons and $\mathbf{S}^2 = S^z = 0$.

Using that $[H,\eta^+] = -2\mu\eta^+$ we can thus express the current-current correlator in the form

$$\begin{aligned} C_{\mathrm{JJ}}(\ell,t) &= \langle GS|J_{j+\ell}(t)J_j(0)|GS\rangle \\ &= \sum_{\mathbf{m}}\langle GS|J_{j+\ell}|LWS;\mathbf{m}\rangle\langle LWS;\mathbf{m}|J_j|GS\rangle e^{-i(E_{\mathbf{m}}-E_{GS})t} \\ &+ \sum_{\mathbf{m}}\frac{\langle GS|J_{j+\ell}\eta^+|LWS;\mathbf{m}\rangle\langle LWS;\mathbf{m}|\eta^- J_j|GS\rangle}{2\eta^z_{\mathbf{m}}} e^{-i(E_{\mathbf{m}}-E_{GS}-2\mu)t}. \end{aligned} \tag{2.14}$$

The factor of $(2\eta^z_{\mathbf{m}})^{-1}$ arises from the normalisation of the state $\eta^+|LWS,\mathbf{m}\rangle$. We note that $\mu < 0$ and hence -2μ is a positive energy shift. It is not obvious how to understand the second term in the framework of a mobile impurity model. However, using the lowest-weight property $\eta^-|GS\rangle = 0$, we can rewrite (2.14) in the form

$$\begin{aligned} C_{\mathrm{JJ}}(\ell,t) &= \sum_{\mathbf{m}}\langle GS|J_{j+\ell}|LWS;\mathbf{m}\rangle\langle LWS;\mathbf{m}|J_j|GS\rangle e^{-i(E_{\mathbf{m}}-E_{GS})t} \\ &+ \sum_{\mathbf{m}}\frac{1}{2\eta^z_{\mathbf{m}}}\langle GS|[J_{j+\ell},\eta^+]|LWS;\mathbf{m}\rangle\langle LWS;\mathbf{m}|[\eta^-,J_j]|GS\rangle e^{-i(E_{\mathbf{m}}-E_{GS}-2\mu)t}. \end{aligned} \tag{2.15}$$

The main advantage of the representation (2.15) is that it only involves regular Bethe Ansatz states, which can be constructed by standard methods. As we concern ourselves only with the threshold behaviours of the optical conductivity, we need only focus on the lower edges of the various excitation continua. As a consequence of kinematic constraints and matrix-element effects, processes with a small number of excitations above the ground state give the dominant contributions to response functions. Defining

$$\mathcal{O}_j = [\eta^-, J_j] = 2it(-1)^j\left(c_{j,\downarrow}c_{j+1,\uparrow} + c_{j+1,\downarrow}c_{j,\uparrow}\right), \tag{2.16}$$

we can recast (2.15) in the form

$$C_{\rm JJ}(\ell,t) = \sum_{\mathbf{m}} |\langle GS|J_j|LWS;\mathbf{m}\rangle|^2 e^{-i(E_{\mathbf{m}}-E_{GS})t+iP_{\mathbf{m}}\ell} + \sum_{\mathbf{m}} \frac{1}{2\eta^z_{\mathbf{m}}} |\langle GS|\mathcal{O}_j^\dagger|LWS;\mathbf{m}\rangle|^2 e^{-i(E_{\mathbf{m}}-E_{GS}-2\mu)t+i(P_{\mathbf{m}}-\pi)\ell} \equiv C^{(1)}_{\rm JJ}(\ell,t) + C^{(2)}_{\rm JJ}(\ell,t). \tag{2.17}$$

Here the additional contribution to the momentum arises because acting with η^+ shifts the momentum by π. If the ground state contains N fermions, the contribution $C^{(2)}_{\rm JJ}(\ell,t)$ is proportional to $1/(L-N+2)$, and can therefore be dropped in the thermodynamic limit away from half filling. However, as we are interested in densities close to one fermion per site it is useful to retain it in view of potential comparisons to numerical results for finite-size systems. The optical conductivity can then be written as

$$\sigma_1(\omega) = \frac{e^2}{2\omega}\left[\sum_{a=1}^{2}\sum_{\ell}\int_{-\infty}^{\infty} dt\; e^{i\omega t}\; C^{(a)}_{\rm JJ}(\ell,t) - \{\omega\to-\omega\}\right] \equiv \sum_{a=1}^{2}\sigma_1^{(a)}(\omega). \tag{2.18}$$

2.2 Bethe Ansatz for the Hubbard model

To gain further insight into the representation (2.17) we now construct the ground state and low-lying excitations above it. We first calculate the energy of such excitations in the thermodynamic limit. This will allow us to identify, on kinematic grounds, which states within the manifold identified earlier are important with respect to the threshold behaviours we aim to describe. We recapitulate some results from Ref. [26] to allow a self-contained discussion. The eigenstates of the Hubbard model can be expressed in terms of the roots of the Takahashi equations, as explained in Section 1.5.2, and the ground state is exhibited in Section 1.5.2.1, upon which we will build the excitations which can contribute to the optical conductivity. In the previously established notation, we denote the ground state defined by the integers of (1.52) by

$$|GS\rangle = |LWS;\{I_j\},\{J^1_\alpha\}\rangle. \tag{2.19}$$

2.2.0.1 Thermodynamic limit

On taking the thermodynamic limit at fixed density n_{GS} and magnetisation m_{GS} the roots of the Takahashi equation corresponding to the choice of integers in (1.52) become dense and we can describe the ground state in terms of root densities $\rho_{c,0}$, $\rho_{s,0}$, which satisfy linear integral equations[26]

$$\rho_{c,0}(k) = \frac{1}{2\pi} + \cos k \int_{-A}^{A} \mathrm{d}\Lambda\, a_1(\sin k - \Lambda)\rho_{s,0}(\Lambda), \tag{2.20}$$

$$\rho_{s,0}(\Lambda) = \int_{-Q}^{Q} \mathrm{d}k\, a_1(\Lambda - \sin k)\rho_{c,0}(k) - \int_{-A}^{A} \mathrm{d}\Lambda'\, a_2(\Lambda - \Lambda')\rho_{s,0}(\Lambda'). \tag{2.21}$$

Here $a_n(x) = \frac{2nu}{2\pi}\frac{1}{(nu)^2+x^2}$ and the integration boundaries Q and A are determined by

$$\int_{-Q}^{Q} \mathrm{d}k\, \rho_{c,0}(k) = n_{GS}, \qquad \int_{-A}^{A} \mathrm{d}\Lambda\, \rho_{s,0}(\Lambda) = \frac{1}{2}\left(n_{GS} - 2m_{GS}\right). \tag{2.22}$$

The energy density of the system is given to $o(1)$ by[26]

$$e_{GS} = \int_{-Q}^{Q} \frac{\mathrm{d}k}{2\pi}\varepsilon_c(k) + u, \tag{2.23}$$

where

$$\varepsilon_c(k) = -2\cos k - \mu - 2u - B + \int_{-A}^{A} \mathrm{d}\Lambda\, a_1(\sin k - \Lambda)\varepsilon_s(\Lambda), \tag{2.24}$$

$$\varepsilon_s(\Lambda) = 2B + \int_{-Q}^{Q} \mathrm{d}k\, \cos k\, a_1(\Lambda - \sin k)\varepsilon_c(k) - \int_{-A}^{A} \mathrm{d}\Lambda'\, a_2(\Lambda - \Lambda')\varepsilon_s(\Lambda'). \tag{2.25}$$

The dressed energies $\varepsilon_c(k)$ and $\varepsilon_s(\Lambda)$ satisfy $\varepsilon_c(\pm Q) = \varepsilon_s(\pm A) = 0$. The dressed momenta are given by[26]

$$p_c(k) = k + \int_{-A}^{A} \mathrm{d}\Lambda\, \rho_{s,0}(\Lambda)\theta\left(\frac{\sin k - \Lambda}{u}\right), \tag{2.26}$$

$$p_s(\Lambda) = \int_{-Q}^{Q} \mathrm{d}k\, \rho_{c,0}(k)\theta\left(\frac{\Lambda - \sin k}{u}\right) - \int_{-A}^{A} \mathrm{d}\Lambda'\, \rho_{s,0}(\Lambda')\theta\left(\frac{\Lambda - \Lambda'}{2u}\right). \tag{2.27}$$

2.2.1 Excitations contributing to $C^{(1)}_{\mathrm{JJ}}(\ell, t)$.

We now turn to excited states that contribute to the spectral representation (2.17) of $C^{(1)}_{\mathrm{JJ}}(\ell, t)$. These are lowest weight states of the spin and η-pairing SU(2) algebras with quantum numbers $N = N_{GS}$, $M = M_{GS}$.

2.2.1.1 "Particle-hole" excitation with $N = N_{GS}$, $M = M_{GS}$.

Creating a particle-hole excitation in the charge degrees of freedom yields a state with the same charge and spin quantum numbers as the ground state, but with a finite momentum and energy difference. The (half-odd) integers for this type of excitation are given by

$$I_j = \begin{cases} -\frac{N_{GS}+1}{2} + j + \Theta\left(-\frac{N_{GS}+1}{2} + j - I^h\right), & j = 1, \ldots, N_{GS}-1 \\ I^p, & j = N_{GS} \end{cases}, \tag{2.28}$$

$$J_\alpha = -\frac{M_{GS}+1}{2} + \alpha, \qquad \alpha = 1, \ldots, M_{GS}, \tag{2.29}$$

where $\Theta(x) = 1$ for $x \geq 0$ and 0 otherwise. The arrangement for these integers is shown in Fig. 2.1. This excitation is two-parametric and has an energy and momen-

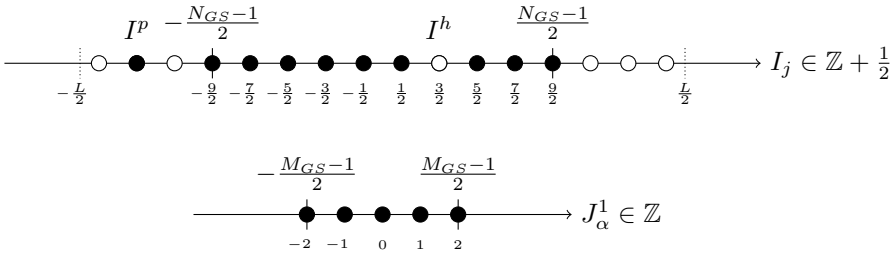

Figure 2.1: Configuration of the integers for the particle-hole excitation above the ground state, explicit numbers given are for $L = 16$, $N_{GS} = 10$, $M_{GS} = 5$

tum of the form

$$\begin{aligned} E &= e_{GS}L + \varepsilon_c(k^p) - \varepsilon_c(k^h) + o(1), \\ P &= p_c(k^p) - p_c(k^h) + o(1), \end{aligned} \tag{2.30}$$

where the rapidities are determined by $z_c(k^h) = \frac{2\pi I^h}{L}$, $z_c(k^p) = \frac{2\pi I^p}{L}$. This forms a continuum of excitations above the ground state, shown in Fig. 2.2.

2.2.1.2 "k-Λ string" excitation

We start by considering excitations with $N = N_{GS}$, $M = M_{GS}$ involving a single ("k-Λ string") bound state. This excitation has been considered previously e.g. in Section 7.7.2 of Ref. [26]. It involves having a single (half-odd) integer in the sector corresponding to the set $\{J'^1_\alpha\}$. The lowest-energy bound state which can be created

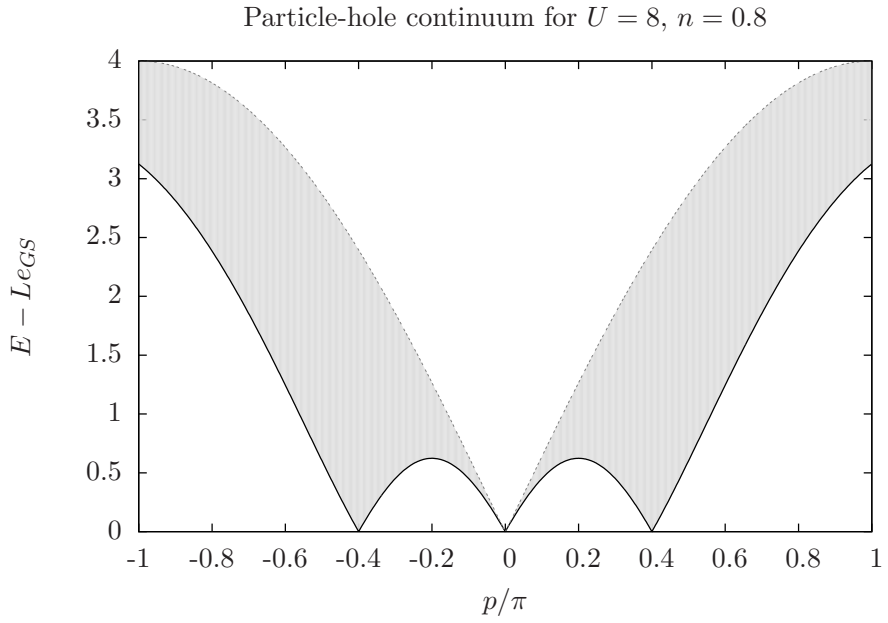

Figure 2.2: Particle-hole excitation continuum above the ground state

comprises of two ks and one Λ forming a string pattern in the complex plane. The Takahashi equations describe the real centres of these and other root patterns. The case we consider is realised by the integer configuration

$$I_j = -\frac{N_{GS}-2}{2} - \frac{1}{2} + j, \qquad j = 1, \ldots, N_{GS}-2, \tag{2.31}$$

$$J^1_\alpha = -\frac{M_{GS}-1}{2} - \frac{1}{2} + \alpha, \qquad \alpha = 1, \ldots, M_{GS}-1, \tag{2.32}$$

$$J'^1_\beta = J'^p, \qquad \beta = 1, \tag{2.33}$$

which is displayed in Fig. 2.3. In the notations used above, we can denote this excited state by $|LWS; \{I_j\}, \{J^1_\alpha\}, \{J'^1_\beta\}\rangle$. We can again take the thermodynamic limit and compare the energy of this excited state with that of the ground state. Following similar manipulations to the case of the ground state energy, the $\mathcal{O}(1)$ corrections can be calculated[26]. The energy is given by

$$E = Le_{\rm GS} + \varepsilon_{k\Lambda}(\Lambda^p) + o(1), \tag{2.34}$$

where

$$\varepsilon_{k\Lambda}(\Lambda) = 4{\rm Re}\sqrt{1-(\Lambda - iu)^2} - 2\mu - 4u + \int_{-Q}^{Q} dk \cos k \; a_1(\sin k - \Lambda)\; \varepsilon_c(k). \tag{2.35}$$

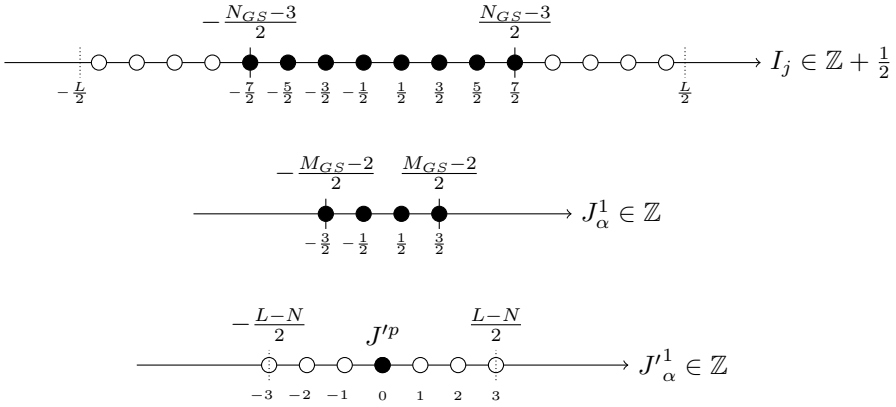

Figure 2.3: Configuration of the integers for the k-Λ string excited state

The momentum is given by $P = p_{k\Lambda}(\Lambda^p)$, where

$$p_{k\Lambda}(\Lambda') = -2\mathrm{Re}\arcsin(\Lambda' + iu) + \int_{-Q}^{Q} \mathrm{d}k\, \rho_{c,0}(k)\theta\left(\frac{\Lambda' - \sin k}{u}\right), \tag{2.36}$$

and Λ^p is determined by $z_1'(\Lambda^p) = \frac{2\pi J'^p}{L}$. This form can be readily interpreted physically as a particle-like excitation above the ground state. The k-Λ string dispersion describes the threshold of an excitation continuum obtained by adding e.g. particle-hole excitations in the charge sector. The dispersion relation for this excitation and the particle-hole continuum is shown in Fig. 2.4. The existence of such a continuum at $p = 0$ is necessary to understand the problem within the mobile impurity approach to threshold singularities.

2.2.2 Excitations contributing to $C^{(2)}_{\mathrm{JJ}}(\ell, t)$.

We now turn to excited states that contribute to the spectral representation (2.17) of $C^{(2)}_{\mathrm{JJ}}(\ell, t)$. As we have re-expressed $C^{(2)}_{\mathrm{JJ}}(\ell, t)$ in terms of matrix elements of the operator $\mathcal{O}_j^\dagger$ defined in (2.16), we will focus on excited states $|LWS; \mathbf{m}\rangle$ that have non-vanishing matrix elements $\langle GS|\mathcal{O}_j^\dagger|LWS; \mathbf{m}\rangle \neq 0$ These are lowest weight states of the spin and η-pairing SU(2) algebras and their quantum numbers are $N = N_{GS} - 2$, $M = M_{GS} - 1$. It is of course straightforward to translate back to excitations contributing to the original spectral representation (2.14): all that is required is to act with $\eta^\dagger$ on the states we discuss in the following.

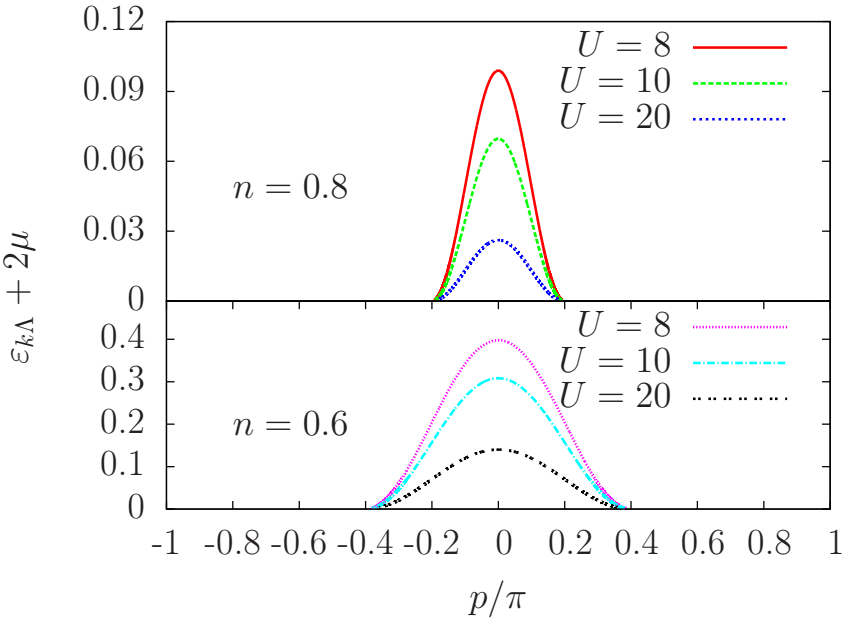

(a) Dispersion relation $\varepsilon_{k\Lambda}(\Lambda(p))$ for the k-Λ string for various U and n. Each curve has been shifted down by -2μ.

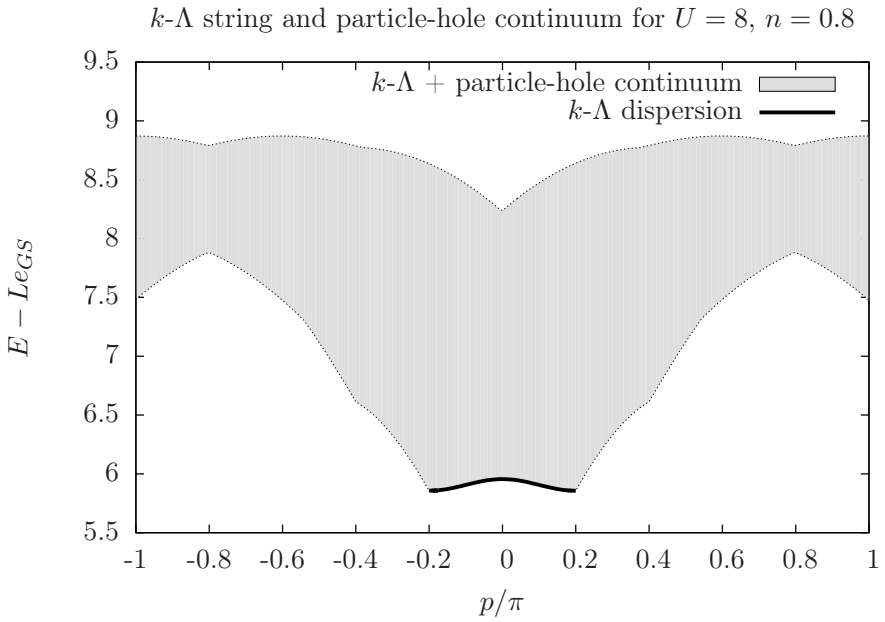

(b) k-Λ and charge particle-hole excitation continuum.

Figure 2.4: k-Λ string dispersion for various U and n, and particle-hole excitation continuum above this for $U = 8$, $n = 0.8$. For small momenta, the k-Λ string dispersion marks the lower edge of a continuum described by additional excitations e.g. particle-hole excitations in the charge sector.

2.2.2.1 "Particle-hole" excitation with $N = N_{GS} - 2$, $M = M_{GS} - 1$.

The integer configuration for this type of excitation is given by

$$I_j = \begin{cases} -\frac{N_{GS}}{2} + j + \Theta\left(\frac{-N_{GS}}{2} + j - I^h\right), & j = 1, \ldots, N_{GS} - 3 \\ I^p, & j = N_{GS} - 2 \end{cases}, \tag{2.37}$$

$$J_\alpha = -\frac{M_{GS}}{2} + \alpha, \qquad \alpha = 1, \ldots, M_{GS} - 1 \quad . \tag{2.38}$$

This is shown graphically in Fig. 2.5.

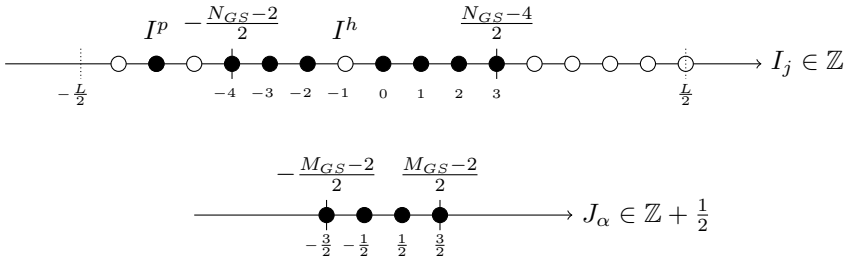

Figure 2.5: Integer configuration for the particle-hole excitation, explicit numbers for $L = 16$, $N_{GS} = 10$, $M_{GS} = 5$.

In complete analogy to the previous case, the energy and momentum of this state are given by

$$\begin{aligned} E &= L e_{\mathrm{GS}} + \varepsilon_c(k^p) - \varepsilon_c(k^h) + o(1), \\ P &= p_c(k^p) - p_c(k^h) \pm 2k_F + o(1), \end{aligned} \tag{2.39}$$

where k^p and k^h are determined by $z_c(k^p) = \frac{2\pi I^p}{L}$, $z_c(k^h) = \frac{2\pi I^h}{L}$. The contributions $\pm 2k_F$ arise from the asymmetry of the charge "Fermi sea", leaving a choice of two parity-related states. The continuum of excitations given by (2.39) is shown in Fig. 2.6, and consists of the union of two copies of the continuum depicted in Fig. 2.2 shifted by $\pm 2k_F$ respectively. We note that in order to make closer contact with the spectral representation (2.17) we have shifted the momentum by π.

2.2.2.2 "Two particle" excitation with $N = N_{GS} - 2$, $M = M_{GS} - 1$.

A closely related type of excitation corresponds to the choice of (half-odd) integers

$$I_j = \begin{cases} -\frac{N_{GS}-4}{2} + j, & j = 1, \ldots, N_{GS} - 4 \\ I^{p_1}, & j = N_{GS} - 3, \\ I^{p_2}, & j = N_{GS} - 2 \end{cases}, \tag{2.40}$$

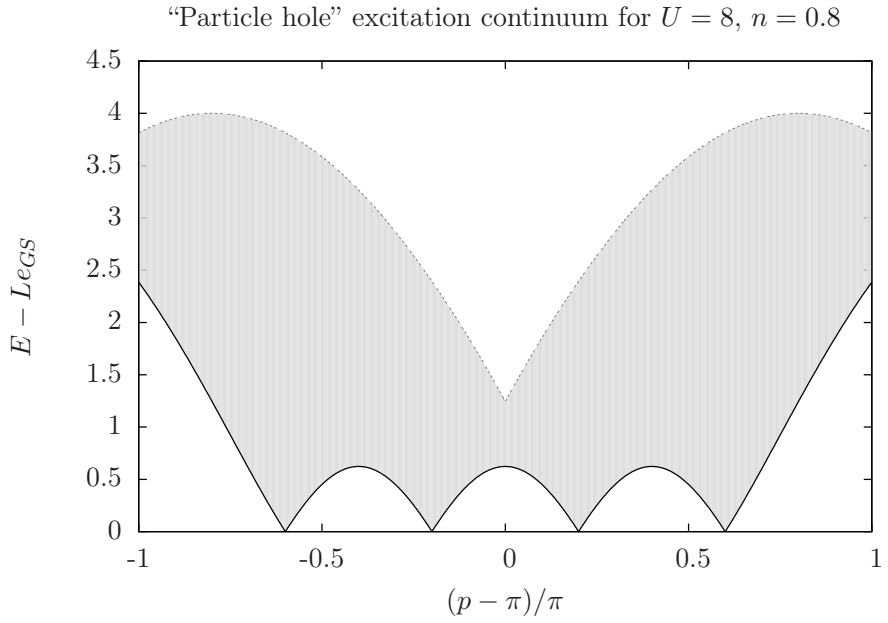

Figure 2.6: Continuum for particle-hole excitation with momentum shifted for clarity.

$$J_\alpha = -\frac{M_{GS}}{2} + \alpha, \qquad \alpha = 1, \ldots, M_{GS} - 1. \tag{2.41}$$

Such a configuration is shown in Fig. 2.7 and can be thought of as involving two particles associated with I^{p_1} and I^{p_2} respectively. The energy and momentum of this

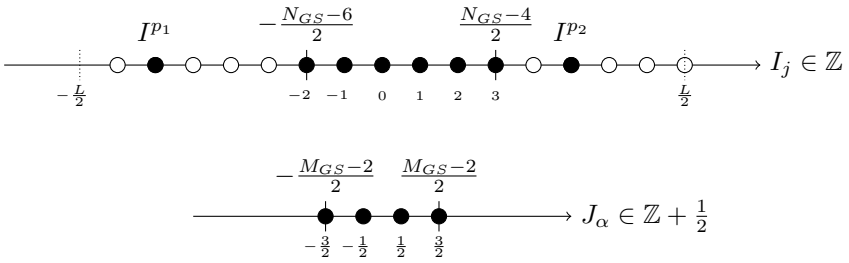

Figure 2.7: Integer configuration for the particle-particle excitation, explicit numbers for $L = 16$, $N_{GS} = 10$, $M_{GS} = 5$.

excitation are

$$\begin{aligned} E &= Le_{\mathrm{GS}} + \varepsilon_c(k^{p_1}) + \varepsilon_c(k^{p_2}) + o(1), \\ P &= p_c(k^{p_1}) + p_c(k^{p_2}) \pm 2k_F + o(1), \end{aligned} \tag{2.42}$$

with $z_c(k^{p_i}) = \frac{2\pi I^{p_i}}{L}$. The continua corresponding to (2.42) are shown in Fig. 2.8. We note that both possible choices $\pm 2k_F$ have been taken into account, and we have again

shifted the total momentum by π in order to make closer contact with the spectral representation (2.17) of our correlator.

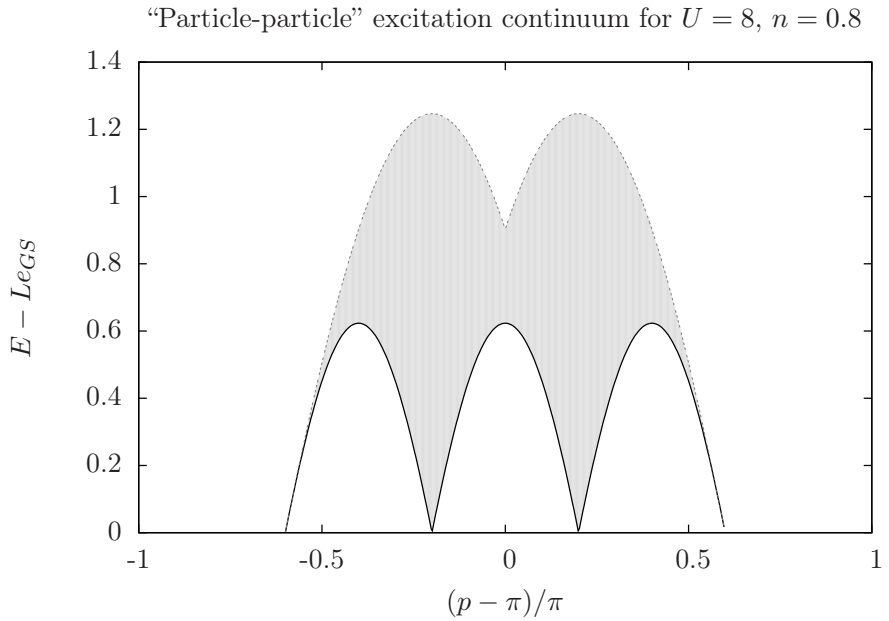

Figure 2.8: Continuum for particle-particle excitation with momentum shifted for clarity.

2.2.2.3 "Two hole" excitation with $N = N_{GS} - 2$, $M = M_{GS} - 1$.

Finally, we consider excitations characterised by the distribution of (half-odd) integers

$$\begin{aligned} I_j &= -\frac{N_{GS}}{2} + j + \Theta\left(-\frac{N_{GS}}{2} + j - I^{h_1}\right) \\ &\quad + \Theta\left(-\frac{N_{GS}}{2} + j - I^{h_2}\right), \qquad j = 1, \ldots, N_{GS} - 2, \\ J_\alpha &= -\frac{M_{GS}}{2} + \alpha, \qquad \alpha = 1, \ldots, M_{GS} - 1, \end{aligned} \tag{2.43}$$

which is displayed in Fig. 2.9. We see that these states can be viewed as involving two holes associated with I^{h_1} and I^{h_2} respectively. The energy and momentum of this excitation are given by

$$\begin{aligned} E &= Le_{\rm GS} - \varepsilon_c(k^{h_1}) - \varepsilon_c(k^{h_2}) + o(1), \\ P &= -p_c(k^{h_1}) - p_c(k^{h_2}) \pm 2k_F + o(1), \end{aligned} \tag{2.44}$$

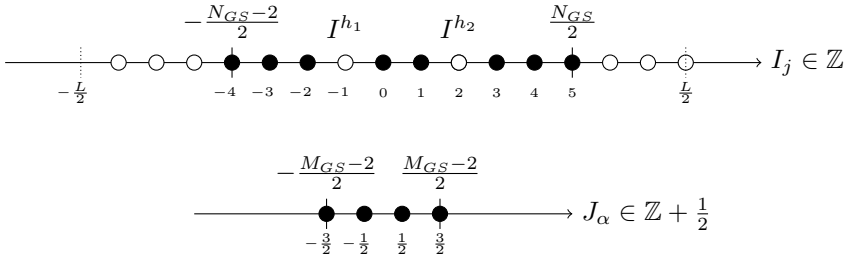

Figure 2.9: Integer configuration for two hole excited state, explicit numbers for $L = 16$, $N_{GS} = 10$, $M_{GS} = 5$.

with $z_c(k^{h_i}) = \frac{2\pi I^{h_i}}{L}$. The continua for these excitations are shown in Fig. 2.10, where we have taken both possible choices of $\pm 2k_F$ into account and we again have shifted the total momentum by π in order to make closer contact with the spectral representation (2.17) of our correlator.

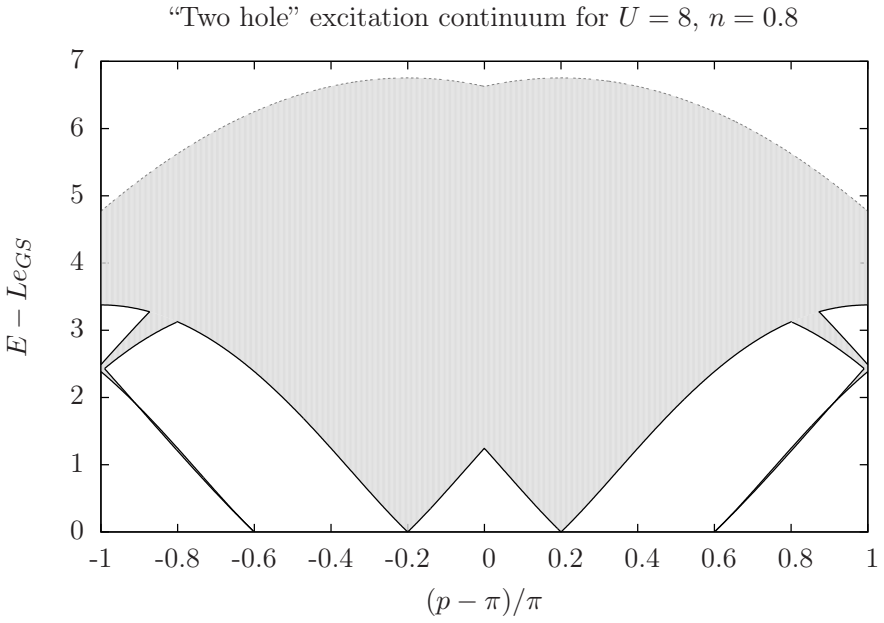

Figure 2.10: Continuum for two hole excitation with momentum shifted for clarity.

2.2.3 Excitation thresholds at commensurate fillings

By considering additional excitations around the "Fermi points" in the charge sector we can construct other excitations that are degenerate in energy (to $o(1)$), but differ in

their momenta by integer multiples of $4k_F$. As we consider the case of zero magnetic field, there is no freedom to rearrange the integers in the spin sector that leads to a lower energy for a given momentum. In this way we can determine the thresholds for a given class of excited states.

1. The absolute threshold is obtained by combining the particle-hole excitation of Sec. 2.2.1.1 with zero-energy particle-hole excitations at the "Fermi points" in the charge sector, which shift the momentum by multiples of $4k_F$. It is depicted by a dashed red line in Fig. 2.11. At zero momentum, the relevant value for the optical conductivity, the absolute threshold occurs at zero energy. At low energies the optical conductivity is dominated by particle-hole excitations. Close to half-filling, the spectral weight of this contribution is small and tends to zero for $n \to 1$. In the vicinity of half-filling most of the spectral weight concomitantly occurs above a "pseudo-gap" that is close in value to the Mott gap of the half-filled system.

2. Above an energy scale that tends to the Mott gap as the band filling approaches one from below, excitations involving a single k-Λ string of length two exist. Their threshold is shown as a dashed black line in Fig. 2.11. Precisely at half filling these excitations do not contribute to the optical conductivity [25, 26, 118] as a result of the enhanced symmetry: at half filling this excitation describes a singlet of the η-pairing SU(2) algebra and does not contribute to $\sigma_1(\omega)$.

3. For band fillings close to $n = 1$ there are other excitations of the form $\eta^+|LWS, \mathbf{m}\rangle$ that contribute to the optical conductivity. At half-filling these are the only states contributing to $\sigma_1(\omega)$ in the frequency regime $2\Delta \leq \omega \leq 4\Delta$, where Δ is the Mott gap. Below half-filling, their contribution to $\sigma_1(\omega)$ can be cast in the form of $C^{(2)}_{\mathrm{JJ}}(\ell, t)$ in (2.17), and the states to be considered are then given by Sec. 2.2.2.1, 2.2.2.2 and 2.2.2.3.

The thresholds shown in Fig. 2.11 are at a high commensurability: $5(4k_F) = 8\pi$. We note that thresholds involving high-order umklapp processes are suppressed in

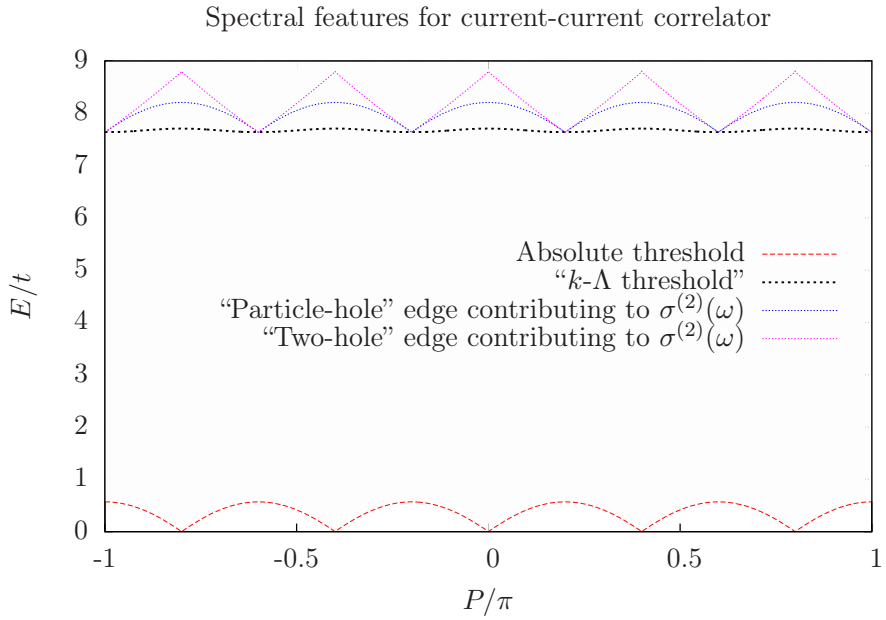

Figure 2.11: The continuum of lowest-lying excitations of the Hubbard model involving only the charge sector for $n = 0.8$, $U = 10$. As the optical conductivity is defined at zero momentum, only the features encountered at $P = 0$ are relevant. The k-Λ string dispersion defines the lower edge of a continuum of excitations involving the k-Λ string. The contributions to $\sigma^{(2)}(\omega)$ are shifted by -2μ, in accordance with the spectral representation (2.17).

$\sigma_1(\omega)$, cf. Refs. [98, 100, 101]. Analytic forms for the "high-energy" thresholds are given below in eqns (2.52), (2.214) and (2.231). These results show that the contributions from $\sigma^{(2)}(\omega)$ do not constitute the "pseudo-gap threshold", and moreover are suppressed by a factor $1/L$ as we have pointed out before. Hence they do not play an important role in the initial growth of $\sigma_1(\omega)$, even for finite-size systems, and we therefore relegate their discussion to Appendix 2.F.

2.3 Mobile impurity approach to threshold singularities

Our goal is to determine the behaviour of the optical conductivity in the metallic phase of the Hubbard model close to half-filling above the excitation thresholds occurring in the vicinity of the Mott gap at $n = 1$. This can be achieved by following the

mobile impurity approach to the Hubbard chain set out in Ref. [59]. In the main cases of interest to us here, the mobile impurity model describes low-energy degrees of freedom in the presence of a single high-energy excitation with momentum q and takes the general form

$$H = H_{\rm LL} + H_{\rm imp} + H_{\rm int}, \tag{2.45}$$

$$H_{\rm LL} = \int dx \Big[\sum_{\alpha=c,s} \frac{v_\alpha}{16\pi} \left(\frac{1}{2K_\alpha} \big(\partial_x \Phi^*_\alpha\big)^2 + 2K_\alpha \big(\partial_x \Theta^*_\alpha\big)^2 \right) \Big], \tag{2.46}$$

$$H_{\rm imp} = \int {\rm d}x\, B^\dagger(x) \left[\epsilon(q) - i\epsilon'(q)\partial_x - \frac{1}{2}\epsilon''(q)\partial_x^2 \right] B(x)\ , \tag{2.47}$$

$$H_{\rm int} = \int dx\ B^\dagger(x) B(x) \left[f_\alpha(q)\partial_x \varphi^*_\alpha(x) + \bar{f}_\alpha(q)\partial_x \bar{\varphi}^*_\alpha(x) \right] + \dots\ . \tag{2.48}$$

Here $v_{c,s}$ and $K_{c,s}$ are respectively the velocities and Luttinger parameters of low-energy collective spin and charge degrees of freedom, $\varphi^*_{c,s}$, $\bar{\varphi}^*_{c,s}$ are chiral charge and spin Bose fields, and

$$\Phi^*_\alpha = \varphi^*_\alpha + \bar{\varphi}^*_\alpha\ , \quad \Theta^*_\alpha = \varphi^*_\alpha - \bar{\varphi}^*_\alpha\ , \qquad \alpha = c, s. \tag{2.49}$$

The high-energy excitation under consideration has a "bare" dispersion $\epsilon(q)$ and is described in terms of the field $B(x)$. Finally, the functions $f_{c,s}(q)$ and $\bar{f}_{c,s}(q)$ parametrise the interactions between the high-energy excitation and the low-energy degrees of freedom. Our Bose fields are related to the usual spin and charge bosons[40, 41] by a canonical transformation

$$\Phi_\alpha = \frac{\Phi^*_\alpha}{\sqrt{2}}\ , \quad \Theta_\alpha = \sqrt{2}\Theta^*_\alpha\ , \tag{2.50}$$

and were introduced in Ref. [59] by bosonising the physical fermionic spin and charge excitations in the Hubbard model. The form of $H_{\rm int}$ is fixed by symmetry considerations and assuming the high-energy excitation to be a point-like object. Within the mobile impurity model the current operator is represented as

$$J_j \to B^\dagger(x)\mathcal{O}_{\rm LL}(x), \tag{2.51}$$

where $\mathcal{O}_{\rm LL}(x)$ is an operator acting in the Luttinger liquid sector of the model (2.48) only. In order to fully specify our problem we proceed as follows:

1. The spin and charge velocities and Luttinger parameters are determined directly from the exact solution of the Hubbard model, see Appendix 2.A for a brief summary.

2. The relevant ("dressed") dispersion relations for the various excitations we need to consider have already been determined above in section 2.2.

3. For a given threshold, the projection $\mathcal{O}_{\mathrm{LL}}$ of the current operator onto the Luttinger liquid sector is determined by bosonisation/refermionisation techniques. This is done in sections 2.3.1.1, 2.F.1.1 and 2.F.2.1 below.

4. Finally, the interaction parameters $f_{c,s}(q)$, $\bar{f}_{c,s}(q)$ are determined in sections 2.3.1.4, 2.F.1.4 and 2.F.2.4 by comparing finite-size corrections to excitation energies in the Hubbard model and the mobile impurity model (2.45).

2.3.1 k-Λ threshold in $\sigma^{(1)}(\omega)$

This threshold is obtained when the entire $\mathcal{O}(1)$ contribution to the excitation energy and momentum are carried by the k-Λ string. The functional form of the threshold is

$$\begin{aligned} E^{k\text{-}\Lambda}_{\mathrm{thres}}(q) &= \varepsilon_{k\Lambda}\big(\Lambda(q)\big), \\ q &= -2\,\mathrm{Re}\,\arcsin(\Lambda+iu) + \int_{-Q}^{Q} dk\,\theta\left(\frac{\Lambda-\sin k}{u}\right)\rho_{c,0}(k), \end{aligned} \tag{2.52}$$

where $\rho_{c,0}(k)$ is the ground state root density (2.20). It important to note that in the case relevant for the optical conductivity the k-Λ string sits at $q = 0$, which corresponds to a *maximum* of $\varepsilon_{k\Lambda}(\Lambda)$. The mobile impurity Hamiltonian appropriate for the description of this case is therefore of the form

$$H_{\mathrm{imp}} = \int \mathrm{d}x\, B^\dagger(x)\left(\epsilon(0) - \frac{1}{2}\epsilon''(0)\partial_x^2\right)B(x), \tag{2.53}$$

where $\epsilon''(0) < 0$. We note that by virtue of the interactions between the mobile impurity and the Luttinger liquid degrees of freedom, the bare dispersion $\epsilon(q)$ is differs from the actual threshold $\varepsilon_{k\Lambda}\big(\Lambda(q)\big)$. The relationship between the two quantities is established below. The threshold $\varepsilon_{k\Lambda}(0)$ is shown in Fig. 2.12 for various U and n

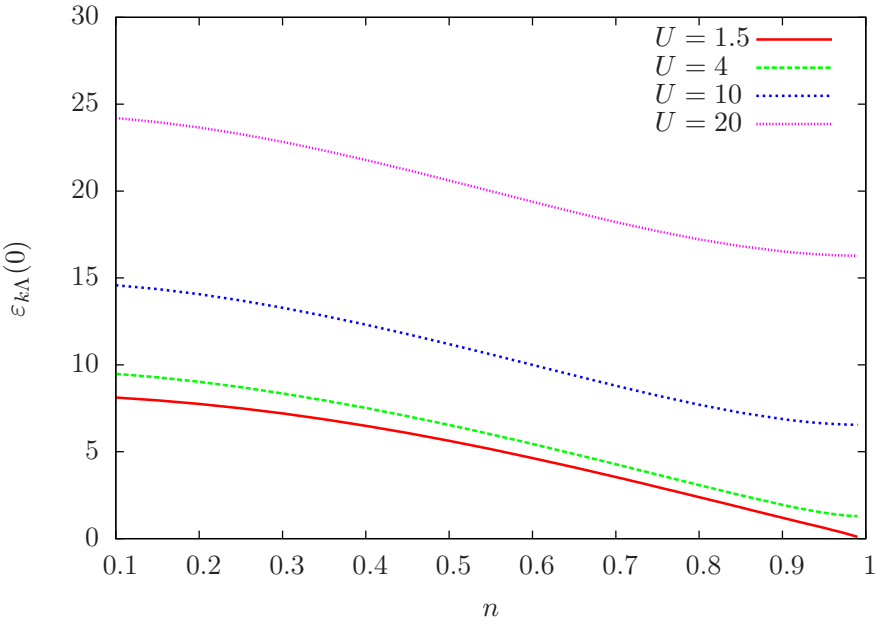

Figure 2.12: The threshold of the k-Λ string $\varepsilon_{k\Lambda}(0)$ is shown for various U and n

2.3.1.1 Projection of the current operator

Having identified the state involving the k-Λ string as contributing to $\sigma_1^{(1)}(\omega)$, we wish to project the current operator (2.6) onto the operators involved in the mobile impurity model. To this end we introduce the Hubbard projection operators[26], defined on site j as

$$X_j^{ab} := |a\rangle_{jj}\langle b|, \qquad a, b = 0, \uparrow, \downarrow, 2\,(\uparrow\downarrow). \tag{2.54}$$

The current operator is expressed in terms of the X_j^{ab} as

$$J_j = -it \sum_\sigma \left(\sigma X_j^{2\bar{\sigma}} + X_j^{\sigma 0}\right)\left(\sigma X_{j+1}^{\bar{\sigma}2} + X_{j+1}^{0\sigma}\right) - \left(\sigma X_{j+1}^{2\bar{\sigma}} + X_{j+1}^{\sigma 0}\right)\left(\sigma X_j^{\bar{\sigma}2} + X_j^{0\sigma}\right). \tag{2.55}$$

In order to proceed further, we now consider the large-U limit, in which the k-Λ string corresponds to a doubly-occupied site. The current operator J can be decomposed into three terms: a piece which increases the double occupancy by one (J^+), a piece which decreases it by one (J^-) and a piece that leaves the double occupancy unchanged (J^0) i.e.

$$J_j = J_j^+ + J_j^- + J_j^0 \ . \tag{2.56}$$

As we are concerned with creating an excitation involving double-occupation, we are interested in J_j^+ only. This is given by

$$J_j^+ = -it \sum_\sigma \sigma X_j^{2\bar{\sigma}} X_{j+1}^{0\sigma} - \sigma X_{j+1}^{2\bar{\sigma}} X_j^{0\sigma}, \tag{2.57}$$

and can be suggestively rewritten as

$$J_j^+ = -it \left[X_j^{20} \left(X_j^{0\downarrow} X_{j+1}^{0\uparrow} - X_j^{0\uparrow} X_{j+1}^{0\downarrow} \right) - X_{j+1}^{20} \left(X_{j+1}^{0\downarrow} X_j^{0\uparrow} - X_{j+1}^{0\uparrow} X_j^{0\downarrow} \right) \right]. \tag{2.58}$$

As, in the large-U limit, a k-Λ string corresponds to a doubly occupied site, while the ground state has zero double occupancy, we can identify the operator creating the k-Λ string as $B^\dagger(x) \sim X_j^{20}$. This allows us to recast J^+ in the form

$$\begin{aligned} J_j^+ \sim -it \left[B_j^\dagger - B_{j+1}^\dagger \right] \Big(& c_{j,\downarrow} c_{j+1,\uparrow} \left(1 - n_{j,\uparrow} \right) \left(1 - n_{j+1,\downarrow} \right) \\ & - c_{j,\uparrow} c_{j+1,\downarrow} \left(1 - n_{j,\downarrow} \right) \left(1 - n_{j+1,\uparrow} \right) \Big). \end{aligned} \tag{2.59}$$

In order to complete the projection of the current operator onto the mobile impurity model we simply bosonise all remaining electron operators. The final result is

$$J_{k\Lambda}(x) \sim \left(\partial_x B^\dagger(x) \right) e^{-i\Theta_c^*(x)/\sqrt{2}} \sin\left(\frac{\Phi_s^*}{2\sqrt{2}} \right) + \dots \tag{2.60}$$

2.3.1.2 Finite-size corrections to excitation energies in the mobile impurity model

Energies of excited states in the mobile impurity model in a large, finite volume can be calculated following Refs. [55, 59]. The chiral spin and charge Bose fields have mode expansions

$$\varphi_\alpha^*(x) = \varphi_{\alpha,0}^* + \frac{x}{L} Q_\alpha^* + \sum_{n=1}^{\infty} \sqrt{\frac{2}{n}} \left[e^{i\frac{2\pi n}{L}x} a_{\alpha,R,n} + e^{-i\frac{2\pi n}{L}x} a_{\alpha,R,n}^\dagger \right], \tag{2.61}$$

$$\bar{\varphi}_\alpha^*(x) = \bar{\varphi}_{\alpha,0}^* + \frac{x}{L} \bar{Q}_\alpha^* + \sum_{n=1}^{\infty} \sqrt{\frac{2}{n}} \left[e^{-i\frac{2\pi n}{L}x} a_{\alpha,L,n} + e^{i\frac{2\pi n}{L}x} a_{\alpha,L,n}^\dagger \right]. \tag{2.62}$$

Here Q_α^*, $\bar{Q}_\alpha^*$, $\varphi_{\alpha,0}$, $\bar{\varphi}_{\alpha,0}$ are zero-mode operators, obeying the commutation relations

$$[\varphi_{\alpha,0}^*, Q_\alpha^*] = -[\bar{\varphi}_{\alpha,0}^*, \bar{Q}_\alpha^*] = -4\pi i. \tag{2.63}$$

The eigenvalues q_α, $\bar{q}_\alpha$ of the operators Q^*_α, $\bar{Q}^*_\alpha$ depend on the boundary conditions of the fields $\varphi^*_\alpha(x)$, $\bar{\varphi}^*_\alpha(x)$. These boundary conditions are, crucially, influenced by the presence of a mobile impurity: coupling the impurity to the Luttinger liquid will change the boundary conditions and therefore modify the eigenvalue spectrum, causing a shift in the $\mathcal{O}(L^{-1})$ spectrum. It is precisely this relationship that will allow us to determine the coupling constants by examining the finite-size spectrum of the Hubbard model in the presence of a high-energy excitation. An important distinction from previous calculations is that the dispersion of the mobile impurity is quadratic in our case and has negative curvature.

The interactions between the impurity and the LL degrees of freedom in (2.45) can be removed by a unitary transformation of the form [49, 59]

$$U = e^{-i\int_{-\infty}^{\infty} dx \ \sum_\alpha (\gamma_\alpha \varphi^*_\alpha(x) + \bar{\gamma}_\alpha \bar{\varphi}^*_\alpha(x)) B^\dagger(x) B(x)}. \tag{2.64}$$

The transformed fields are given by

$$\begin{aligned}
\varphi^\circ_\alpha &= U\varphi^*_\alpha U^\dagger = \varphi^*_\alpha(x) - 2\pi\gamma_\alpha C(x), \\
\bar{\varphi}^\circ_\alpha &= U\bar{\varphi}^*_\alpha U^\dagger = \bar{\varphi}^*_\alpha(x) + 2\pi\bar{\gamma}_\alpha C(x), \\
\widetilde{B}(x) &= UB(x)U^\dagger = B(x) e^{i\sum_\alpha(\gamma_\alpha\varphi^*_\alpha(x) + \bar{\gamma}_\alpha\bar{\varphi}^*_\alpha(x))} e^{-i\pi\sum_\alpha(\gamma^2_\alpha - \bar{\gamma}^2_\alpha)C(x)},
\end{aligned} \tag{2.65}$$

where

$$C(x) = \int_{-\infty}^{\infty} \mathrm{d}y \, \mathrm{sgn}(x-y) B^\dagger(y) B(y). \tag{2.66}$$

By choosing the parameters γ_α, $\bar{\gamma}_\alpha$ to fulfil

$$\begin{pmatrix} f_\alpha \\ \bar{f}_\alpha \end{pmatrix} = \begin{pmatrix} -v^+_\alpha & -v^-_\alpha \\ v^-_\alpha & v^+_\alpha \end{pmatrix} \begin{pmatrix} \gamma_\alpha \\ \bar{\gamma}_\alpha \end{pmatrix}, \qquad v^\pm_\alpha = \frac{v_\alpha}{2}\left(2K_\alpha \pm \frac{1}{2K_\alpha}\right), \tag{2.67}$$

we find that, retaining only the most relevant terms, the impurity decouples in the new basisi.e.

$$\begin{aligned}
H = &\int \mathrm{d}x \left[\sum_{\alpha=c,s} \frac{v_\alpha}{16\pi}\left(\frac{1}{2K_\alpha}\left(\partial_x \Phi^\circ_\alpha\right)^2 + 2K_\alpha\left(\partial_x\Theta^\circ_\alpha\right)^2\right)\right] \\
&+ \int \mathrm{d}x \, \widetilde{B}^\dagger(x)\left[\widetilde{\epsilon}(q) - \frac{1}{2}\widetilde{\epsilon}''(q)\partial_x^2\right]\widetilde{B}(x) + \ldots.
\end{aligned} \tag{2.68}$$

We note that the "dressed" impurity dispersion for momenta $k \approx q$ is $\widetilde{\epsilon}(q) - \frac{1}{2}\widetilde{\epsilon}''(q)(k-q)^2$ and differs from its "bare" value $\epsilon(k)$ by a constant[1]. Importantly, it is the *dressed* dispersion that relates directly to the Bethe Ansatz result for $E^{k\text{-}\Lambda}_{\text{thres}}(k)$ in (2.52). In the decoupled theory of (2.68) it is a straightforward matter to calculate the spectrum of *low-energy* excitations above the ground state in the presence of an impurity. The result is[59]

$$\begin{aligned}\Delta E_{LL} = \sum_{\alpha=c,s} \frac{2\pi v_\alpha}{L} \Bigg[& \frac{1}{4K_\alpha}\left(\frac{q_\alpha + \bar{q}_\alpha}{4\pi} - \gamma_\alpha + \bar{\gamma}_\alpha\right)^2 \\ & + K_\alpha \left(\frac{q_\alpha - \bar{q}_\alpha}{4\pi} - \gamma_\alpha - \bar{\gamma}_\alpha\right)^2 + \sum_{n>0} n\left[M^+_{n,\alpha} + M^-_{n,\alpha}\right]\Bigg].\end{aligned} \tag{2.69}$$

Here $M^\pm_{n,\alpha}$ are non-negative integers corresponding to particle-hole excitations at the edge of the "Fermi seas". Any operator acting on the ground state will, in general, produce a superposition of energy eigenstates. Noting that the ground state is annihilated by Q^*_α, $\bar{Q}^*_\alpha$, the state $\mathcal{O}(x)|GS\rangle$ has well-defined quantum numbers $q^{(0)}_\alpha$, $\bar{q}^{(0)}_\alpha$ if $\mathcal{O}(x)$ satisfies the relations

$$[Q^*_\alpha, \mathcal{O}(x)] = q^{(0)}_\alpha \mathcal{O}(x), \qquad [\bar{Q}^*_\alpha, \mathcal{O}(x)] = \bar{q}^{(0)}_\alpha \mathcal{O}(x). \tag{2.70}$$

If the operator satisfies such a property then all states in the superposition defined by $\mathcal{O}(x)|GS\rangle$ must have the *same* q_α, $\bar{q}_\alpha$, namely $q^{(0)}_\alpha$, $\bar{q}^{(0)}_\alpha$. The only difference in the energies comes from having different $M^\pm_{n,\alpha}$. We can therefore identify the "minimal" excitation[59]: this is the state with all $M^\pm_{n,\alpha} = 0$ i.e. no particle-hole excitations. For the specific case of interest here, namely acting with the projected current operator $J_{k\Lambda}(x)$ on the ground state, this can be represented pictorially as

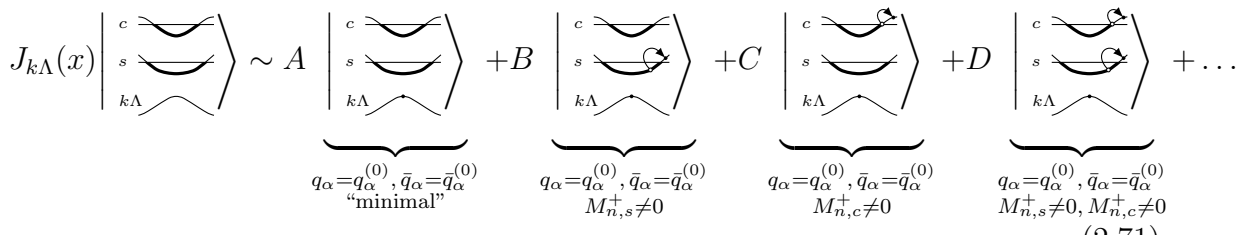

(2.71)

[1] In such a case, the difference between $\varepsilon(q)$ and $\tilde{\varepsilon}(q)$ is simply a constant shift of $\sum_\alpha \pi v_\alpha \left(\frac{(\gamma_\alpha - \bar{\gamma}_\alpha)^2}{2K_\alpha} + 2K_\alpha(\gamma_\alpha + \bar{\gamma}_\alpha)^2\right)$.

From the bosonised expression for $J_{k\Lambda}(x)$, and focussing only on the $e^{i\Phi_s^*/2\sqrt{2}}$ term with the other following from parity, it follows that

$$q_c^{(0)} = \bar{q}_c^{(0)} = 2\pi\sqrt{2}; \qquad q_s^{(0)} = -\bar{q}_s^{(0)} = -\pi\sqrt{2}. \tag{2.72}$$

The total momentum can also be calculated using the mode expansion, and is found to be of the form

$$\begin{aligned} P = &\frac{k_F}{\pi\sqrt{2}}\left(\bar{q}_c - q_c\right) + P_{\text{imp}}(k_L^p) \\ &+ \frac{2\pi}{L}\sum_{\alpha=c,s}\left[\left(\frac{q_\alpha + \bar{q}_\alpha}{4\pi} - \gamma_\alpha + \bar{\gamma}_\alpha\right)\left(\frac{q_\alpha - \bar{q}_\alpha}{4\pi} - \gamma_\alpha - \bar{\gamma}_\alpha\right) + \left(N_\alpha^+ - N_\alpha^-\right)\right], \end{aligned} \tag{2.73}$$

where k_L^p includes finite-size shifts to the rapidity k^p. We can identify the "minimally excited" state with the Bethe Ansatz excitation at the relevant threshold. By matching the expressions for the finite-size energies, we will be able to constrain the parameters γ_α, $\bar{\gamma}_\alpha$.

2.3.1.3 Finite-size corrections to excitation energies from Bethe Ansatz

Finite-size corrections to the energies of states involving both high- and low-energy excitations can be determined from the Bethe Ansatz solution of the Hubbard model following Ref. [68]. The details for the excitations of interest here involving a k-Λ string are given in Appendix 2.B. The final result for zero magnetic field and total momentum $P = \mathcal{O}(L^{-1})$ is

$$\begin{aligned} E = &e_{GS}L + \varepsilon_{k\Lambda}(0) - \frac{\pi}{6L}(v_c + v_s) \\ &+ \frac{2\pi v_c}{L}\left[\frac{(\Delta N_c - N_c^{\text{imp}})^2}{8K_c} + 2K_c\left(D_c - D_c^{\text{imp}} + \frac{D_s - D_s^{\text{imp}}}{2}\right)^2\right] \\ &+ \frac{2\pi v_s}{L}\left[\frac{1}{2}\left(\Delta N_s - \frac{\Delta N_c}{2}\right)^2 + \frac{(D_s - D_s^{\text{imp}})^2}{2}\right]. \end{aligned} \tag{2.74}$$

Here e_{GS} is the ground state energy per site in the thermodynamic limit, while $\varepsilon_{k\Lambda}(0)$ is the contribution due to the (high-energy) k-Λ string excitation and is obtained

from the solution of the integral equations

$$\begin{aligned}\varepsilon_{k\Lambda}(\Lambda) &= 4\mathrm{Re}\sqrt{1-(\Lambda-iu)^2} - 2\mu - 4u + \int_{-Q}^{Q} \mathrm{d}k\, \cos k\, a_1(\sin k - \Lambda)\, \varepsilon_c(k), \\ \varepsilon_c(k) &= -2\cos k - \mu - 2u + \int_{-Q}^{Q} \mathrm{d}k'\, \cos k'\, R(\sin k - \sin k')\varepsilon_c(k'),\end{aligned} \tag{2.75}$$

where the function $R(x)$ is given by

$$R(x) = \int_{-\infty}^{\infty} \frac{d\omega}{2\pi} \frac{e^{i\omega x}}{1+\exp(2u|\omega|)}. \tag{2.76}$$

The spin and charge velocities $v_{s,c}$ and the Luttinger parameter K_c are given in Appendix 2.A, while the quantities N_c^{imp} and $D_{c,s}^{\mathrm{imp}}$ are given by

$$D_c^{\mathrm{imp}} = 0, \quad D_s^{\mathrm{imp}} = 0\ , \quad N_c^{\mathrm{imp}} = \int_{-Q}^{Q} \mathrm{d}k\, \rho_{c,1}(k), \tag{2.77}$$

where

$$\rho_{c,1}(k) = \cos k\, a_1(\sin k - \Lambda'^p) + \cos k \int_{-Q}^{Q} dk'\, \rho_{c,1}(k') R(\sin k - \sin k'). \tag{2.78}$$

Finally, the quantities ΔN_c, ΔN_s, D_c and D_s characterise low-energy excitations of the spin and charge degrees of freedom and for the "minimal" excitation of interest are given by

$$\Delta N_c = -2\ , \quad D_c = 0\ , \quad \Delta N_s = -1\ , \quad D_s = 0. \tag{2.79}$$

We note that in order to fully specify the mobile impurity model we require the value of the curvature of the impurity dispersion at its maximum. This is given by

$$\frac{1}{m} = \left.\frac{\partial^2 \varepsilon_{k\Lambda}(\Lambda)}{\partial p^2}\right|_{\Lambda=0} = \frac{\varepsilon''_{k\Lambda}(0)}{(2\pi\sigma_1'^h(0))^2}, \tag{2.80}$$

where

$$\begin{aligned}\varepsilon''_{k\Lambda}(0) &= -\frac{4}{(1+u^2)^{3/2}} - \int_{-Q}^{Q} \mathrm{d}k\, a_1'(\sin k)\varepsilon_c'(k), \\ 2\pi\sigma_1'^h(0) &= \frac{2}{\sqrt{1+u^2}} - 2\pi \int_{-Q}^{Q} \mathrm{d}k\, a_1(\sin k)\rho_{c,0}(k).\end{aligned} \tag{2.81}$$

The total momentum of the state of interest can also be calculated from the Bethe Ansatz and for the case of interest results in

$$\begin{aligned}P = {} & q_L + 2k_F(2D_c + D_s) \\ & + \frac{2\pi}{L} \sum_{\alpha=c,s} \left[(\Delta N_\alpha - N_\alpha^{\mathrm{imp}})(D_\alpha - D_\alpha^{\mathrm{imp}}) + (N_\alpha^+ - N_\alpha^-)\right],\end{aligned} \tag{2.82}$$

with q_L the contribution, including finite-size shifts of the rapidities, from the high-energy impurity and $N_\alpha^\pm$ are integers corresponding to particle-hole pairs at the edge of the "Fermi seas". The method used for deriving this result is summarised in Appendix 2.E.

2.3.1.4 Fixing the parameters γ_α, $\bar{\gamma}_\alpha$

By equating the Bethe Ansatz results (2.74) and (2.82) for energy and momentum with the ones obtained in the framework of the mobile impurity model (2.69), (2.73) we can fix the parameters γ_α, $\bar{\gamma}_\alpha$ to be

$$\gamma_c = -\bar{\gamma}_c = \frac{1}{\sqrt{2}} + \frac{(\Delta N_c - N_c^{\rm imp})}{2\sqrt{2}}; \qquad \gamma_s = \bar{\gamma}_s = -\frac{1}{2\sqrt{2}}. \tag{2.83}$$

2.3.1.5 Current-current correlator in the mobile impurity model

We are now in a position to work out the current-current correlation function (2.14) in the mobile impurity model framework. Given the expression (2.60) for the projection of the current operator, we have

$$C_{\rm JJ}^{(1)}(\ell, t) \sim G(x,t) = \langle J_{k\Lambda}^\dagger(x,t) J_{k\Lambda}(0,0)\rangle. \tag{2.84}$$

In order to evaluate $G(x,t)$ we go over to the transformed basis, in which the impurity decouples from the LL degrees of freedom. Given (2.83), the leading contribution takes the form

$$\begin{aligned} J_{k\Lambda}(x) \sim\ & \partial_x \widetilde{B}^\dagger(x) e^{i\Theta_c^\circ(x)\frac{\Delta N_c - N_c^{\rm imp}}{2\sqrt{2}}} + i\gamma_c \widetilde{B}^\dagger(x)\partial_x\Theta_c^\circ(x) e^{i\Theta_c^\circ(x)\frac{\Delta N_c - N_c^{\rm imp}}{2\sqrt{2}}} \\ & - \frac{i}{2\sqrt{2}} \widetilde{B}^\dagger(x)\partial_x\Phi_s^\circ(x) e^{i\Theta_c^\circ(x)\frac{\Delta N_c - N_c^{\rm imp}}{2\sqrt{2}}}. \end{aligned} \tag{2.85}$$

Substituting this back into (2.84) leads to three kinds of contributions to the correlator

$$\begin{aligned} G(x,t) = & G_1(x,t)\langle \partial_x \widetilde{B}(x,t)\partial_x\widetilde{B}^\dagger(0,0)\rangle + G_2(x,t)\langle \widetilde{B}(x,t)\widetilde{B}^\dagger(0,0)\rangle \\ & + G_3(x,t) i\left[\langle \partial_x\widetilde{B}(x,t)\widetilde{B}^\dagger(0,0) - \langle \widetilde{B}(x,t)\partial_x\widetilde{B}^\dagger(0,0)\right]. \end{aligned} \tag{2.86}$$

Here $G_j(x,t)$ are correlation functions in the LL sector of the theory and can be evaluated by standard methods. The results are

$$\begin{aligned}
G_1(x,t) &= \frac{1}{(x^2-v_c^2t^2)^\gamma}\ , \\
\frac{G_2(x,t)}{G_1(x,t)} &= -\frac{2\gamma_c^2}{K_c}\left[\frac{x^2+v_c^2t^2}{(x^2-v_c^2t^2)^2}+\frac{2\gamma x^2}{(x^2-v_c^2t^2)^2}\right]-\frac{1}{2}\frac{x^2+v_s^2t^2}{(x^2-v_s^2t^2)^2}\ , \\
\frac{G_3(x,t)}{G_1(x,t)} &= i\gamma_c\sqrt{\frac{\gamma}{K_c}}\mathrm{sgn}(N_c^{\mathrm{imp}}+2)\ \frac{2x}{x^2-v_c^2t^2}\ ,
\end{aligned} \tag{2.87}$$

where we have defined

$$\gamma = \frac{1}{2K_c}\left(1+\frac{N_c^{\mathrm{imp}}}{2}\right)^2. \tag{2.88}$$

The free impurity correlator is given by

$$\langle \widetilde{B}(x,t)\widetilde{B}^\dagger(0,0)\rangle = \int_{-\Lambda}^{\Lambda}\frac{\mathrm{d}p}{2\pi}e^{-ipx}e^{-i\varepsilon(p)t}, \tag{2.89}$$

where $\varepsilon(p)$ is the dispersion relation for the k-Λ string and Λ is a momentum cutoff for the impurity excitation. Using (2.84), (2.86), (2.87) and (2.89) we may now determine the contribution from the k-Λ string excitation to the retarded correlator (2.5). The result can be written in the form

$$\begin{aligned}
\sigma_1(\omega)\Big|_{k\Lambda} \sim \frac{1}{\omega}\int_{-\Lambda}^{\Lambda}\mathrm{d}p\Bigg\{ & \frac{\gamma_c^2}{K_c}\Big((1+\gamma)\left[\widetilde{G}^c_{\gamma+2,\gamma}\big(\omega-\varepsilon(p),p\big)+\widetilde{G}^c_{\gamma,\gamma+2}\big(\omega-\varepsilon(p),p\big)\right] \\
& -2\gamma\widetilde{G}^c_{\gamma+1,\gamma+1}\big(\omega-\varepsilon(p),p\big)\Big) \\
& +\sqrt{\frac{4\gamma}{K_c}}\gamma_c p\left[\widetilde{G}^c_{\gamma+1,\gamma}\big(\omega-\varepsilon(p),p\big)-\widetilde{G}^c_{\gamma,\gamma+1}\big(\omega-\varepsilon(p),p\big)\right] \\
& +p^2\widetilde{G}^c_{\gamma,\gamma}\big(\omega-\varepsilon(p),p\big)+\gamma_s^2\left[\widetilde{G}^s_{\gamma}\big(\omega-\varepsilon(p),p\big)+\widetilde{G}^s_{\gamma}\big(\omega-\varepsilon(p),-p\big)\right]\Bigg\},
\end{aligned} \tag{2.90}$$

where we have defined

$$\begin{aligned}
\widetilde{G}^c_{\gamma_+,\gamma_-}(\omega,p) &= \frac{(2\pi)^2}{\Gamma(\gamma_+)\Gamma(\gamma_-)(2v_c)^{\gamma_++\gamma_--1}}(\omega+v_cp)^{\gamma_+-1}(\omega-v_cp)^{\gamma_--1}\Theta(\omega-v_c|p|)\ , \\
\widetilde{G}^s_{\gamma}(\omega,p) &= \int_0^1\mathrm{d}s\left[\frac{2\pi}{\Gamma(\gamma)}\right]^2\frac{(\omega-v_sp)^{2\gamma-1}}{(v_c^2-v_s^2)^\gamma}\Theta(\omega-v_sp)s^{\gamma-1}(1-s)^{\gamma-1} \\
&\quad\times\left[\frac{2v_c(\omega-v_sp)}{v_c^2-v_s^2}s-\frac{\omega-v_cp}{v_c-v_s}\right]\Theta\Big(\frac{2v_c(\omega-v_sp)}{v_c^2-v_s^2}s-\frac{\omega-v_cp}{v_c-v_s}\Big).
\end{aligned} \tag{2.91}$$

The dependence of (2.90) on the momentum cutoff Λ is shown in Fig. 2.13. We see that over a wide range the result is only weakly cutoff-dependent. Unfortunately, the mobile impurity method provides no simple way of predicting how large the cutoff should be. The only obvious constraint is that it should fulfil $\Lambda \ll \pi(1-n)$. If we approach the threshold from above, i.e. consider the limit $\omega \to \varepsilon_{k\Lambda}(0)$, the remaining integral in (2.90) can be carried out and yields a power-law behaviour of the form

$$\lim_{\omega\to\varepsilon_{k\Lambda}(0)} \sigma_1(\omega)\Big|_{k\Lambda} \sim \frac{1}{\omega}\left[\omega - \varepsilon_{k\Lambda}(0)\right]^{\gamma-1}\Theta\left(\omega-\varepsilon_{k\Lambda}(0)\right). \tag{2.92}$$

This is shown in Fig. 2.13 together with numerical evaluations of (2.90) for several values of the cutoff Λ, and is seen to provide a good approximation across the entire frequency range examined. Importantly, the exponent $\gamma-1$ is always larger than one, which is in disagreement with that of Ref. [127] . Additionally, the exponent γ can

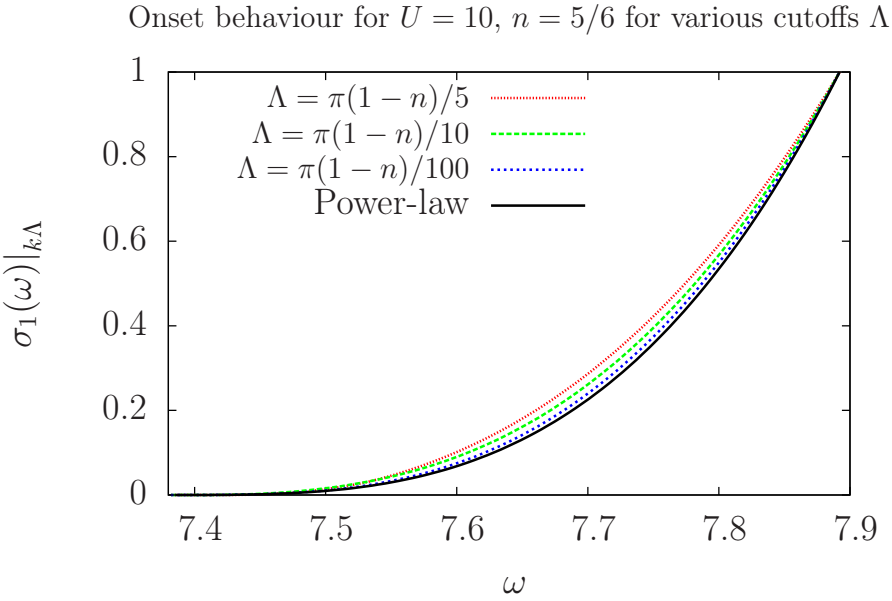

Figure 2.13: Optical conductivity (2.90) for $U = 10$, $n = 5/6$ and several values of the cutoff Λ. The different curves have been normalised such that $\sigma_1(\varepsilon_{k\Lambda}+0.5)\Big|_{k\Lambda} = 1$. For comparison we show the power-law behaviour (2.92), valid for $\omega \to \varepsilon_{k\Lambda}$. We see that the power law in fact provides a good approximation over the entire range of comparison.

be calculated for a variety of parameters, as presented in Fig. 2.14.

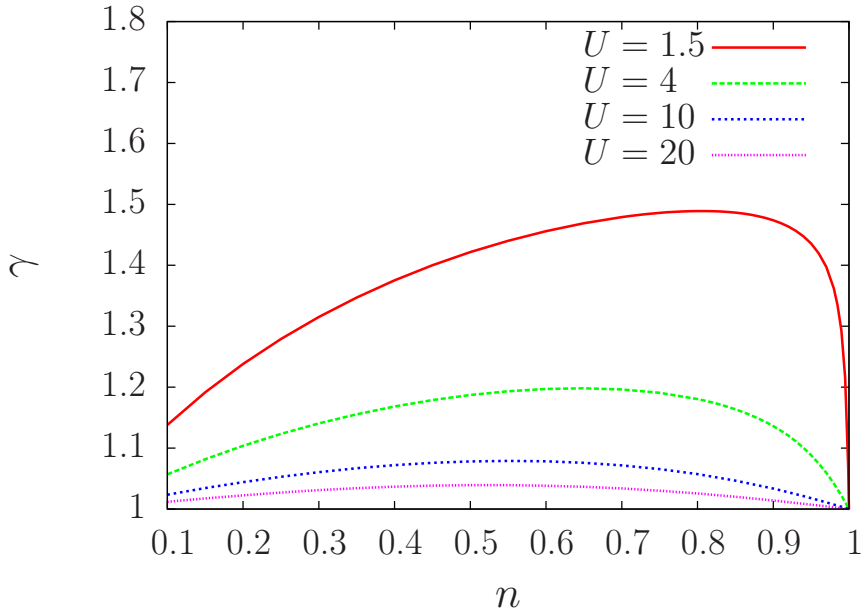

Figure 2.14: Value of the exponent γ in (2.92) characterising the power-law behaviour of $\sigma_1(\omega)$ just above the pseudo-gap, for several values of U and n

2.4 Comparison with numerical results

In Ref. [90] the optical conductivity of the one dimensional Hubbard model has been computed by matrix product methods. The approach requires introduction of a damping parameter $\eta > 0$ and provides Im $\chi^J(\omega + i\eta)$ for a chain of finite length. In order to facilitate a comparison with the results obtained here it is necessary to remove this broadening. In order to do this approximately we proceed as follows. For positive frequencies the zero temperature optical conductivity can be expressed as

$$\begin{aligned} \sigma_1(\omega > 0) &= -\frac{\text{Im } \chi_+(\omega)}{\omega} \ , \\ \chi_+(\omega) &= \frac{e^2}{L} \sum_n \frac{|\langle \text{GS}|J|n\rangle|^2}{\omega + i0 - E_n + E_{\text{GS}}} \ . \end{aligned} \tag{2.93}$$

Ref. [90] provides results for the quantity

$$\chi_+(\omega; L, \eta) = \int_{-\infty+i0}^{\infty+i0} \frac{d\omega'}{2\pi} \, \frac{2\eta}{\eta^2 + (\omega - \omega')^2} \text{Im } \chi_+(\omega') \ , \tag{2.94}$$

where L is the chain length and ω takes values on a regular grid of frequencies. We first use rational function interpolation to extract a continuous function from

the numerical data, which we then deconvolve using the Richardson-Lucy algorithm [133, 134].

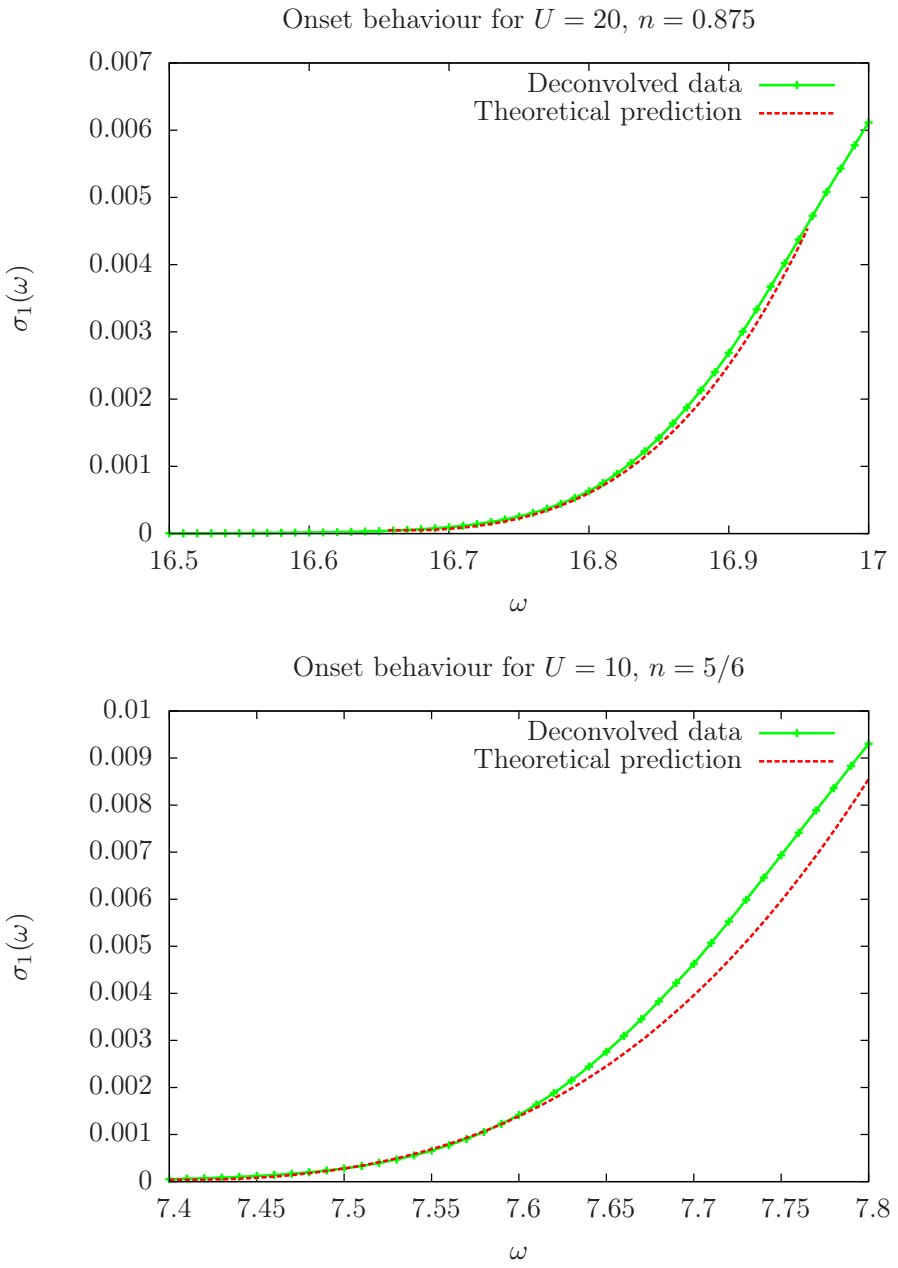

Figure 2.15: Comparison of deconvolved DMRG data from Ref. [90] with the onset as predicted in (2.90), varying the offset and overall scale factor and choosing $\Lambda = (1-n)\pi/10$. The onset value at $n = 1$ is given by $\omega = 16.28, 6.547$ for $U = 20$ and $U = 10$ respectively.

The deconvolved numerical results obtained in this way can then be compared

to the onset predicted at the lowest threshold, as given by (2.90). We allow for an unknown scale factor in the calculation, as well as a small constant contribution from the particle-hole excitations. We choose a specific value of the cutoff Λ, but as noted earlier, the results do not depend strongly on the precise choice. Due to the soft nature of the onset predicted, it is only realistic to compare the initial onset due to the k-Λ string, as when moving away from this point less relevant operators will begin to contribute. Comparisons between the prediction of the MIM and numerical results are shown in Fig. 2.15. The agreement is not perfect, but the results are seen to be compatible. As usual the size of the frequency window in which the MIM prediction applies is not known. The theoretical and numerical results of the onset being convex are in stark contrast to the results of Ref. [127], which for the parameters we consider predicts concave power-law behaviour.

2.5 Away from $q = 0$

One can easily generalise the results here to examine the conductivity at *finite momentum* i.e. consider

$$\chi^J(\omega, q) = -ie^2 \int_0^\infty dt \sum_{l=-L/2}^{L/2-1} e^{i(\omega t - qla_0)} \langle GS|[J_l(t), J_0(0)]|GS\rangle, \tag{2.95}$$

for $q \neq 0$. The analysis proceeds in an identical manner to identify the quantities $N_{c,s}^{\rm imp}$, $D_{c,s}^{\rm imp}$, as the high-energy impurity simply shifts its momentum. However, in order to find the threshold away from $q \in [(n-1)\pi, (1-n)\pi]$, umklapp processes must be involved. For an arbitrary filling, these will generically be of a very large order, which will suppress the contributions. The dispersion relation is generically no longer a saddle point and therefore in the region where one impurity is involved and one can linearise, power-law behaviour for the onset will be obtained. For the k-Λ string at momentum q, one must first solve for Λ^p such that $p_{k\Lambda}(\Lambda^p) = q$, and then $N_c^{\rm imp}(\Lambda^p)$, $D_c^{\rm imp}(\Lambda^p)$ can be calculated. γ is still given by (2.88). The most relevant contribution will then have the form

$$\text{Im } \chi(\omega, q \neq 0) \sim \frac{1}{(\omega - \omega_{\rm th}(q))^{\gamma(\Lambda^p)}}, \tag{2.96}$$

where $\gamma(\Lambda^p)$ is a function of the quantities $N_\alpha^{\rm imp}$, $D_\alpha^{\rm imp}$ and K_α.

2.6 Summary and conclusions

We have studied the optical conductivity $\sigma_1(\omega)$ in the one dimensional Hubbard at zero temperature and close to half filling. Recent DMRG computations [90] have shown that in this regime $\sigma_1(\omega)$ is very small within a "pseudo-gap" and exhibits a rapid increase above an energy scale $E_{\rm opt}$ that depends on doping as well as the interaction strength U. Using the Bethe Ansatz we have identified the relevant excitations that contribute to $\sigma_1(\omega)$ for $\omega > E_{\rm opt}$. One of these, the k-Λ string excitation, had been previously proposed to describe the scale $E_{\rm opt}$ [127]. We then followed Ref. [59] to construct a mobile impurity model describing the behaviour of $\sigma_1(\omega)$ above $E_{\rm opt}$. The analysis of this model entailed several generalisations relating to the projection of lattice operators to local fields in the MIM, the treatment of excitations that are not highest weight states with respect to the η-pairing algebra of the Hubbard model, and considering the mobile impurity to be located at a maximum of its dispersion. We also derived an explicit expression for the finite-size momentum of the relevant Bethe Ansatz states, which is useful in determining the various unknown parameters in the MIM. Our main result is to show that the MIM approach predicts a smooth, slow increase in $\sigma_1(\omega)$ for frequencies above $E_{\rm opt}$. This is in contrast to the half-filled case [25] and previous predictions[127], but consistent with recent dynamical DMRG computations[90]. The results presented in this work are by construction specific to the Hubbard model. However, we expect the gross features seen in the optical conductivity to be quite general for weakly doped Mott insulators. In particular, we expect that such systems to exhibit a rapid increase of $\sigma_1(\omega)$ above a pseudo-gap. As the functional form of the increase is non-universal, it is conceivable that for other models it could be considerably steeper than in the case considered here.

2.A Velocities and Luttinger parameters in zero magnetic field

In zero magnetic field the charge and spin velocities are given in terms of the solutions to the linear integral equations (2.20), (2.21), (2.24), (2.25) for the dressed energies and root densities as

$$v_c = \frac{\varepsilon_c'(Q)}{2\pi\rho_{c,0}(Q)} , \qquad v_s = \frac{\varepsilon_s'(\infty)}{2\pi\rho_{s,0}(\infty)}. \tag{2.97}$$

The spin Luttinger parameter is fixed by spin rotational symmetry to be

$$K_s = 1. \tag{2.98}$$

We stress that all spin excitations relevant to our mobile impurity model description occur at (approximately) zero energy, so that corrections to (2.98) are negligible. The charge Luttinger parameter is

$$K_c = \frac{\xi^2(Q)}{2}, \tag{2.99}$$

where $\xi(k)$ is the solution of the linear integral equation

$$\xi(k) = 1 + \int_{-Q}^{Q} \mathrm{d}k' \, \cos k' \; R(\sin k - \sin k') \; \xi(k'). \tag{2.100}$$

Here $R(x)$ is defined in (2.76).

2.B Bethe Ansatz results for k-Λ string

Having established that the threshold above the low-energy continuum can be explained by a k-Λ string excitation, the simplest equations to consider are the Takahashi equations[26] in the presence of a single k-Λ string of length 2 i.e. consisting of 1 Λ and 2 ks. It is also clear that as the correlator is a zero momentum quantity, k-Λ string is pinned to zero momentum. The Takahashi equations can be analysed for large L, keeping terms to $\mathcal{O}(L^{-2})$ in order to calculate the finite-size corrections

to the energy. The counting functions in this specific case are given by

$$\begin{aligned} Lz_c(k_j) &= k_j L + \sum_{\alpha=1}^{M-1} \theta\left(\frac{\sin k_j - \Lambda_\alpha}{u}\right) + \theta\left(\frac{\sin k_j - \Lambda'^p}{u}\right), \quad j = 1, \ldots, N-2, \\ Lz_s(\Lambda_\alpha) &= \sum_{j=1}^{N-2} \theta\left(\frac{\Lambda - \sin k_j}{u}\right) - \sum_{\beta=1}^{M-1} \theta\left(\frac{\Lambda_\alpha - \Lambda_\beta}{2u}\right), \qquad \alpha = 1, \ldots, M-1. \end{aligned} \tag{2.101}$$

Employing the Euler-Maclaurin summation formula

$$\frac{1}{L}\sum_{n=n_1}^{n_2} f\left(\frac{n}{L}\right) = \int_{\frac{n_-}{L}}^{\frac{n_+}{L}} dx\ f(x) + \frac{1}{24L^2}\left(f'\left(\frac{n_-}{L}\right) - f'\left(\frac{n_+}{L}\right)\right) + \ldots, \tag{2.102}$$

where $n_+ = n_2 + \frac{1}{2}$ and $n_- = n_1 - \frac{1}{2}$, it can be seen that

$$\begin{aligned} z_c(k) &= k + \int_{A_-}^{A_+} \mathrm{d}\Lambda\ \theta\left(\frac{\sin k - \Lambda}{u}\right)\rho_s(\Lambda) + \frac{1}{L}\theta\left(\frac{\sin k - \Lambda'^p}{u}\right) \\ &\quad + \frac{2\pi}{24L^2}\left[\frac{a_1(\sin k - A_+)}{\rho_s(A_+)} - \frac{a_1(\sin k - A_-)}{\rho_s(A_-)}\right], \\ z_s(\Lambda) &= \int_{Q_-}^{Q_+} dk\ \theta\left(\frac{\Lambda - \sin k}{u}\right)\rho_c(k) - \int_{A_-}^{A_+} d\Lambda'\ \theta\left(\frac{\Lambda - \Lambda'}{2u}\right)\rho_s(\Lambda') \\ &\quad + \frac{2\pi}{24L^2}\left[\frac{a_1(\Lambda - \sin Q_+)\cos Q_+}{\rho_c(Q_+)} - \frac{a_1(\Lambda - \sin Q_-)\cos Q_-}{\rho_c(Q_+)}\right. \\ &\quad \left. - \frac{a_2(\Lambda - A_+)}{\rho_s(A_+)} + \frac{a_2(\Lambda - A_-)}{\rho_s(A_-)}\right]. \end{aligned} \tag{2.103}$$

Taking derivatives, equations for the root densities can be found

$$\begin{aligned} \rho_c(k) &= \frac{1}{2\pi} + \int_{A_-}^{A_+} d\Lambda\ \cos k\, a_1(\sin k - \Lambda)\rho_s(\Lambda) + \frac{1}{L}\cos k\, a_1(\sin k - \Lambda'^p) \\ &\quad + \frac{1}{24L^2}\left[\frac{\cos k\, a_1'(\sin k - A_+)}{\rho_s(A_+)} - \frac{\cos k\, a_1'(\sin k - A_-)}{\rho_s(A_-)}\right], \end{aligned} \tag{2.104}$$

$$\begin{aligned} \rho_s(\Lambda) &= \int_{Q_-}^{Q_+} dk\ a_1(\Lambda - \sin k)\rho_c(k) - \int_{A_-}^{A_+} d\Lambda'\ a_2(\Lambda - \Lambda')\rho_s(\Lambda') \\ &\quad + \frac{1}{24L^2}\left[\frac{a_1'(\Lambda - \sin Q_+)\cos Q_+}{\rho_c(Q_+)} - \frac{a_1'(\Lambda - \sin Q_-)\cos Q_-}{\rho_c(Q_-)}\right. \\ &\quad \left. - \frac{a_2'(\Lambda - A_+)}{\rho_s(A_+)} + \frac{a_2'(\Lambda - A_-)}{\rho_s(A_-)}\right]. \end{aligned} \tag{2.105}$$

As the integral equations are linear, we can write

$$\rho_\alpha(z_\alpha) := \rho_{\alpha,0}(z_\alpha) + \frac{1}{L}\rho_{\alpha,1}(z_\alpha) + \frac{1}{24L^2}\sum_{\beta,\sigma}\frac{f_{\alpha\beta}^{(\sigma)}(z)}{\rho_\beta(X_\sigma^\beta)}, \tag{2.106}$$

here $X^c_\sigma = Q_\sigma$, $X^s_\sigma = A_\sigma$. The integral equations satisfied by the first two terms in (2.106) are

$$\rho_{\alpha,a}(z) = \rho^{(0)}_{\alpha,a}(z) + K_{\alpha\beta} * \rho_{\beta,a}, \qquad a = 0, 1, \tag{2.107}$$

with $K_{\alpha\beta} * f_\beta$ denoting the convolution $\sum_\beta \int_{X^\beta_-}^{X^\beta_+} \mathrm{d}z_\beta \, K_{\alpha\beta}(z_\alpha, z_\beta) f_\beta(z_\beta)$, the kernels defined by

$$\begin{aligned} K_{cc}(k,k') &= 0, \qquad & K_{cs}(k,\Lambda) &= \cos k \, a_1(\sin k - \Lambda), \\ K_{sc}(\Lambda,k) &= a_1(\Lambda - \sin k), \qquad & K_{ss}(\Lambda,\Lambda') &= -a_2(\Lambda - \Lambda'), \end{aligned} \tag{2.108}$$

and the driving terms given by

$$\rho^{(0)}_{\alpha,0} = \frac{\delta_{\alpha,c}}{2\pi}, \tag{2.109}$$

$$\rho^{(0)}_{\alpha,1} = \delta_{\alpha,c} \cos k \; a_1(\sin k - \Lambda'^p). \tag{2.110}$$

The final integral equation is determined by

$$f^{(\sigma)}_{\alpha\beta} = d^{(\sigma)}_{\alpha\beta} + K_{\alpha\gamma} * f^{(\sigma)}_{\gamma\beta}, \tag{2.111}$$

where

$$d^{(\sigma)}_{\alpha\beta} = -\sigma \frac{\partial}{\partial z'} K_{\alpha\beta}(z,z') \Big|_{z'=X^\beta_\sigma}. \tag{2.112}$$

The exact finite-size energy of the system is given by (1.49). Using the Euler-Maclaurin summation formula (2.102) again, corrections can be kept to $\mathcal{O}(L^{-1})$, yielding

$$E = Lu + L \sum_\alpha \int_{X^\alpha_-}^{X^\alpha_+} dz \; \varepsilon^{(0)}_\alpha(z) \rho_\alpha(z) + \varepsilon^{(0)}_{k\Lambda}(\Lambda'^p). \tag{2.113}$$

Expanding in powers of L and exploiting the identical kernels of the integral equations for dressed charge and root density equations, if the energy is now considered as a functional of the integration boundaries, performing an expansion about σX^α to second order (the first order term vanishes)[68], it can be shown that

$$\begin{aligned} E &= L e_{GS}(\{X^\alpha\}) + \varepsilon_{k\Lambda}(\Lambda'^p) \\ &\quad + L\pi \sum_\alpha v_\alpha \left\{ \left(\rho_{\alpha,0}(X^\alpha)(X^\alpha_+ - X^\alpha)\right)^2 + \left(\rho_{\alpha,0}(X^\alpha)(X^\alpha_- + X^\alpha)\right)^2 \right\} \end{aligned} \tag{2.114}$$

2.B.1 Impurity densities

The following are taken as definitions

$$n_\alpha = \int_{X_-^\alpha}^{X_+^\alpha} dz\ \rho_\alpha(z), \tag{2.115}$$

$$2D_c = I_+ + I_- = \frac{L}{2\pi}\left[z_c(Q_+) + z_c(Q_-)\right], \tag{2.116}$$

$$2D_s = J_+ + J_- = \frac{L}{2\pi}\left[z_s(A_+) + z_s(A_-)\right]. \tag{2.117}$$

The corrections from adding the "impurity" i.e. the high-energy excitation can be identified and separated off from the terms that would be present without it. This is achieved by using that

$$\lim_{\Lambda\to\infty} z_s(\Lambda) = -\lim_{\Lambda\to-\infty} z_s(\Lambda), \tag{2.118}$$

$$\lim_{k\to\pm\pi} z_c(k) = -\int_{A_-}^{A_+} d\Lambda\ \theta\left(\frac{\Lambda}{u}\right)\rho_s(\Lambda) - \theta\left(\frac{\Lambda'^p}{u}\right). \tag{2.119}$$

This allows the "quantum numbers" to be expressed in terms of integrals of the root densities, which can then be split off order-by-order in $1/L$. More explicitly, one finds that

$$\begin{aligned} 2D_s &= L\left(\int_{-\infty}^{A_-} d\Lambda\ \rho_s(\Lambda) - \int_{A_+}^{\infty} d\Lambda\ \rho_s(\Lambda)\right), \\ &= L\left(\int_{-\infty}^{A_-} d\Lambda\ \rho_{s,0}(\Lambda) - \int_{A_+}^{\infty} d\Lambda\ \rho_{s,0}(\Lambda)\right) + 2D_s^{\text{imp}}, \end{aligned} \tag{2.120}$$

where

$$2D_s^{\text{imp}} = \int_{-\infty}^{-A} d\Lambda\ \rho_{s,1}(\Lambda) - \int_{A}^{\infty} d\Lambda\ \rho_{s,1}(\Lambda). \tag{2.121}$$

Similarly for the charge sector

$$\begin{aligned} 2D_c &= \frac{L}{2\pi}\left(z_c(Q_+) + z_c(Q_-) - z_c(\pi) - z_c(-\pi) - 2\int_{A_-}^{A_+} d\Lambda\ \rho_s(\Lambda)\theta\left(\frac{\Lambda}{u}\right) - \frac{2}{L}\theta\left(\frac{\Lambda'^p}{u}\right)\right), \\ &= L\left(\int_{-\pi}^{Q_-} dk\ \rho_{c,0}(k) - \int_{Q_+}^{\pi} dk\ \rho_{c,0}(k) - \frac{1}{\pi}\int_{A_-}^{A_+} d\Lambda\ \rho_{s,0}(\Lambda)\theta\left(\frac{\Lambda}{u}\right)\right) + 2D_c^{\text{imp}}, \end{aligned} \tag{2.122}$$

$$2D_c^{\text{imp}} = \int_{-\pi}^{-Q} dk\ \rho_{c,1}(k) - \int_{Q}^{\pi} dk\ \rho_{c,1}(k) - \frac{1}{\pi}\int_{-A}^{A} d\Lambda\ \rho_{s,1}(\Lambda)\theta\left(\frac{\Lambda}{u}\right) - \frac{1}{\pi}\theta\left(\frac{\Lambda'^p}{u}\right). \tag{2.123}$$

Similarly,

$$N_\alpha^{\rm imp} = \int_{-X^\alpha}^{X^\alpha} dz\ \rho_{\alpha,1}(z). \tag{2.124}$$

2.B.2 Relation between $X_\sigma^\alpha - \sigma X^\alpha$ and the impurity densities

Following Ref. [68], considering the variation of the integration bounds X_σ^α with respect to n_β, it can be seen that, in terms of the dressed charge matrix[26] $Z_{\alpha\beta}$, defined by

$$\begin{aligned} Z_{\alpha\beta} &= \xi_{\alpha\beta}(X^\beta), \\ \xi_{\alpha\beta}(z_\beta) &= \delta_{\alpha\beta} + \xi_{\alpha\gamma} * K_{\gamma\beta}, \end{aligned} \tag{2.125}$$

with $K_{\alpha\beta}$ given by (2.108), one finds

$$X_\sigma^\alpha - \sigma X^\alpha = \sigma \frac{1}{2} \frac{Z^{-1}_{\alpha\beta}}{\rho_{\alpha,0}(X^\alpha)} \left(\Delta n_\beta - \frac{1}{L} N_\beta^{\rm imp} \right) + \frac{Z^\top_{\alpha\beta}}{\rho_{\alpha,0}(X^\alpha)} \left(d_\beta - \frac{1}{L} D_\beta^{\rm imp} \right). \tag{2.126}$$

These results can be inserted into the finite-size energy, which now reads as

$$\begin{aligned} E = L e_{GS}(\{X^\alpha\}) + \varepsilon_{k\Lambda}(0) + \frac{1}{L} \Big(& -\frac{\pi}{6}(v_s + v_c) \\ & + 2\pi \left[\frac{1}{4} \Delta\widetilde{N}_\alpha (Z^\top)^{-1}_{\alpha\gamma} v_\gamma Z^{-1}_{\gamma\beta} \Delta\widetilde{N}_\beta + \widetilde{D}_\alpha Z_{\alpha\gamma} v_\gamma Z^\top_{\gamma\beta} \widetilde{D}_\beta \right] \Big), \end{aligned} \tag{2.127}$$

where

$$\widetilde{D}_\alpha = D_\alpha - D_\alpha^{\rm imp}, \tag{2.128}$$

$$\Delta\widetilde{N}_\alpha = \Delta N_\alpha - N_\alpha^{\rm imp}. \tag{2.129}$$

2.B.3 Simplifications for zero magnetic field

In the $B \to 0$ limit, the integration boundary $A \to \infty$ and many results simplify by use of Fourier transforms. Useful identities used can be found in Ch. 17 of Ref. [26]. First, the dressed charge matrix adopts the simple form

$$Z = \begin{pmatrix} \xi & 0 \\ \frac{\xi}{2} & \frac{1}{\sqrt{2}} \end{pmatrix}, \tag{2.130}$$

where $\xi = \xi(Q)$ and $\xi(k)$ obeys (2.100). Following a similar method to Ref. [68], the root densities can be shown to simplify as

$$\rho_{c,1}(k) = \cos k\ a_1(\sin k - \Lambda'^p) + \cos k \int_{-Q}^{Q} dk'\ \rho_{c,1}(k') R(\sin k - \sin k'), \tag{2.131}$$

$$\rho_{s,1}(\Lambda) = \int_{-Q}^{Q} dk\ \rho_{c,1}(k)\ s(\Lambda - \sin k), \tag{2.132}$$

where

$$s(x) = \frac{1}{4u \cosh\left(\frac{\pi x}{2u}\right)}. \tag{2.133}$$

Considering the Fourier transform of (2.132), it can be shown that

$$N_s^{\text{imp}} = \frac{1}{2} N_c^{\text{imp}}. \tag{2.134}$$

In the $\Lambda'^p \to 0$ limit, both $\rho_{c,1}(k)$ and $\rho_{s,1}(\Lambda)$ are even functions and therefore

$$D_c^{\text{imp}} = D_s^{\text{imp}} = 0. \tag{2.135}$$

It is useful to note that the dressed energies take the form

$$\varepsilon_c(k) = -2\cos k - \mu - 2u + \int_{-Q}^{Q} \mathrm{d}k'\ \cos k'\ R(\sin k - \sin k')\varepsilon_c(k'), \tag{2.136}$$

$$\varepsilon_s(\Lambda) = \int_{-Q}^{Q} dk\ \ \cos k\ s\left[\Lambda - \sin k\right]\ \varepsilon_c(k), \tag{2.137}$$

$$\varepsilon_{k\Lambda}(\Lambda) = 4\mathrm{Re}\sqrt{1 - (\Lambda - iu)^2} - 2\mu - 4u + \int_{-Q}^{Q} dk \cos k\ a_1(\sin k - \Lambda)\ \varepsilon_c(k). \tag{2.138}$$

The value of $\varepsilon_{k\Lambda}(0)$ provides the location of the threshold at zero momentum in this sector. The finite-size energy can therefore be simply written as

$$\begin{aligned} E = {} & L e_{GS}(\{X^\alpha\}) + \varepsilon_{k\Lambda}(0) - \frac{\pi v_c}{6L} \\ & + \frac{2\pi v_c}{L}\left[\frac{(\Delta N_c - N_c^{\text{imp}})^2}{4\xi^2} + \xi^2\left(D_c - D_c^{\text{imp}} + \frac{D_s - D_s^{\text{imp}}}{2}\right)^2\right]. \end{aligned} \tag{2.139}$$

2.C Bethe Ansatz results for high-energy charge particle

2.C.1 Bethe Ansatz calculation

Starting from the Takahashi equations

$$\begin{aligned} Lz_c(k_j) &= k_j L + \sum_{\alpha=1}^{M} \theta\left(\frac{\sin k_j - \Lambda_\alpha}{u}\right), && j = 1, \ldots, N, \\ Lz_s(\Lambda_\alpha) &= \sum_{j=1}^{N} \theta\left(\frac{\Lambda_\alpha - \sin k_j}{u}\right) - \sum_{\beta=1}^{M} \theta\left(\frac{\Lambda_\alpha - \Lambda_\beta}{2u}\right), && \alpha = 1, \ldots, M. \end{aligned} \tag{2.140}$$

We can use the Euler-Maclaurin formula (2.102) to recast this as

$$z_c(k) = k + \int_{A_-}^{A^+} \mathrm{d}\Lambda\, \theta\left(\frac{\sin k - \Lambda}{u}\right) \rho_s(\Lambda) + \frac{2\pi}{24L^2}\left[\frac{a_1(\sin k - A_+)}{\rho_s(A_+)} - \frac{a_1(\sin k - A_-)}{\rho_s(A_-)}\right], \tag{2.141}$$

$$\begin{aligned} z_s(\Lambda) = &\int_{Q_-}^{Q_+} \mathrm{d}k\, \theta\left(\frac{\Lambda - \sin k}{u}\right) \rho_c(k) - \int_{A_-}^{A_+} \mathrm{d}\Lambda' \theta\left(\frac{\Lambda - \Lambda'}{2u}\right) \rho_s(\Lambda') + \frac{1}{L}\theta\left(\frac{\Lambda - \sin k^p}{u}\right) \\ &+ \frac{2\pi}{24L^2}\left[\frac{a_1(\Lambda - \sin Q_+)\cos Q_+}{\rho_c(Q_+)} - \frac{a_1(\Lambda - \sin Q_-)\cos Q_-}{\rho_c(Q_-)} - \frac{a_2(\Lambda - A_+)}{\rho_s(A_+)} + \frac{a_2(\Lambda - A_-)}{\rho_s(A_-)}\right]. \end{aligned} \tag{2.142}$$

Taking derivatives gives the root densities

$$\rho_c(k) = \frac{1}{2\pi} + \int_{A_-}^{A_+} \mathrm{d}\Lambda a_1(\sin k - \Lambda)\rho_s(\Lambda)\cos k + \frac{1}{24L^2}\cos k\left[\frac{a_1'(\sin k - A_+)}{\rho_s(A_+)} - \frac{a_1'(\sin k - A_-)}{\rho_s(A_-)}\right], \tag{2.143}$$

$$\begin{aligned} \rho_s(\Lambda) = &\int_{Q_-}^{Q_+} \mathrm{d}k a_1(\Lambda - \sin k)\rho_c(k) - \int_{A_-}^{A_+} \mathrm{d}\Lambda' a_2(\Lambda - \Lambda')\rho_s(\Lambda') + \frac{1}{L} a_1(\Lambda - \sin k^p) \\ &+ \frac{1}{24L^2}\left[\frac{a_1'(\Lambda - \sin Q_+)\cos Q_+}{\rho_c(Q_+)} - \frac{a_1'(\Lambda - \sin Q_-)\cos Q_-}{\rho_c(Q_-)} + \frac{a_2'(\Lambda - A_-)}{\rho_s(A_-)} - \frac{a_2'(\Lambda - A_+)}{\rho_s(A_+)}\right]. \end{aligned} \tag{2.144}$$

We can again split these linear integral equations into the form (2.106), (2.107), (2.111) where in this case

$$\rho_{\alpha,0}^{(0)} = \frac{\delta_{\alpha,c}}{2\pi}, \qquad \rho_{\alpha,1}^{(0)}(z_\alpha) = \delta_{\alpha,s} a_1(z_\alpha - \sin k^p). \tag{2.145}$$

and the integral kernels are again given by (2.108). We can then construct the impurity densities

$$N_\alpha^{\rm imp} = \int_{-X_\alpha}^{X^\alpha} {\rm d}z_\alpha \rho_{\alpha,1}(z_\alpha), \tag{2.146}$$

$$2D_c^{\rm imp} = \int_Q^\pi {\rm d}k \left[\rho_{c,1}(-k) - \rho_{c,1}(k)\right] - \frac{1}{\pi}\int_{-A}^{A} {\rm d}\Lambda\, \rho_{s,1}(\Lambda)\, \theta\left(\frac{\Lambda}{u}\right), \tag{2.147}$$

$$2D_s^{\rm imp} = \int_A^\infty {\rm d}\Lambda\, \left[\rho_{s,1}(-\Lambda) - \rho_{s,1}(\Lambda)\right]. \tag{2.148}$$

To determine the thermodynamic rapidity k^p and the finite-size correction δk^p, we can examine the requirements that

$$z_c(k_L^p) = \frac{2\pi I^p}{L}, \tag{2.149}$$

$$z_{c,0}(k^p) = \frac{2\pi I^p}{L}, \tag{2.150}$$

with $k_L^p = k^p + \frac{\delta k^p}{L}$. Expanding (2.149) in the deviation δk^p and using (2.150) yields

$$\delta k^p = -\frac{L}{2\pi\rho_{c,0}(k^p)}\left[\sum_{\beta,\sigma}\Psi_\beta^{(\sigma)}(k^p)(X_\beta^\sigma - \sigma X^\beta)\right] - \frac{1}{2\pi\rho_{c,0}(k^p)}\int_{-A}^{A}{\rm d}\Lambda\rho_{s,1}(\Lambda)\theta\left(\frac{\Lambda-\sin k^p}{u}\right), \tag{2.151}$$

where

$$\Psi_\beta^{(\sigma)}(k) = \sigma\rho_{s,0}(A)\theta\left(\frac{\sigma A - \sin k}{u}\right)\delta_{s,\beta} + \int_{-A}^{A}{\rm d}\Lambda\, r_{s,\beta}^{(\sigma)}(\Lambda)\theta\left(\frac{\Lambda-\sin k}{u}\right), \tag{2.152}$$

$$r_{\alpha\beta}^{(\sigma)} = \sigma\rho_{\beta,0}(X^\beta)K_{\alpha\beta}(z_\alpha, \sigma X^\beta) + K_{\alpha\gamma} * r_{\gamma\beta}^{(\sigma)}. \tag{2.153}$$

Using the results of Appendix 2.E, this can be shown to reduce to

$$\delta k^p = \frac{1}{\rho_{c,0}(k^p)}\sum_{\alpha=c,s}\left(N_\alpha^{\rm imp}D_\alpha + D_\alpha^{\rm imp}\Delta N_\alpha - D_\alpha^{\rm imp}N_\alpha^{\rm imp}\right). \tag{2.154}$$

We then have that

$$E = e_{GS}L + \varepsilon_c(k^p) + \varepsilon_c'(k^p)\frac{\delta k^p}{L} - \frac{\pi}{6L}(v_s+v_c) + \frac{2\pi}{L}\left[\frac{1}{4}\Delta\widetilde{N}_\gamma(Z^\top)^{-1}_{\gamma\alpha}v_\alpha Z^{-1}_{\alpha\beta}\Delta\widetilde{N}_\beta + \widetilde{D}_\gamma Z_{\gamma\alpha}v_\alpha Z^\top_{\alpha\beta}\widetilde{D}_\beta\right], \tag{2.155}$$

with the form of $\widetilde{D}_\alpha$, $\Delta\widetilde{N}_\alpha$ and $Z_{\alpha\beta}$ given by (2.128), (2.129), (2.125).

2.C.2 Simplification for $B \to 0$

In the $B \to 0$ limit, the integral equations describing the impurity densities are given by

$$\rho_{c,1}(k) = \cos k\, R(\sin k - \sin k^p) + \cos k \int_{-Q}^{Q} \mathrm{d}k'\, R(\sin k - \sin k')\rho_{c,1}(k'), \tag{2.156}$$

$$N_c^{\mathrm{imp}} = \int_{-Q}^{Q} \mathrm{d}k \rho_{c,1}(k), \qquad N_s^{\mathrm{imp}} = \frac{1}{2}(1 + N_c^{\mathrm{imp}}), \tag{2.157}$$

$$\begin{aligned} 2D_c^{\mathrm{imp}} = &\int_Q^{\pi} \mathrm{d}k \left[\rho_{c,1}(-k) - \rho_{c,1}(k)\right] + \frac{i}{\pi}\left\{\ln\left[\frac{\Gamma\left(\frac{1}{2} - i\frac{\sin k^p}{4u}\right)\Gamma\left(1 + i\frac{\sin k^p}{4u}\right)}{\Gamma\left(\frac{1}{2} + i\frac{\sin k^p}{4u}\right)\Gamma\left(1 - i\frac{\sin k^p}{4u}\right)}\right]\right\} \\ &+ \frac{i}{\pi}\int_{-Q}^{Q} \mathrm{d}k \rho_{c,1}(k)\left\{\ln\left[\frac{\Gamma\left(\frac{1}{2} - i\frac{\sin k}{4u}\right)\Gamma\left(1 + i\frac{\sin k}{4u}\right)}{\Gamma\left(\frac{1}{2} + i\frac{\sin k}{4u}\right)\Gamma\left(1 - i\frac{\sin k}{4u}\right)}\right]\right\}, \end{aligned} \tag{2.158}$$

$$D_s^{\mathrm{imp}} = 0. \tag{2.159}$$

This gives the finite-size corrections to the energy as

$$\begin{aligned} E = &e_{GS}L + \varepsilon_c(k^p) + \varepsilon'(k^p)\frac{\delta k^p}{L} - \frac{\pi v_c}{6L} \\ &+ \frac{2\pi v_c}{L}\left[\frac{(\Delta N_c - N_c^{\mathrm{imp}})^2}{4\xi^2} + \xi^2\left(D_c - D_c^{\mathrm{imp}} + \frac{D_s}{2}\right)^2\right] \\ &+ \frac{2\pi v_s}{L}\left[\frac{1}{2}\left(\Delta N_s - \frac{\Delta N_c}{2} - \frac{1}{2}\right)^2 + \frac{D_s^2}{2}\right], \end{aligned} \tag{2.160}$$

where $\xi = \xi(Q)$ and $\xi(k)$ obeys (2.100).

2.D Bethe Ansatz results for two high-energy charge hole excitations

We again start from (2.140). Following similar steps to Appendices 2.B and 2.C, applying the Euler-Maclaurin summation formula (2.102) then allows us to write

$$\rho_\alpha(z_\alpha) = \rho_{\alpha,0}(z_\alpha) + \frac{1}{L}\rho_{\alpha,1}(z_\alpha) + \frac{1}{24L^2}\sum_{\beta,\sigma}\frac{f_{\alpha\beta}^{(\sigma)}(z_\alpha)}{\rho_\beta(X_\sigma^\beta)}. \tag{2.161}$$

We can again split these linear integral equations into the form (2.106), (2.107), (2.111) where in this case

$$\rho^{(0)}_{\alpha,0} = \frac{\delta_{\alpha,c}}{2\pi}, \tag{2.162}$$

$$\rho^{(0)}_{\alpha,1} = -\delta_{\alpha,s}\left[a_1(\Lambda - \sin k^{h_1}) + a_1(\Lambda - \sin k^{h_2})\right]. \tag{2.163}$$

and the integral kernels are given by (2.108). We can now determine

$$2D_c^{\text{imp}} = \int_Q^\pi \mathrm{d}k\,[\rho_{c,1}(-k) - \rho_{c,1}(k)] - \frac{1}{\pi}\int_{-A}^{A}\mathrm{d}\Lambda\,\theta\left(\frac{\Lambda}{u}\right)\rho_{s,1}(\Lambda), \tag{2.164}$$

$$2D_s^{\text{imp}} = \int_A^\infty \mathrm{d}\Lambda\,\left[\rho_{s,1}(-\Lambda) - \rho_{s,1}(\Lambda)\right]. \tag{2.165}$$

We also have that

$$z_c(k_L^{h_i}) = \frac{2\pi I^{h_i}}{L}, \qquad z_{c,0}(k^{h_i}) = \frac{2\pi I^{h_i}}{L}, \tag{2.166}$$

with $k_L^{h_i} = k^{h_i} + \frac{\delta k^{h_i}}{L}$, yielding

$$\delta k^{h_i} = -\frac{L}{2\pi\rho_{c,0}(k^{h_i})}\left[\sum_{\beta,\sigma}\Psi^{(\sigma)}_\beta(k^{h_i})(X^\sigma_\beta - \sigma X^\beta)\right] - \frac{1}{2\pi\rho_{c,0}(k^{h_i})}\int_{-A}^{A}\mathrm{d}\Lambda\rho_{s,1}(\Lambda)\theta\left(\frac{\Lambda - \sin k^{h_i}}{u}\right), \tag{2.167}$$

with $\Psi^{(\sigma)}(k)$ given by (2.152). We now have all of the quantities required to evaluate the finite-size spectrum in the presence of the two high-energy holons:

$$\begin{aligned} E = {} & e_{GS}L - \varepsilon_c(k^{h_1}) - \varepsilon_c(k^{h_2}) - \varepsilon_c'(k^{h_1})\frac{\delta k^{h_1}}{L} - \varepsilon_c'(k^{h_2})\frac{\delta k^{h_2}}{L} - \frac{\pi}{6L}(v_s + v_c) \\ & + \frac{2\pi}{L}\left[\frac{1}{4}\Delta\widetilde{N}_\gamma(Z^\top)^{-1}_{\gamma\alpha}v_\alpha Z^{-1}_{\alpha\beta}\Delta\widetilde{N}_\beta + \widetilde{D}_\gamma Z_{\gamma\alpha}v_\alpha Z^\top_{\alpha\beta}\widetilde{D}_\beta\right], \end{aligned} \tag{2.168}$$

with the form of $\widetilde{D}_\alpha$, $\Delta\widetilde{N}_\alpha$ and $Z_{\alpha\beta}$ given by (2.128), (2.129), (2.125).

2.D.1 Zero field

In zero field, the integral equations for the functions $\rho_{c,1}$, $\rho_{s,1}$ simplify due to $A \to \infty$ allowing the use of a Fourier transform, specifically

$$\rho_{c,1}(k) = -\cos k\left[R(\sin k - \sin k^{h_1}) + R(\sin k - \sin k^{h_2})\right] + \cos k\int_{-Q}^{Q}\mathrm{d}k'\,R(\sin k - \sin k')\rho_{c,1}(k'), \tag{2.169}$$

$$\rho_{s,1} = -s(\Lambda - \sin k^{h_1}) - s(\Lambda - \sin k^{h_2}) + \int_{-Q}^{Q}\mathrm{d}k\,s(\Lambda - \sin k)\rho_{c,1}(k). \tag{2.170}$$

We also have

$$N_s^{\text{imp}} = \frac{1}{2}N_c^{\text{imp}} - 1. \tag{2.171}$$

The finite-size spectrum can then be written as

$$\begin{aligned} E = e_{GS}L - \varepsilon_c(k^{h_1}) - \varepsilon_c(k^{h_2}) - \frac{\delta k^{h_1}}{L}\varepsilon_c'(k^{h_1}) - \frac{\delta k^{h_2}}{L}\varepsilon_c'(k^{h_2}) - \frac{\pi}{6L}(v_c + v_s) \\ + \frac{2\pi v_c}{L}\left[\frac{(\Delta N_c - N_c^{\text{imp}})^2}{4\xi^2} + \xi^2\left(D_c - D_c^{\text{imp}} + \frac{D_s - D_s^{\text{imp}}}{2}\right)^2\right] \\ + \frac{2\pi v_s}{L}\left[\frac{1}{2}\left(\Delta N_s - \frac{\Delta N_c}{2} + 1\right)^2 + \frac{(D_s - D_s^{\text{imp}})^2}{2}\right]. \end{aligned} \tag{2.172}$$

2.E Finite-size momentum spectrum

As well as the finite-size energies, it is also possible to match the finite-size momentum spectra. We consider here the simple case of a single high-energy charge excitation, but the reasoning is the same for other excitations.

2.E.1 Mobile impurity model momentum spectrum

We bosonise the Hubbard chain at $U = 0$, decomposing the fermionic annihilation operator as

$$c_\sigma(x) = R_\sigma(x)e^{ik_F x} + L_\sigma(x)e^{-ik_F x}. \tag{2.173}$$

To identify the momentum operator, we consider it as the generator of translations by one site i.e.

$$e^{-ia_0 P}c_\sigma(x)e^{ia_0 P} = c_\sigma(x + a_0). \tag{2.174}$$

Which means that $R_\sigma(x) \to R_\sigma(x + a_0)e^{ik_F a_0}$. By utilising the refermionisation identities[59]

$$R_\uparrow \sim \prod_{\alpha=c,s} e^{-\frac{i}{\sqrt{2}}\varphi_\alpha^* + \frac{i}{4\sqrt{2}}\Phi_\alpha^*}, \qquad L_\uparrow \sim \prod_{\alpha=c,s} e^{\frac{i}{\sqrt{2}}\bar{\varphi}_\alpha^* - \frac{i}{4\sqrt{2}}\Phi_\alpha^*}, \tag{2.175}$$

we can identify that, in terms of the mode expansion of the spin and charge modes, the momentum operator is given by

$$\begin{aligned} P = &\frac{k_F}{\pi\sqrt{2}}\left(\bar{Q}_c^* - Q_c^*\right) + \frac{1}{8\pi L}\left[Q_c^{*2} - \bar{Q}_c^{*2} + Q_s^{*2} - \bar{Q}_s^{*2}\right] \\ &+ i\int \mathrm{d}x B^\dagger(x)\partial_x B(x) + \sum_{\alpha=c,s}\sum_{n=1}^{\infty}\frac{2\pi n}{L}\left(c^\dagger_{\alpha,R,n}c_{\alpha,R,n} - c^\dagger_{\alpha,L,n}c_{\alpha,L,n}\right). \end{aligned} \tag{2.176}$$

Employing the unitary transformation, this can be written as

$$\begin{aligned} P = &\frac{k_F}{\pi\sqrt{2}}\left(\bar{Q}_c^\circ - \bar{Q}_c^\circ - 4\pi\gamma_c + 4\pi\bar{\gamma}_c\right) + \frac{1}{8\pi L}\left[Q_c^{\circ 2} - \bar{Q}_c^{\circ 2} + Q_s^{\circ 2} - \bar{Q}_s^{\circ 2}\right] + i\int \mathrm{d}x \widetilde{B}^\dagger\partial_x\widetilde{B} \\ &+ \sum_{\alpha=c,s}\sum_{n=1}^{\infty}\frac{2\pi n}{L}\left(c^\dagger_{\alpha,R,n}c_{\alpha,R,n} - c^\dagger_{\alpha,L,n}c_{\alpha,L,n}\right). \end{aligned} \tag{2.177}$$

This therefore predicts a finite-size spectrum of the form

$$\begin{aligned} P = &\frac{k_F}{\pi\sqrt{2}}\left(\bar{q}_c - q_c\right) + P_{mimp}(k^p) + \frac{2\pi}{L}\left[\left(\frac{q_c+\bar{q}_c}{4\pi} - \gamma_c + \bar{\gamma}_c\right)\left(\frac{q_c-\bar{q}_c}{4\pi} - \gamma_c - \bar{\gamma}_c\right) + \right. \\ &\left.\left(\frac{q_s+\bar{q}_s}{4\pi} - \gamma_s + \bar{\gamma}_s\right)\left(\frac{q_s-\bar{q}_s}{4\pi} - \gamma_s - \bar{\gamma}_s\right)\right] + \frac{2\pi}{L}\sum_{k=c,s}\left(N_k^+ - N_k^-\right), \end{aligned} \tag{2.178}$$

where the $N_k^\pm$ are non-negative integers enumerating the number of particle-hole pairs in the vicinity of the "Fermi points".

2.E.2 Bethe Ansatz calculation: high-energy charge particle

We wish to know the momentum contribution from the high-energy charge particle: there will be finite-size contributions to this from interactions with the low-energy sector. As we know precisely the integers forming this state from (2.38), we can simply sum these integers to find the momentum. This approach, however, yields no information on which contributions come from the finite-size shift of the rapidity and which contributions come from interactions between the high-energy and low-energy degrees of freedom. The solution is to explicitly include the finite-size shift of the rapidity and calculate the remaining corrections in terms of the quantites N_α^{imp}, D_α^{imp}, N_α, D_α, as we had for the finite-size energy.

2.E.2.1 Basic integral equations

The solution for $\rho_{\alpha,1}$ implicitly defined by (2.145), can be formally written as

$$\rho_{\alpha,1}(z_\alpha) = \left(K_{\alpha\beta} * (1-\hat{K})^{-1}_{\beta c}\right)(z_\alpha, k^p). \tag{2.179}$$

We introduce the shift functions[27]

$$\begin{aligned} F^{(0)}_{cc}(k,k') &= 0, \qquad F^{(0)}_{cs}(k,\Lambda) = \frac{1}{2\pi}\theta\left(\frac{\sin k - \Lambda}{u}\right), \\ F^{(0)}_{sc}(\Lambda,k) &= \frac{1}{2\pi}\theta\left(\frac{\Lambda - \sin k}{u}\right), \qquad F_{ss}(\Lambda,\Lambda') = -\frac{1}{2\pi}\theta\left(\frac{\Lambda-\Lambda'}{2u}\right), \end{aligned} \tag{2.180}$$

and the "dressed" shift functions

$$F_{\alpha\beta}(z_\alpha, z_\beta) = F^{(0)}_{\alpha\beta}(z_\alpha, z_\beta) + \left(F_{\alpha\gamma} * K_{\gamma\beta}\right)(z_\alpha, z_\beta). \tag{2.181}$$

It is useful to note that

$$K_{\alpha\beta}(z_\alpha, z_\beta) = \partial_{z_\alpha} F^{(0)}_{\alpha\beta}. \tag{2.182}$$

Both the finite-size energy and momentum spectra involve the function

$$\tilde{r}^{(\sigma)}_{\alpha\beta}(z_\alpha) = K_{\alpha\beta}(z_\alpha, \sigma X^\beta) + K_{\alpha\gamma} * \tilde{r}^{(\sigma)}_{\gamma\beta}. \tag{2.183}$$

2.E.2.2 Finite-size momentum spectrum

As for the energy of the system, the momentum can also be expanded as an asymptotic series in powers of L^{-1}. In the analysis of the finite-size energy calculation, when determining δk^p as in (2.151), one finds

$$\begin{aligned} z_c(k^p_L) = z_{c,0}(k^p) &+ z'_{c,0}(k^p)\frac{\delta k^p}{L} \\ &+ \sum_{\sigma,\beta} \sigma\rho_{\beta,0}(X^\beta)\left[\theta\left(\frac{\sin k^p - \sigma X^\beta}{u}\right)\delta_{\beta,s}\right. \\ &\left. + \int_{-A}^{A} \mathrm{d}\Lambda\,\theta\left(\frac{\sin k^p - \Lambda}{u}\right)\tilde{r}^{(\sigma)}_{s\beta}(\Lambda)\right]\left[X^\beta_\sigma - \sigma X^\beta\right] \\ &+ \frac{1}{L}\int_{-A}^{A}\mathrm{d}\Lambda\,\theta\left(\frac{\sin k^p - \Lambda}{u}\right)\rho_{s,1}(\Lambda). \end{aligned} \tag{2.184}$$

We will first look at the term in the sum multiplied by $X^\beta_\sigma - \sigma X^\beta$. (2.181) and (2.183) imply that

$$F_{\alpha\beta} = F^{(0)}_{\alpha\gamma} * (1-\hat{K})^{-1}_{\gamma\beta}, \qquad \tilde{r}^{(\sigma)}_{\alpha\beta} = (1-\hat{K})^{-1}_{\alpha\gamma} * K_{\gamma\beta}(z_\alpha, \sigma X^\beta), \tag{2.185}$$

allowing us to write

$$F^{(0)}_{c\beta}(k^p, \sigma X^\beta) + F^{(0)}_{c\alpha} * \tilde{r}^{(\sigma)}_{\alpha\beta}(k^p) = F_{c\beta}(k^p, \sigma X^\beta). \tag{2.186}$$

It can also be shown that

$$\int_{-A}^{A} \mathrm{d}\Lambda\, \theta\left(\frac{\sin k - \Lambda}{u}\right) \rho_{s,1}(\Lambda) = 2\pi F_{cc}(k, k^p). \tag{2.187}$$

The finite-size momentum can therefore be written in terms of the dressed shift functions as

$$\begin{aligned} z_c(k^p_L) = z_{c_0}(k^p) + z'_{c,0}(k^p)\frac{\delta k^p}{L} \\ + \sum_{\sigma,\beta} \sigma 2\pi \rho_{\beta,0}(X^\beta) F_{c\beta}(k^p, \sigma X^\beta)\left[X^\beta_\sigma - \sigma X^\beta\right] + \frac{2\pi}{L} F_{cc}(k^p, k^p). \end{aligned} \tag{2.188}$$

We now wish to relate the functions $F_{\alpha\beta}(z_\alpha, z_\beta)$ to the impurity densities N^{imp}_α, D^{imp}_α.

2.E.2.3 Relating shift functions to impurity densities

By using (2.179) and (2.182) in (2.146) and (2.147), it can be shown that

$$2D^{\mathrm{imp}}_\alpha = F_{\alpha c}(X^\alpha, k^p) + F_{\alpha c}(-X^\alpha, k^p), \tag{2.189}$$

$$N^{\mathrm{imp}}_\alpha = F_{\alpha c}(X^\alpha, k^p) - F_{\alpha c}(-X_\alpha, k^p), \tag{2.190}$$

i.e.

$$D^{\mathrm{imp}}_\alpha \pm \frac{N^{\mathrm{imp}}_\alpha}{2} = F_{\alpha c}(\pm X^\alpha, k^p). \tag{2.191}$$

2.E.2.4 A useful identity

To express the finite-size momentum (2.188) in terms of the N^{imp}_α, D^{imp}_α (2.191), we need to relate $F_{\alpha c}(\sigma X^\alpha, k^p)$ to $F_{c\beta}(k^p, \sigma' X^\beta)$. Here we derive a result which explicitly relates the two. In short: we consider the Neumann series of (2.185) and integrate by parts. By definition, we have that

$$F_{\alpha\beta}(z_\alpha, z_\beta) = F^{(0)}_{\alpha\beta}(z_\alpha, z_\beta) + \left(F_{\alpha\gamma} * K_{\gamma\beta}\right)(z_\alpha, z_\beta). \tag{2.192}$$

We can rewrite this as

$$F_{\alpha\beta} = F^{(0)}_{\alpha\gamma} * (1 - \hat{K})^{-1}_{\gamma\beta}, \tag{2.193}$$

$$F_{\alpha\beta} = F^{(0)}_{\alpha\gamma} * \sum_{n=0}^{\infty} (K^n)_{\gamma\beta}. \tag{2.194}$$

Expanding this explicitly, we can write this as (dropping the explicit arguments)

$$F_{\alpha\beta}(z_\alpha, z_\beta) = \sum_{n=0}^{\infty} \left\{ \sum_{\gamma_1,\ldots,\gamma_n} \int \mathrm{d}z_{\gamma_1} \cdots \mathrm{d}z_{\gamma_n} F^{(0)}_{\alpha\gamma_1} K_{\gamma_1,\gamma_2} \cdots K_{\gamma_n,\beta}. \right\} \tag{2.195}$$

Using (2.182), we can recast this as

$$F_{\alpha\beta}(z_\alpha, z_\beta) = \sum_{n=0}^{\infty} \left\{ \sum_{\gamma_1,\ldots,\gamma_n} \int \mathrm{d}z_{\gamma_1} \cdots \mathrm{d}z_{\gamma_n} F^{(0)}_{\alpha\gamma_1} \partial_{\gamma_1} F^{(0)}_{\gamma_1,\gamma_2} \cdots \partial_{\gamma_n} F^{(0)}_{\gamma_n,\beta} \right\}. \tag{2.196}$$

Focussing on just a single term

$$\begin{aligned}
F^{(0)}_{\alpha\gamma} * K_{\gamma\delta} &= \sum_{\gamma} \int \mathrm{d}z_\gamma F^{(0)}_{\alpha\gamma}(z_\alpha, z_\gamma) \partial_\gamma F^{(0)}_{\gamma\delta}(z_\gamma, z_\delta) \\
&= \sum_{\gamma} \int \mathrm{d}z_\gamma \left\{ \partial_\gamma \left[F^{(0)}_{\alpha\gamma}(z_\alpha, z_\gamma) F^{(0)}_{\gamma\delta}(z_\gamma, z_\delta) \right] - \left[\partial_\gamma F^{(0)}_{\alpha\gamma}(z_\alpha, z_\gamma) \right] F^{(0)}_{\gamma\delta}(z_\gamma, z_\delta) \right\} \\
&= \sum_{\gamma\sigma} \sigma F^{(0)}_{\alpha\gamma}(z_\alpha, \sigma X^\gamma) F^{(0)}_{\gamma\delta}(\sigma X^\gamma, z_\delta) - \sum_{\gamma} \int \mathrm{d}z_\gamma \left[\partial_\gamma F^{(0)}_{\alpha\gamma}(z_\alpha, z_\gamma) \right] F^{(0)}_{\gamma\delta}(z_\gamma, z_\delta) \\
&= \sum_{\gamma\sigma} \sigma F^{(0)}_{\alpha\gamma}(z_\alpha, \sigma X^\gamma) F^{(0)}_{\gamma\delta}(\sigma X^\gamma, z_\delta) + K_{\gamma\alpha} \circ F^{(0)}_{\gamma\delta},
\end{aligned} \tag{2.197}$$

$$F^{(0)}_{\alpha\gamma} * K_{\gamma\delta} = F^{(0)}_{\alpha\gamma} \square F^{(0)}_{\gamma\delta} + K_{\gamma\alpha} \circ F^{(0)}_{\gamma\delta}. \tag{2.198}$$

We have defined $\square$ by

$$A_{\alpha\beta} \square B_{\beta\gamma} = \sum_{\sigma,\beta} \sigma A_{\alpha\beta}(z_\alpha, \sigma X^\beta) B_{\beta\gamma}(\sigma X^\beta, z_\gamma), \tag{2.199}$$

and $\circ$ to be convolution over the *first* index i.e.

$$A_{\alpha\beta} \circ B_{\alpha\gamma} = \sum_{\alpha} \int_{-X^\alpha}^{X^\alpha} \mathrm{d}z_\alpha A_{\alpha\beta}(z_\alpha, z_\beta) B_{\alpha\gamma}(z_\alpha, z_\gamma). \tag{2.200}$$

This provides a way of "moving the $F^{(0)}$ to the right". Repeatedly employing this yields

$$\begin{aligned}
F^{(0)}_{\alpha\gamma} * (K^n)_{\gamma\beta} &= \left(F_{\alpha\gamma_1} \square + K_{\gamma_1,\alpha} \circ\right) \left(F_{\gamma_1\gamma_2} \square + K_{\gamma_2,\gamma_1} \circ\right) \cdots \left(F_{\gamma_{n-1}\gamma_n} \square + K_{\gamma_n,\gamma_{n-1}} \circ\right) F^{(0)}_{\gamma_n,\beta}, \\
&= -F^{(0)}_{\beta,\gamma_n} \left(* K_{\gamma_n,\gamma_{n-1}} - \square F_{\gamma_n,\gamma_{n-1}} \right) \cdots \left(* K_{\gamma_1,\alpha} - \square F_{\gamma_1,\alpha} \right).
\end{aligned} \tag{2.201}$$

Putting this all together, this yields the useful identity:

$$F_{\alpha\beta}(z_\alpha, z_\beta) + F_{\beta\alpha}(z_\beta, z_\alpha) = -\sum_{\gamma,\sigma} \sigma F_{\gamma\alpha}(\sigma X^\gamma, z_\alpha) F_{\gamma\beta}(\sigma X^\gamma, z_\beta). \tag{2.202}$$

2.E.2.5 Determining boundary terms

To establish the desired relationship, (2.202) implies that we require the values $F_{\alpha\beta}(\tau X^\alpha, \tau' X^\beta)$. It is simple to show that

$$F_{\alpha\beta}(X^\alpha, X^\beta) - F_{\alpha\beta}(-X^\alpha, X^\beta) = Z_{\alpha\beta} - \delta_{\alpha\beta}, \tag{2.203}$$

with Z the dressed charge matrix as defined in (2.125). (2.202) also implies that

$$\begin{aligned} F_{\alpha\beta}(X^\alpha, X^\beta) + F_{\beta\alpha}(X^\beta, X^\alpha) = -\sum_\gamma \big[& F_{\gamma\alpha}(X^\gamma, X^\alpha) F_{\gamma\beta}(X^\gamma, X^\beta) \\ & - F_{\gamma\alpha}(-X^\gamma, X^\alpha) F_{\gamma\beta}(-X^\gamma, X^\beta) \big] . \end{aligned} \tag{2.204}$$

Substituting (2.203) into (2.204) and simplifying, if we define F to be the matrix $F_{\alpha\beta}(X^\alpha, X^\beta)$, then it satisfies the equation

$$Z^\top F + F^\top Z = (1 - Z)^\top (1 - Z). \tag{2.205}$$

Considering

$$F_{\beta\alpha}(-X^\beta, X^\alpha) - F_{\alpha\beta}(-X^\alpha, X^\beta) = \sum_{\sigma,\gamma} \sigma F_{\gamma\alpha}(\sigma X^\gamma, X^\alpha) F_{\gamma\beta}(-\sigma X^\gamma, X^\beta), \tag{2.206}$$

and using (2.203) again, we find the similar equation

$$Z^\top F - F^\top Z = Z - Z^\top . \tag{2.207}$$

(2.205) and (2.207) determine F uniquely, giving

$$F_{\alpha\beta}(\tau X^\alpha, \tau' X^\beta) = \frac{\tau}{2} (Z - 1)_{\alpha\beta} + \frac{\tau'}{2} \left(Z^{-1^\top} - 1 \right)_{\alpha\beta} . \tag{2.208}$$

This therefore allows us to write down the dressed shift functions appearing in (2.188) in terms of the known quantities N_α^{imp}, D_α^{imp}, viz.

$$F_{cc}(k^p, k^p) = -\sum_\gamma D_\gamma^{\mathrm{imp}} N_\gamma^{\mathrm{imp}}, \tag{2.209}$$

$$F_{c\alpha}(k^p, \tau X^\alpha) = -\sum_\gamma \left(\frac{\tau}{2} N_\gamma^{\mathrm{imp}} {Z^{-1}}^\top_{\gamma\alpha} + D_\gamma^{\mathrm{imp}} Z_{\gamma\alpha} \right) . \tag{2.210}$$

Combining the previous results, we find

$$z_c(k_L^p) = z_{c,0}(k^p) + z'_{c,0}(k^p) \frac{\delta k^p}{L} - \frac{2\pi}{L} \sum_\alpha \left[N_\alpha^{\mathrm{imp}} D_\alpha + D_\alpha^{\mathrm{imp}} \Delta N_\alpha - D_\alpha^{\mathrm{imp}} N_\alpha^{\mathrm{imp}} \right] . \tag{2.211}$$

Using Eq. (8.38) from Ref. [26], the full finite-size momentum spectrum in the presence of a high-energy charge particle is given by

$$\begin{aligned} P = {} & 2D_c k_{F,\uparrow} + 2(D_c + D_s)k_{F,\downarrow} + z_{c,0}(k^p) + 2\pi\rho_{c,0}(k^p)\frac{\delta k^p}{L} \\ & + \frac{2\pi}{L}\left(\Delta\widetilde{\mathbf{N}}^\top \cdot \Delta\widetilde{\mathbf{D}} + \sum_{k\in\{c,s\}} (N_k^+ - N_k^-)\right), \end{aligned} \tag{2.212}$$

where the $N_k^\pm$ are non-negative integers enumerating the number of particle-hole pairs in the vicinity of the Fermi points and $k_{F,\uparrow(\downarrow)} = \frac{1}{2}(\pi n_c \pm 2\pi m)$. In the zero-field limit $m = 0$ and therefore $k_{F,\uparrow} = k_{F,\downarrow} = k_F$, giving

$$\begin{aligned} P = {} & 2k_F\,(2D_c + D_s) + z_{c,0}(k^p) + 2\pi\rho_{c,0}(k^p)\frac{\delta k^p}{L} \\ & + \frac{2\pi}{L}\left(\Delta\widetilde{\mathbf{N}}^\top \cdot \Delta\widetilde{\mathbf{D}} + \sum_{k\in\{c,s\}} (N_k^+ - N_k^-)\right). \end{aligned} \tag{2.213}$$

2.F Mobile impurity contributions to $\sigma^{(2)}(\omega)$

2.F.1 Threshold of the "particle-hole" continuum in $\sigma^{(2)}(\omega)$

Next we examine the thresholds in the second contribution (2.18) to the optical conductivity. The lowest threshold arises in the "particle-hole" and "two-particle" excitations considered in 2.2.2.1 and 2.2.2.2 respectively. The threshold in both cases is given by

$$\begin{aligned} E^{\mathrm{ph}}_{\mathrm{thres}}(q) &= \varepsilon_c(k(q)) - 2\mu, \\ q &= k + \int_{-\infty}^{\infty} \mathrm{d}\Lambda\, \theta\left(\frac{\sin k - \Lambda}{u}\right)\rho_{s,0}(\Lambda), \end{aligned} \tag{2.214}$$

where $\rho_{s,0}(\Lambda)$ is the ground state root density (2.21). The threshold for the particle-hole (two-particle) excitation is obtained by fixing the position of the hole (one of the particles) in momentum space at one of the "Fermi points", so that it contributes only at $\mathcal{O}(L^{-1})$ to the excitation energy. Hence the impurity degree of freedom corresponds to a particle in both cases.

2.F.1.1 Projection of the operator $\mathcal{O}_j$

We will use the representation (2.17) to determine the contribution $C^{(2)}_{\rm JJ}(\ell,t)$ to the current-current correlator. Hence we require the projection of the operator $\mathcal{O}_j$ defined in (2.16) to the mobile impurity model (2.48). This can be worked out by following Ref. [59]. We start by taking the continuum limit of the lattice fermion operators

$$c_{j,\sigma} \sim R_\sigma(x)e^{ik_F x} + L_\sigma(x)e^{-ik_F x} + \dots, \quad x = ja_0 \tag{2.215}$$

where a_0 is the lattice spacing. The continuum limit of $\mathcal{O}_j$ then takes the form

$$\mathcal{O}(x) \sim e^{ix(2k_F-\pi)}R_c\partial_x R_c e^{i\pi\int_{-\infty}^{x}\mathrm{d}x'\,Q_c(x')} + \dots\,, \tag{2.216}$$

with $Q_c(x) = R_c^\dagger(x)R_c(x) + L_c^\dagger(x)L_c(x)$. Next we decompose the charge part into the low-energy and impurity pieces

$$R_c(x) \sim r_c + B^\dagger(x)e^{i(\pi-2k_F)x} + \dots\,. \tag{2.217}$$

Substituting this back into (2.216) and then bosonising the low-energy degrees of freedom we obtain

$$\mathcal{O}(x) \sim B^\dagger(x)e^{-\frac{i}{2\sqrt{2}}\Theta_c^*(x)} + \dots, \tag{2.218}$$

where we have retained only the most relevant piece in the sector with a single impurity.

2.F.1.2 Finite-size excitation energy in the Mobile Impurity Model

As the mobile impurity model is again given by (2.46) to (2.48), and the impurity again is located at a maximum of its dispersion, we can follow through the same steps as in our analysis of the k-Λ string threshold. The finite-size spectrum is, accordingly, of the same form as (2.69). The values of $q_\alpha^{(0)}$ follow from the form of the Luttinger liquid part of (2.218) to be

$$q_c^{(0)} = \bar{q}_c^{(0)} = \pi\sqrt{2}; \qquad q_s^{(0)} = \bar{q}_s^{(0)} = 0. \tag{2.219}$$

2.F.1.3 Finite-size excitation energy from Bethe Ansatz

We consider again the excitation described in Section 2.2.2.1. The finite-size corrections to the excitation energy are calculated in Appendix 2.C. The final result is of the form

$$\begin{aligned} E = {} & e_{GS}L + \varepsilon_c(k^p) + \frac{\delta k^p}{L}\varepsilon_c'(k^p) - \frac{\pi}{6L}(v_c + v_s) \\ & + \frac{2\pi v_c}{L}\left[\frac{(\Delta N_c - N_c^{\mathrm{imp}})^2}{8K_c} + 2K_c\left(D_c - D_c^{\mathrm{imp}} + \frac{D_s - D_s^{\mathrm{imp}}}{2}\right)^2\right] \\ & + \frac{2\pi v_s}{L}\left[\frac{1}{2}\left(\Delta N_s - N_s^{\mathrm{imp}} - \frac{\Delta N_c - N_c^{\mathrm{imp}}}{2}\right)^2 + \frac{(D_s - D_s^{\mathrm{imp}})^2}{2}\right]. \end{aligned} \tag{2.220}$$

Here the ground state energy per site e_{GS} and dressed energy $\varepsilon_c(k)$ are given in (2.23) and (2.24) respectively, while the velocities $v_{s,c}$ and the Luttinger parameter K_c are calculated in Appendix 2.A. The thermodynamic value k^p of the impurity rapidity and its finite-size correction δk^p are determined by (2.150) and (2.154). Finally, we have

$$\Delta N_c = -3\ , \qquad \Delta N_s = -1\ , \qquad D_c = 0\ , \qquad D_s = 0\ , \tag{2.221}$$

$$N_c^{\mathrm{imp}} = 2N_s^{\mathrm{imp}} - 1 = \int_{-Q}^{Q} \mathrm{d}k\, \rho_{c,1}(k)\ , \qquad D_s^{\mathrm{imp}} = 0, \tag{2.222}$$

$$\begin{aligned} 2D_c^{\mathrm{imp}} = {} & \int_Q^{\pi} \mathrm{d}k\, [\rho_{c,1}(-k) - \rho_{c,1}(k)] + \frac{i}{\pi}\left\{\ln\left[\frac{\Gamma\left(\frac{1}{2} - i\frac{\sin k^p}{4u}\right)\Gamma\left(1 + i\frac{\sin k^p}{4u}\right)}{\Gamma\left(\frac{1}{2} + i\frac{\sin k^p}{4u}\right)\Gamma\left(1 - i\frac{\sin k^p}{4u}\right)}\right]\right\} \\ & + \frac{i}{\pi}\int_{-Q}^{Q} \mathrm{d}k\, \rho_{c,1}(k)\left\{\ln\left[\frac{\Gamma\left(\frac{1}{2} - i\frac{\sin k}{4u}\right)\Gamma\left(1 + i\frac{\sin k}{4u}\right)}{\Gamma\left(\frac{1}{2} + i\frac{\sin k}{4u}\right)\Gamma\left(1 - i\frac{\sin k}{4u}\right)}\right]\right\}, \end{aligned} \tag{2.223}$$

where $\rho_{c,1}(k)$ is the solution of the integral equation

$$\rho_{c,1}(k) = \cos k\, R(\sin k - \sin k^p) + \cos k \int_{-Q}^{Q} \mathrm{d}k'\, R(\sin k - \sin k')\rho_{c,1}(k'). \tag{2.224}$$

In order to fully specify our mobile impurity model we also require the the curvature of the dispersion relations of $\varepsilon_c(k)$ at $k = \pi$, which is given by

$$-\frac{1}{m} = \left.\frac{\mathrm{d}^2\varepsilon_c(k(q))}{\mathrm{d}q^2}\right|_{k=\pi} = \frac{2 + \int_{-Q}^{Q} \mathrm{d}k\, R'(\sin k)\varepsilon_c'(k)}{(2\pi\rho_{c,0}(\pi))^2}. \tag{2.225}$$

2.F.1.4 Fixing the parameters γ_α, $\bar{\gamma}_\alpha$

By matching the expressions (2.220) and (2.69) for the finite-size energies we can fix the parameters γ_α, $\bar{\gamma}_\alpha$

$$\begin{aligned} \gamma_c &= \frac{1}{2\sqrt{2}} + \frac{1}{2\sqrt{2}}(\Delta N_c - N_c^{\rm imp}) \ , \qquad \gamma_s = 0 \ , \\ \bar{\gamma}_c &= -\frac{1}{2\sqrt{2}} - \frac{1}{2\sqrt{2}}(\Delta N_c - N_c^{\rm imp}) \ , \qquad \bar{\gamma}_s = 0. \end{aligned} \tag{2.226}$$

2.F.1.5 Current-current correlator in the mobile impurity model

Given the expression (2.218) for the projection of the operator $\mathcal{O}_j$, we have

$$\begin{aligned} C^{(2)}_{\rm JJ}(\ell,t) \sim H(x,t) &= \langle \mathcal{O}^\dagger(x,t)\mathcal{O}(0,0)\rangle \\ &\sim \langle B(x,t) e^{\frac{i}{2\sqrt{2}}\Theta_c^*(x,t)} B^\dagger(0,0) e^{-\frac{i}{2\sqrt{2}}\Theta_c^*(0,0)}\rangle. \end{aligned} \tag{2.227}$$

This is readily calculated using the unitary transformation (2.64). In the new basis the correlator factorises

$$\begin{aligned} H(x,t) &\sim \langle e^{\frac{i}{2\sqrt{2}}(\Delta N_c - N_c^{\rm imp})\Theta_c^\circ(x,t)} e^{-\frac{i}{2\sqrt{2}}(\Delta N_c - N_c^{\rm imp})\Theta_c^\circ(0,0)}\rangle \langle \widetilde{B}(x,t)\widetilde{B}^\dagger(0,0)\rangle \\ &\sim \frac{1}{(x^2 - v_c^2 t^2)^\eta} \int_{-\Lambda}^{\Lambda} \frac{{\rm d}p}{2\pi} e^{-ipx} e^{-i\varepsilon(p)t}, \end{aligned} \tag{2.228}$$

where in this case $\varepsilon(p)$ is given by $\varepsilon_c(\pi + p)$ and

$$\eta = \frac{1}{2K_c}\left(\frac{3}{2} + \frac{N_c^{\rm imp}}{2}\right)^2. \tag{2.229}$$

Fourier transforming and using (2.18) we arrive at

$$\sigma_1^{(2)}(\omega)\Big|_{ph} \sim \frac{1}{\omega}\int_{-\Lambda}^{\Lambda} {\rm d}p\, \widetilde{G}^c_{\eta,\eta}\big(\omega - \varepsilon(p), p\big) \ , \tag{2.230}$$

where $\widetilde{G}^c_{\eta,\eta}(\omega,p)$ is given by (2.91). The behaviour of (2.230) is shown in Fig. 2.16. We see that the contribution vanishes smoothly at the threshold and increases slowly above it.

2.F.2 Threshold of the two-hole continuum in $\sigma_1^{(2)}(\omega)$

Last but not least we wish to consider the threshold of the contribution of the two-hole continuum to $\sigma_1^{(2)}(\omega)$. This occurs at a higher energy than the threshold of the

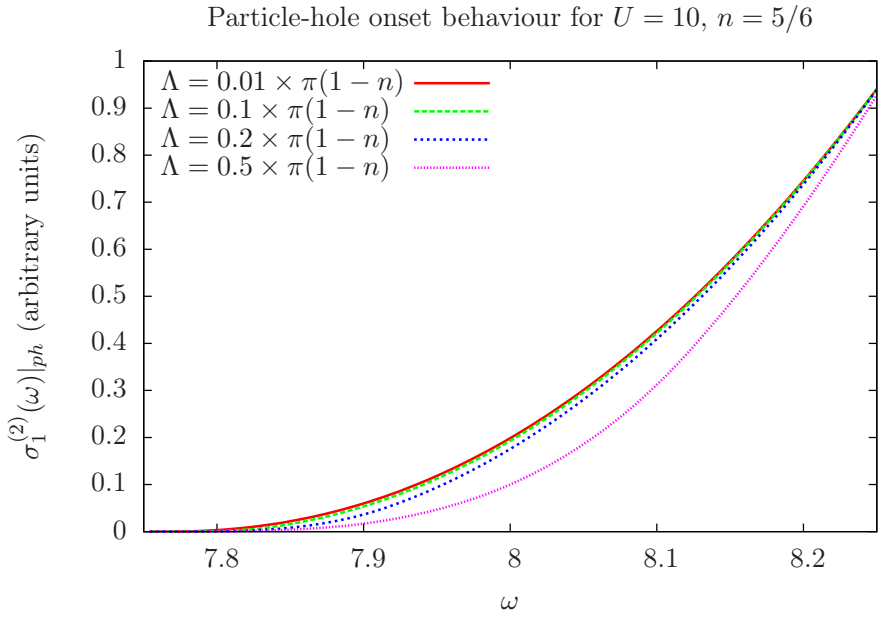

Figure 2.16: Contribution to onset of $\sigma_1^{(2)}(\omega)$ from particle-hole excitation in (2.230) for $U = 10$, $n = 5/6$

particle-hole and particle-particle continua, but unlike the latter two persists as we approach half-filling. The threshold is parametrised by

$$E^{\text{hh}}_{\text{thres}}(q) = -2\varepsilon_c\left(\frac{k(q)}{2}\right) - 2\mu, \tag{2.231}$$

where $k(q)$ is again fixed by (2.214). The threshold corresponds to having *two* high-energy hole excitations with momentum $q/2$ each. As we are now dealing with two impurities with equal momenta, the appropriate mobile impurity model is of the form (2.48), but we now have to retain impurity-impurity interactions

$$\begin{aligned} H_{\text{imp}} = \int \mathrm{d}x \Big[& B^\dagger(x)(\varepsilon - iu\partial_x - \frac{1}{2m}\partial_x^2)B(x) \\ & + V\, B^\dagger(x)\partial_x B^\dagger(x)\; B(x)\partial_x B(x)\Big]. \end{aligned} \tag{2.232}$$

2.F.2.1 Projection of the operator $\mathcal{O}_j$

Next we require the projection of the operator $\mathcal{O}_j$ onto the mobile impurity model. This proceeds as before, cf. eqns (2.215), (2.216), but now we take

$$R_c(x) \sim r_c(x) + B^\dagger(x)e^{-iqx/2}. \tag{2.233}$$

Substituting this into the expression (2.216) for $\mathcal{O}(x)$ we find

$$\mathcal{O}(x) \sim e^{i(2k_F-\pi-q)x} B^\dagger(x)\partial_x B^\dagger(x) e^{\frac{i}{2\sqrt{2}}\Phi_c^*(x)} + \dots \ , \tag{2.234}$$

where we have retained only the most relevant term in the sector with two impurities.

2.F.2.2 Finite-size corrections to excitation energies in the mobile impurity model

The interactions between the mobile impurities and the Luttinger liquid degrees of freedom can again be removed by the unitary transformation (2.64). In the transformed basis finite-size corrections to the excitation energies in the LL part of the theory can then be calculated as before, and lead to the result (2.69).

The zero mode eigenvalues for the "minimal" excitation (cf. (2.70)) associated with $\mathcal{O}(x)$ as defined in (2.234) are

$$q_c^{(0)} = -\pi\sqrt{2} \ , \quad \bar{q}_c^{(0)} = \pi\sqrt{2} \ , \quad q_s^{(0)} = 0 \ , \quad \bar{q}_s^{(0)} = 0. \tag{2.235}$$

2.F.2.3 Finite-size corrections to excitation energies from the Bethe Ansatz

The two-hole excitation has been constructed in 2.2.2.3, and the threshold of interest here occurs when, in the thermodynamic limit, the two holes have equal momentum. The finite-size corrections to the excitation energy can be calculated following Ref. [68], details are given in Appendix 2.D. The final result in zero magnetic field is

$$\begin{aligned} E = e_{GS}L - \varepsilon_c(k^{h_1}) - \varepsilon_c(k^{h_2}) - \frac{\delta k^{h_1}}{L}\varepsilon_c'(k^{h_1}) - \frac{\delta k^{h_2}}{L}\varepsilon_c'(k^{h_2}) - \frac{\pi}{6L}(v_c+v_s) \\ + \frac{2\pi v_c}{L}\left[\frac{(\Delta N_c - N_c^{\rm imp})^2}{8K_c} + 2K_c\left(D_c - D_c^{\rm imp} + \frac{D_s - D_s^{\rm imp}}{2}\right)^2\right] \\ + \frac{2\pi v_s}{L}\left[\frac{1}{2}\left(\Delta N_s - N_s^{\rm imp} - \frac{\Delta N_c - N_c^{\rm imp}}{2}\right)^2 + \frac{(D_s - D_s^{\rm imp})^2}{2}\right]. \end{aligned} \tag{2.236}$$

Here the ground state energy per site e_{GS} and dressed energy $\varepsilon_c(k)$ are given in (2.23) and (2.24) respectively, while the velocities $v_{s,c}$ and the Luttinger parameter K_c are calculated in Appendix 2.A. The thermodynamic values k^{h_i} of the impurity rapidities and the finite-size corrections δk^{h_i} are determined by (2.166) and (2.167). Finally, we

have

$$\Delta N_c = 0\ , \qquad \Delta N_s = -1\ , \qquad D_c = \frac{1}{2}\ , \qquad D_s = 0\ , \tag{2.237}$$

$$N_c^{\rm imp} = 2(N_s^{\rm imp}+1) = \int_{-Q}^{Q} {\rm d}k\, \rho_{c,1}(k)\ , \qquad D_s^{\rm imp} = 0, \tag{2.238}$$

$$\begin{aligned} 2D_c^{\rm imp} = &\int_Q^\pi {\rm d}k\, [\rho_{c,1}(-k)-\rho_{c,1}(k)] - \sum_{j=1,2}\frac{i}{\pi}\left\{\ln\left[\frac{\Gamma\left(\frac{1}{2}-i\frac{\sin k^{h_j}}{4u}\right)\Gamma\left(1+i\frac{\sin k^{h_j}}{4u}\right)}{\Gamma\left(\frac{1}{2}+i\frac{\sin k^{h_j}}{4u}\right)\Gamma\left(1-i\frac{\sin k^{h_j}}{4u}\right)}\right]\right\} \\ &+\frac{i}{\pi}\int_{-Q}^{Q}{\rm d}k\,\rho_{c,1}(k)\left\{\ln\left[\frac{\Gamma\left(\frac{1}{2}-i\frac{\sin k}{4u}\right)\Gamma\left(1+i\frac{\sin k}{4u}\right)}{\Gamma\left(\frac{1}{2}+i\frac{\sin k}{4u}\right)\Gamma\left(1-i\frac{\sin k}{4u}\right)}\right]\right\}, \end{aligned} \tag{2.239}$$

where $\rho_{c,1}(k)$ is the solution of the integral equation

$$\begin{aligned} \rho_{c,1}(k) = &-\cos k\ \left[R(\sin k-\sin k^{h_1})+R(\sin k-\sin k^{h_2})\right] \\ &+\cos k\int_{-Q}^{Q} dk'\ \rho_{c,1}(k')R(\sin k-\sin k'). \end{aligned} \tag{2.240}$$

2.F.2.4 Fixing the parameters γ_α, $\bar\gamma_\alpha$

By comparing the finite-size spectra calculated from the Bethe Ansatz (2.236) with those obtained from the mobile impurity model (2.69) we are again able to determine the parameters γ_α, $\bar\gamma_\alpha$. In the case at hand we obtain

$$\gamma_c+\bar\gamma_c = -\sqrt{2}D_c^{\rm imp}\ , \quad \gamma_c-\bar\gamma_c = -\frac{1}{\sqrt{2}}N_c^{\rm imp}\ , \quad \gamma_s=\bar\gamma_s=0. \tag{2.241}$$

2.F.2.5 Current-current correlator in the mobile impurity model

Given the expression (2.234) for the projection of the operator $\mathcal{O}_j$, we have

$$\begin{aligned} C^{(2)}_{\rm JJ}(\ell,t) &\sim \langle \mathcal{O}^\dagger(x,t)\mathcal{O}(0,0)\rangle \\ &\sim \langle \partial_x B(x,t)B(x,t)e^{-i\Phi_c^*(x,t)/2\sqrt{2}}B^\dagger(0,0)\partial_x B^\dagger(0,0)e^{i\Phi_c^*(0,0)/2\sqrt{2}}\rangle \equiv L(x,t). \end{aligned} \tag{2.242}$$

This is readily calculated using the unitary transformation (2.64). In the new basis the correlator factorises

$$\begin{aligned} L(x,t) = &\langle \partial_x\widetilde{B}(x,t)\widetilde{B}(x,t)\widetilde{B}^\dagger(0,0)\partial_x\widetilde{B}^\dagger(0,0)\rangle \\ &\times\left\langle e^{-i\frac{\frac{1}{2}-2D_c^{\rm imp}}{\sqrt{2}}\Phi_c^\circ(x,t)+i\frac{N_c^{\rm imp}}{\sqrt{2}}\Theta_c^\circ(x,t)}e^{i\frac{\frac{1}{2}-2D_c^{\rm imp}}{\sqrt{2}}\Phi_c^\circ(0,0)-i\frac{N_c^{\rm imp}}{\sqrt{2}}\Theta_c^\circ(0,0)}\right\rangle. \end{aligned} \tag{2.243}$$

The Luttinger liquid part of the correlator is readily calculated

$$L(x,t) = \langle \partial_x \widetilde{B}(x,t)\widetilde{B}(x,t)\widetilde{B}^\dagger(0,0)\partial_x\widetilde{B}^\dagger(0,0)\rangle \big(x - v_c t\big)^{-\nu_+}\big(x + v_c t\big)^{-\nu_-}, \qquad (2.244)$$

where

$$\begin{aligned} \nu_\pm &= 2\left[\sqrt{K_c}\left(\frac{1}{2} - 2D_c^{\rm imp}\right) \mp \frac{N_c^{\rm imp}}{2\sqrt{K_c}}\right]^2, \\ \nu &= \nu_+ + \nu_- = 4K_c\left(\frac{1}{2} - 2D_c^{\rm imp}\right)^2 + \frac{\left(N_c^{\rm imp}\right)^2}{K_c}. \end{aligned} \qquad (2.245)$$

In the absence of interactions between our two high-energy impurities ($V = 0$) the impurity part of the correlator is readily calculated as

$$\langle \partial_x \widetilde{B}(x,t)\widetilde{B}(x,t)\widetilde{B}^\dagger(0,0)\partial_x\widetilde{B}^\dagger(0,0)\rangle \sim \frac{1}{t^{3/2}}\delta(x - ut). \qquad (2.246)$$

In order to gain some insight in the importance of interactions, they can be taken into account in a random phase approximation in the impurity-impurity interaction. Summing up the RPA bubble diagrams does not change the behaviour sufficiently close to the threshold. Putting everything together we find

$$L(x,t) \sim \frac{1}{(x - v_c t)^{\nu_+}}\frac{1}{(x + v_c t)^{\nu_-}}\frac{\delta(x - ut)}{t^{3/2}} + \ldots \qquad (2.247)$$

The resulting contribution to $\sigma_1^{(2)}(\omega)$ for frequencies close to $\omega_0 = -2\mu - 2\varepsilon_c\left(\frac{k(q))}{2}\right)$ is thus

$$\sigma_1^{(2)}(\omega)\Big|_{\rm two-hole} \sim \frac{1}{\omega}\left(\omega - \omega_0\right)^{\nu+\frac{1}{2}}\,\Theta(\omega - \omega_0). \qquad (2.248)$$

As we have pointed out before, the excitation with two high-energy holes persists at half-filling. Importantly, this contribution is no longer suppressed at half-filling, and in fact gives rise to the square root increase above the absolute threshold in the optical conductivity in this limit[25, 109, 118]. Our result (2.248) is reconciled with this behaviour by noting that the frequency range $\omega - \omega_0$ over which (2.248) holds is related to the cutoff Λ_c of the charge sector of the Luttinger liquid degrees of freedom. As we approach half-filling this cutoff tends to zero i.e. the frequency window in which (2.248) applies vanishes. At sufficiently high frequencies $\omega > \omega_0 + \Lambda_c$ we expect on general grounds to recover the square root behaviour observed at half-filling.

Chapter 3

Quantum disentangled liquids in the half-filled Hubbard model

In this chapter, we investigate the existence of quantum disentangled liquid (QDL) states in the half-filled Hubbard model on bipartite lattices. In the one dimensional case we employ a combination of integrability and strong coupling expansion methods to argue that there are indeed finite energy-density eigenstates that exhibit a "weak" form of QDL behaviour. In particular we show that measuring the spin degrees of freedom in these states leaves the system in an area-law entangled state order-by-order in the strong coupling expansion. The states exhibiting the QDL property are atypical in the sense that their entropy density is smaller than that of thermal states at the same energy density. We argue that within a certain temperature window parametrically large in U, the thermal states also exhibit a weaker form of the QDL property.

The question of how isolated many-particle quantum systems relax and how to describe their steady state behaviour has attracted attention for a long time[135]. The past decade has witnessed a tremendous resurgence of interest in this problem, which was largely motivated by ground-breaking experiments on systems of trapped ultra-cold atoms[136–146]. It is now understood that generic many-body systems relax towards thermal equilibrium distributions at an effective temperature fixed by the energy density, which is by definition conserved for isolated systems. This behaviour follows from the eigenstate thermalisation hypothesis (ETH)[32, 72, 87, 147]. When

a system thermalises the only information about the initial state that is retained at late times is its energy density. This does not, however, exhaust the theoretically understood paradigms of relaxation: quantum integrable systems possess conservation laws which constrain the system to retain information on more than just the energy density. As such, they do not thermalise, but instead relax towards Generalised Gibbs Ensembles [33, 73–77]. This can be understood in terms of a generalised ETH[78, 148]. Sufficiently strong disorder is another mechanism that can preclude thermalisation[79–82, 149, 150]. This can again be related to the existence of conservation laws[84, 85, 150], although, unlike in the integrable case, no fine-tuning is required. Moreover, in (many-body) localised systems eigenstates at finite energy densities exhibit an area-law scaling of the entanglement entropy. This is qualitatively different to cases in which the ETH holds and differs dramatically from the situation encountered in integrable models as well.

Recently it has been proposed that the eigenstates of certain systems may fail to thermalise in the conventional sense. The corresponding state of matter has been dubbed the "quantum disentangled liquid" (QDL)[86]. A characteristic feature of such systems is that they comprise both heavy and light degrees of freedom. The basic premise of the QDL concept is that while the heavy degrees of freedom are fully thermalised, the light ones, which are enslaved to the heavy particles, are not independently thermalised. A convenient diagnostic for such a state of matter is the bipartite entanglement entropy (EE) after a projective measurement of the heavy particles. The possibility of realising a QDL in the one dimensional Hubbard model was subsequently investigated by exact diagonalisation of small systems in Ref. [88]. Given the limitations on accessible system sizes it is difficult to draw definite conclusions from these results. Motivated by these studies we have recently explored the possibility of realising a QDL in the half-filled Hubbard model on bipartite lattices by analytic means[91]. The Hamiltonian of the one-dimensional Hubbard model is

$$H = -t \sum_{j,\sigma=\uparrow,\downarrow} \left(c^{\dagger}_{j,\sigma} c_{j+1,\sigma} + c^{\dagger}_{j+1,\sigma} c_{j,\sigma} \right) + U \sum_{j} \left(n_{j,\uparrow} - \frac{1}{2} \right) \left(n_{j,\downarrow} - \frac{1}{2} \right). \tag{3.1}$$

We recall that at half-filling (one electron per site) (3.1) is invariant under the η-

pairing SU(2) symmetry with generators[151]

$$\eta^z = \frac{1}{2}\sum_j \left(n_{j,\uparrow} + n_{j,\downarrow} - 1\right), \qquad \eta^\dagger = \sum_j (-1)^j c^\dagger_{j,\uparrow} c^\dagger_{j,\downarrow} \equiv (\eta)^\dagger . \tag{3.2}$$

The outline of this chapter is as follows. In Section 3.1 we briefly recall necessary facts from the exact solution of the Hubbard model. In Section 3.2 we consider typical states at finite temperature. In Section 3.3 we employ methods of integrability to show that it is possible to construct particular eigenstates at finite energy densities for which the charge degrees of freedom do not contribute to the volume term in the bipartite EE, corroborating the notion of the QDL diagnostic proposed in Ref. [86]. In Section 3.5 we show that there exists a parametrically large regime in which thermal states support a weaker version of QDL as proposed in Ref. [91]. We turn to strong-coupling techniques in Section 3.6 to address the question at the level of the wavefunction,

3.1 Eigenstates of the Hubbard Hamiltonian

The one-dimensional Hubbard model is exactly solvable by the Bethe Ansatz method [26]. Within the framework of the string hypothesis, eigenstates in the Hubbard model are determined by solutions to *Takahashi's equations*[26]. For a state with N electrons, M of which are spin-down, the Takahashi equations can be found in Section 1.5.2 on page 25. In the framework of the string hypothesis each set $\{I_j, J^n_\alpha, J'^m_\beta\}$ of (half-odd) integers gives rise to a unique eigenstate of the Hubbard Hamiltonian. In particular, the ground state for even lattice length L, even total number of electrons N_{GS} and odd number of down spins M_{GS} is obtained by the choice[26]

$$I_j = -\frac{N_{GS}}{2} - \frac{1}{2} + j, \qquad j = 1, \ldots, N_{GS}, \tag{3.3}$$

$$J^1_\alpha = -\frac{M_{GS}}{2} - \frac{1}{2} + \alpha, \qquad \alpha = 1, \ldots, M_{GS}. \tag{3.4}$$

3.1.1 Macro states at finite energy densities

Taking the thermodynamic limit, the Bethe Ansatz allows a description of macro states corresponding to smooth root distributions. We now use this framework to

identify a class of macro states that exhibits characteristic properties of a QDL. Using the string hypothesis general macro states in the one dimensional Hubbard model can be described by sets of particle and hole densities $\{\rho^p(k), \rho^h(k), \sigma_n^p(\Lambda), \sigma_n^h(\Lambda), {\sigma'_n}^p(\Lambda), {\sigma'_n}^h(\Lambda) | n \in \mathbb{N}\}$ that are subject to the thermodynamic limit of the Bethe Ansatz equations[26]

$$\begin{aligned}
\rho^p(k) + \rho^h(k) &= \frac{1}{2\pi} + \cos k \sum_{n=1}^{\infty} \int_{-\infty}^{\infty} \mathrm{d}\Lambda\, a_n(\Lambda - \sin k) \left[{\sigma'_n}^p(\Lambda) + \sigma_n^p(\Lambda)\right] \ , \\
\sigma_n^h(\Lambda) &= -\sum_{m=1}^{\infty} \int_{-\infty}^{\infty} d\Lambda' A_{nm}(\Lambda - \Lambda')\ \sigma_m^p(\Lambda') + \int_{-\pi}^{\pi} \mathrm{d}k\, a_n(\sin k - \Lambda)\ \rho^p(k) \ , \\
{\sigma'_n}^h(\Lambda) &= \frac{1}{\pi} \mathrm{Re} \frac{1}{\sqrt{1 - (\Lambda - inu)^2}} - \sum_{m=1}^{\infty} \int_{-\infty}^{\infty} d\Lambda' A_{nm}(\Lambda - \Lambda')\ {\sigma'_m}^p(\Lambda') \\
&\quad - \int_{-\pi}^{\pi} \mathrm{d}k\, a_n(\sin k - \Lambda)\ \rho^p(k) \ .
\end{aligned} \tag{3.5}$$

Here $u = U/4t$ and

$$\begin{aligned}
a_n(x) &= \frac{1}{2\pi} \frac{2nu}{(nu)^2 + x^2} \ , \\
A_{nm}(x) &= \delta(x) + (1 - \delta_{m,n}) a_{|n-m|}(x) + 2a_{|n-m|+2}(x) + \cdots + 2a_{|n+m|-2}(x) + a_{n+m}(x).
\end{aligned} \tag{3.6}$$

The energy and thermodynamic entropy per site are then given by

$$\begin{aligned}
e &= u + \int_{-\pi}^{\pi} \mathrm{d}k\, [-2\cos k - \mu - 2u]\, \rho^p(k) + 4 \sum_{n=1}^{\infty} \int d\Lambda\, {\sigma'_n}^p(\Lambda)\, \mathrm{Re} \sqrt{1 - (\Lambda + inu)^2}, \\
s &= \int_{-\pi}^{\pi} \mathrm{d}k\, \mathcal{S}\left[\rho^p(k), \rho^h(k)\right] + u + \sum_{n=1}^{\infty} \int_{-\infty}^{\infty} d\Lambda\ \mathcal{S}\left[{\sigma'_n}^p(\Lambda), {\sigma'_n}^h(\Lambda)\right] \\
&\quad + \sum_{n=1}^{\infty} \int_{-\infty}^{\infty} d\Lambda\ \mathcal{S}\left[{\sigma_n}^p(\Lambda), {\sigma_n}^h(\Lambda)\right] ,
\end{aligned} \tag{3.7}$$

where we have defined

$$\mathcal{S}[f, g] = \big[f(x) + g(x)\big] \ln\big(f(x) + g(x)\big) - f(x) \ln\big(f(x)\big) - g(x) \ln\big(g(x)\big) \ . \tag{3.8}$$

The ground state of the half-filled Hubbard model in zero magnetic field is obtained by choosing

$$\rho^h(k) = 0 = \sigma_1^h(\Lambda) \ , \qquad {\sigma'}_n^p(\Lambda) = 0 = \sigma_{n\geq 2}^p(\Lambda) \ . \tag{3.9}$$

3.2 Typical vs atypical energy eigenstates

A characteristic property of integrable models is that at finite energy densities relative to the ground state there exist thermal states as well as *atypical finite entropy density states* that have rather different properties. The existence of such states is intimately related to the presence of an extensive number of higher conservation laws. Their nature can be easily understood by considering the special limit of non-interacting fermions ($U = 0$). Here the half-filled ground state is simply

$$|\mathrm{GS}\rangle_{U=0} = \prod_{\sigma,|k_j|<\pi/2} c^\dagger_\sigma(k_j)|0\rangle \ , \tag{3.10}$$

where $c_\sigma(k) = L^{-1/2}\sum_j e^{ikj}c_{j,\sigma}$. Thermal states at finite energy densities are Fock states with momentum distribution function

$$\rho^p_\sigma(k) = \frac{1}{2\pi[1+e^{-2\cos(k)/T}]} \ . \tag{3.11}$$

In a large, finite volume we can construct thermal Fock states by using the relation $\rho^p_\sigma(k_j) = \frac{1}{L(k_{j+1}-k_j)} + o(1)$. A simple atypical state at a finite energy density above the ground state is obtained by splitting the Fermi sea

$$|\text{split FS}\rangle = \prod_{\sigma,\frac{\pi}{4}<|k_j|<\frac{3\pi}{4}} c^\dagger_\sigma(k_j)|0\rangle \ . \tag{3.12}$$

The energy eigenstate (3.12) is clearly not thermal. Moreover, the corresponding macro state has zero entropy density in the thermodynamic limit. However, it is easy to see that by considering other arrangements of the momentum quantum numbers one can arrive at atypical states that have finite entropy densities in the thermodynamic limit [152]. The situation in integrable models is a straightforward generalisation of this construction. The relevant quantum numbers are the (half-odd)integer numbers that characterise the solutions of the Bethe Ansatz equations.

3.2.1 Thermal states in the Hubbard model

Thermal states are by construction the most likely states at a given energy density. To obtain their description in terms of particle and hole distribution functions we

need to maximise the entropy density s at a fixed energy density e. To that end it is customary to extremise the free energy per site $f = e - Ts$, where e and s are given in (3.7)

$$\begin{aligned} 0 = \delta f = &\int_{-\pi}^{\pi} \mathrm{d}k \left[\frac{\delta f}{\delta \rho^p(k)} \delta \rho^p(k) + \frac{\delta f}{\delta \rho^h(k)} \delta \rho^h(k) \right] \\ &+ \sum_{n=1}^{\infty} \int_{-\infty}^{\infty} d\Lambda \left[\frac{\delta f}{\delta {\sigma'}_n^p(\Lambda)} \delta {\sigma'}_n^p(\Lambda) + \frac{\delta f}{\delta {\sigma'}_n^h(\Lambda)} \delta {\sigma'}_n^h(\Lambda) \right. \\ &\left. + \frac{\delta f}{\delta \sigma_n^p(\Lambda)} \delta \sigma_n^p(\Lambda) + \frac{\delta f}{\delta \sigma_n^h(\Lambda)} \delta \sigma_n^h(\Lambda) \right]. \end{aligned} \tag{3.13}$$

The relations (3.5) connect hole and particle densities and need to be taken into account as constraints. The extremisation leads to a system of non-linear integral equations that fixes the ratios

$$\zeta(k) = \frac{\rho^h(k)}{\rho^p(k)}\,, \quad \eta_n(\Lambda) = \frac{\sigma_n^h(\Lambda)}{\sigma_n^p(\Lambda)}\,, \quad \eta'_n(\Lambda) = \frac{{\sigma'}_n^h(\Lambda)}{{\sigma'}_n^p(\Lambda)}. \tag{3.14}$$

For the Hubbard model in zero magnetic field the resulting *Thermodynamic Bethe Ansatz equations* read [26, 153]

$$\begin{aligned} \ln \zeta(k) = &\frac{-2\cos k - \mu - 2u}{T} + \sum_{n=1}^{\infty} \int_{-\infty}^{\infty} \mathrm{d}\Lambda\, a_n(\sin k - \Lambda) \ln\left(1 + \frac{1}{\eta'_n(\Lambda)}\right) \\ &- \sum_{n=1}^{\infty} \int_{-\infty}^{\infty} \mathrm{d}\Lambda\, a_n(\sin k - \Lambda) \ln\left(1 + \frac{1}{\eta_n(\Lambda)}\right), \\ \ln\left(1 + \eta_n(\Lambda)\right) = &- \int_{-\pi}^{\pi} \mathrm{d}k\ \cos(k)\ a_n(\sin k - \Lambda) \ln\left(1 + \frac{1}{\zeta(k)}\right) + \sum_{m=1}^{\infty} A_{nm} * \ln\left(1 + \frac{1}{\eta_m}\right)\Bigg|_{\Lambda}, \\ \ln\left(1 + \eta'_n(\Lambda)\right) = &\frac{4\mathrm{Re}\sqrt{1 - (\Lambda - inu)^2} - 2n\mu - 4nu}{T} \\ &- \int_{-\pi}^{\pi} \mathrm{d}k\ \cos(k)\ a_n(\sin k - \Lambda) \ln\left(1 + \frac{1}{\zeta(k)}\right) + \sum_{m=1}^{\infty} A_{nm} * \ln\left(1 + \frac{1}{\eta'_m}\right)\Bigg|_{\Lambda}. \end{aligned} \tag{3.15}$$

The system (3.15) can be solved numerically to calculate the energy density and other simple thermodynamic properties of typical states at finite energy density. The free energy per site is given in terms of the solution of (3.15) by[26]

$$f = -T \int_{-\pi}^{\pi} \frac{\mathrm{d}k}{2\pi} \ln\left(1 + \frac{1}{\zeta(k)}\right) + u - T \sum_{n=1}^{\infty} \int_{-\infty}^{\infty} \frac{\mathrm{d}\Lambda}{\pi} \ln\left(1 + \frac{1}{\eta'_n(\Lambda)}\right) \mathrm{Re} \frac{1}{\sqrt{1 - (\Lambda - inu)^2}}. \tag{3.16}$$

3.2.2 Simple families of atypical finite entropy density states in the Hubbard model

It is instructive to explicitly construct families of atypical macro states with finite entropy densities, which allow one to obtain closed-form expressions for the energy density and double occupancy

$$d = \frac{1}{L}\Big\langle \sum_j n_{j,\uparrow} n_{j,\downarrow} \Big\rangle \ , \tag{3.17}$$

in the thermodynamic limit. In terms of the Bethe Ansatz, the states we wish to consider involve "freezing" the microscopic configuration of the charge sector to that of the ground state at half-filling. More precisely, we consider the following two-parameter family of macro states

$$\sigma'^p_n(\Lambda) = 0 \ , \quad \rho^h(k) = 0 \ , \quad \sigma^h_1(\Lambda) = x\sigma^p_1(\Lambda), \qquad \sigma^h_n(\Lambda) = y\sigma^p_n(\Lambda). \tag{3.18}$$

The choice (3.18) enables us to solve the thermodynamic limit of the Bethe Ansatz equations (3.5) by Fourier techniques. In particular we find that the Fourier transforms of the particle densities in the spin sector $\widetilde{\sigma}_n(\omega) = \int \mathrm{d}\Lambda e^{i\omega\Lambda}\sigma^p_n(\Lambda)$ fulfil

$$\begin{gathered}\begin{pmatrix}\widetilde{\sigma}_1(\omega)\\ \widetilde{\sigma}_n(\omega)\end{pmatrix} = M^{-1}\begin{pmatrix}J_0(\omega)e^{-u|\omega|}\\ J_0(\omega)e^{-nu|\omega|}\end{pmatrix},\\ M = \begin{pmatrix}1+x+e^{-2u|\omega|} & 2e^{-nu|\omega|}\cosh u\omega\\ 2e^{-nu|\omega|}\cosh u\omega & 1+y+2\frac{e^{-2nu|\omega|}-e^{-2u|\omega|}}{e^{-2u|\omega|}-1}+e^{2nu|\omega|}\end{pmatrix}.\end{gathered} \tag{3.19}$$

We are particularly interested in spin singlet states. By the theorem of Refs [154, 155] a sufficient condition for obtaining a singlet is for the S^z eigenvalue to be zero, which imposes the constraint

$$\widetilde{\sigma}_1(0) + n\widetilde{\sigma}_n(0) = \frac{1}{2}. \tag{3.20}$$

Combining this with (3.19) leads to the n-independent requirement $xy = 0$. As $x = 0$ corresponds to the ground state we choose $y = 0$. This corresponds to a finite density of holes for 1-strings and a filled Fermi sea for n-strings. The energy density for the atypical macro states constructed in this way is

$$e_n(x) = -4\int_0^\infty \frac{\mathrm{d}\omega}{\omega} J_0(\omega)J_1(\omega)\frac{1+e^{-2u\omega}+e^{(2-2n)u\omega}(-1+x)-e^{-2nu\omega}(1+x)}{(1+e^{-2u\omega})(1-e^{(4-2n)u\omega}+e^{2u\omega}(1+x)-e^{(2-2n)u\omega}(1+x))}. \tag{3.21}$$

By taking derivatives with respect to u, we can calculate the double occupancy d as

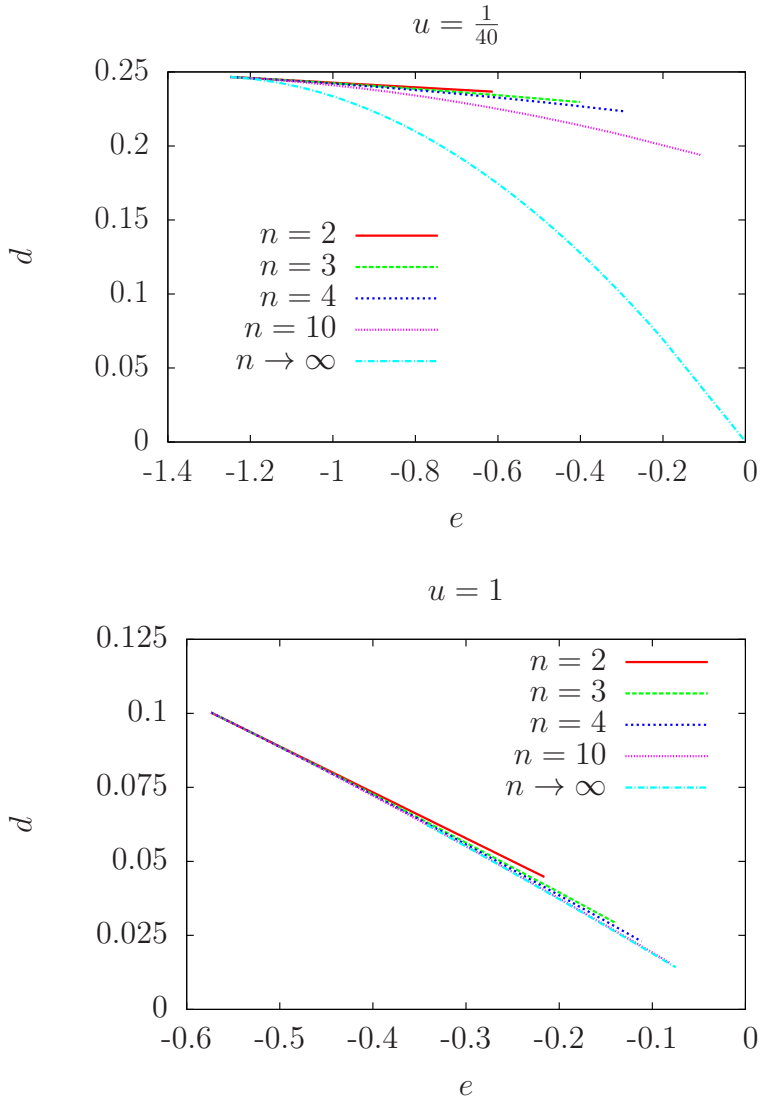

Figure 3.1: e vs d curves for $u = 1/40$ and $u = 1$ respectively, showing states occupying 1-strings and n-strings

a function of x, and combining this with (3.21) we can study how d changes with e for the different families n. The results are shown in Fig. 3.1.

3.2.3 Double occupancy for thermal vs atypical states

It is interesting to compare the behaviour of the double occupancy in thermal states and the particular family of atypical states as identified above in Section 3.2.2. We

can calculate the energy density and double occupancy for typical states using the free energy of (3.16) as

$$\langle e\rangle_\beta = \frac{\partial}{\partial\beta}(\beta f), \qquad \langle d\rangle_\beta = \frac{\partial f}{\partial U} + \frac{1}{4}, \tag{3.22}$$

where we have used the fact that we are working at half-filling. This determines d as an implicit function of e for thermal states. We note that this is of experimental relevance, as recent ultra-cold atomic experiments are able to directly measure the double occupancy in realisations of the one-dimensional Hubbard model[156].

In Fig. 3.2 we present results for the double occupancy as a function of the energy density for thermal states at several values of the interaction strength u. These are compared to the corresponding results for the finite entropy density atypical states with $n = 4$ constructed in Section 3.2.2. We see that as the interaction strength

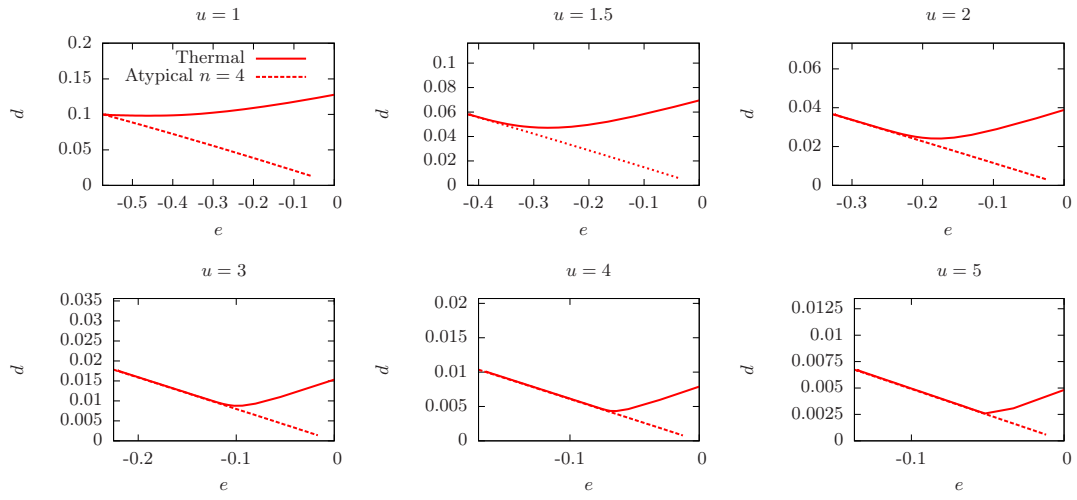

Figure 3.2: Double occupancy d as a function of the energy density for thermal (solid lines) and atypical states (dashed lines).

u is increased, the results for thermal and atypical states track one another for an increasing range of energy densities. On the other hand, for small values of u the double occupancies of thermal and atypical states are very different at all energy densities. These results can be used to shed some light on the role played by finite-size effects in the exact diagonalisation results of Ref. [88]. There the double occupancy was computed on lattices of up to $L = 12$ sites and a very interesting change in

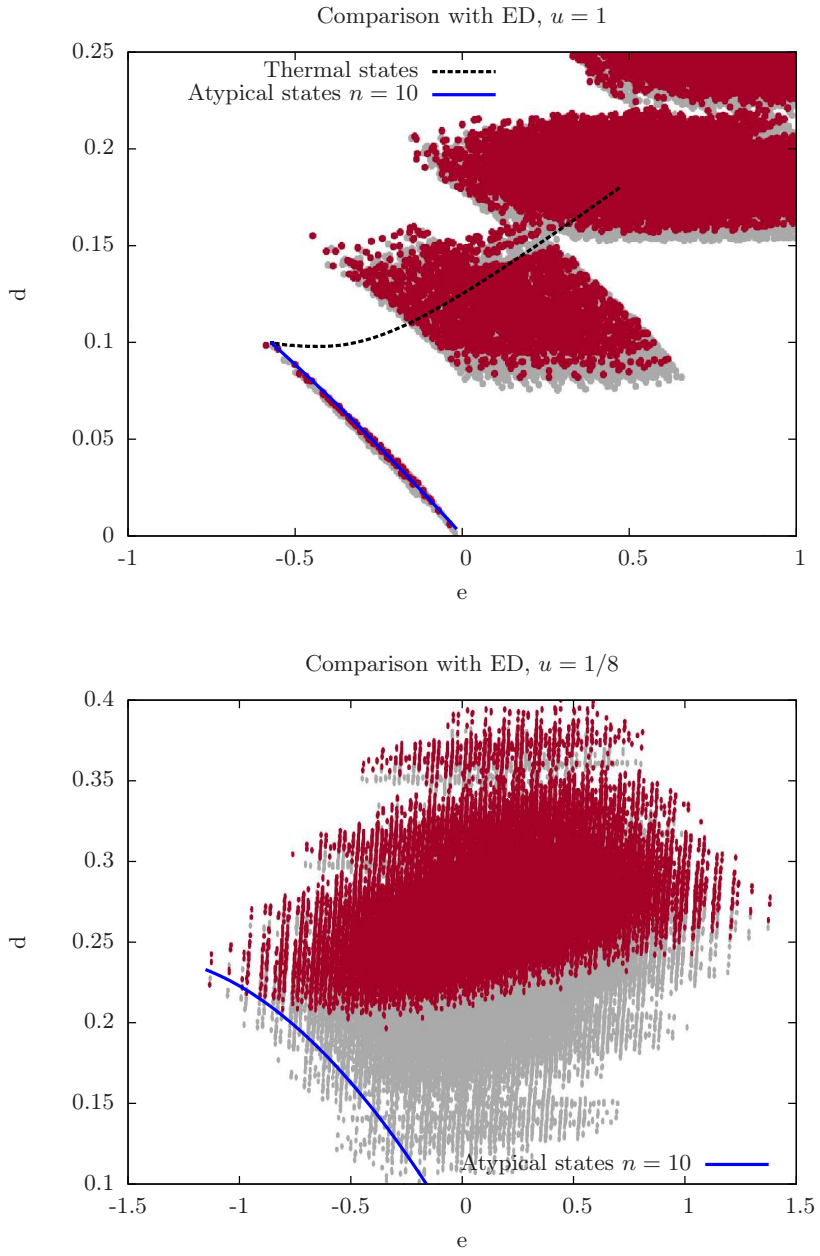

Figure 3.3: Comparison of thermal and typical states with exact diagonalisation data of Ref. [88]. Here the points indicate expectation values for eigenstates of the Hubbard model, where the spin singlets are highlighted in red.

behaviour of $e(d)$ was observed as a function of u. As shown in Fig. 3.3, for sufficiently large values of u the there is a "band" of eigenstates in the $d-e$ plane that minimises d at fixed e and is separated from the region traced out by the other eigenstates. This

is easily understood in terms of typical and atypical eigenstates. The special band of states is seen to track the $d(e)$ of our $n = 10$ family of atypical states, while for most of the states $d(e)$ is centred around the result for typical states in the thermodynamic limit (as the system size in the numerical study is quite small we expect a significant spread around the thermodynamic limit result). At small values of u the atypical states are no longer visible in $L = 12$ numerical data, which are now all spread around the thermal thermodynamic limit result. This discrepancy has its origin in the strength of finite-size effects, which are more pronounced in the small-u limit.

3.3 Particular atypical energy eigenstates: the "Heisenberg sector"

In Ref. [88] it was suggested that a particular class of eigenstates of the Hubbard Hamiltonian possess the *quantum disentangled liquid* property. These states were identified for short chains by considering the strong coupling regime $t \ll U$. In this regime the spectrum breaks up into a sequence of narrow "bands" of states, which can be characterised by the expectation value of the double occupancy number operator. The states of interest constitute the lowest such band and are adiabatically connected to eigenstates without any doubly occupied sites in the limit $t/U \to 0$. As we are interested in the limit $L \to \infty$ at fixed U our first task is to identify such states in terms of the Bethe Ansatz solution. This can be done either at the level of micro states in a (large) finite volume, or in terms of macro states in the thermodynamic limit [91].

3.3.1 Micro states

An important property of the exact solution of the Hubbard model is that it makes it possible to follow the evolution of particular eigenstates with the interaction parameter u. In the framework of the string hypothesis[26] there is a one-to-one correspondence between energy eigenstates and solutions to the Bethe Ansatz equations (1.45), which in turn are uniquely characterised by sets of (half-odd) integers I_j, J_α^n,

J'^n_α. Fixing a particular set $\{I_j, J^n_\alpha, J'^n_\alpha\}$ we may follow the corresponding solution of (1.45) as a function of u. This allows us to identify the special states considered in Ref. [88] as follows. In the limit $U \to \infty$ at fixed L and half filling, the lowest energy states are obtained by setting

$$M' = 0 \ , \tag{3.23}$$

i.e. considering only states that do not contain any k-Λ strings. This is because the latter contribute $\mathcal{O}(u)$ to the total energy,*cf.* (1.49). These states are characterised by the quantum numbers J^n_α, which have ranges

$$|J^n_\alpha| \leq \frac{1}{2}\left(\frac{L}{2} - \sum_{n=1}^{\infty} t_{nm} M_m - 1\right), \quad \alpha = 1, \ldots, M_n. \tag{3.24}$$

There is no freedom in choosing the I_j: they are given by

$$I_j = \begin{cases} -\frac{L}{2} + j & \text{if } \sum_m M_m \text{ is even} \\ -\frac{L+1}{2} + j & \text{if } \sum_m M_m \text{ is odd} \end{cases}, \quad j = 1, \ldots L. \tag{3.25}$$

Importantly, the I_j form a completely filled Fermi sea, just as they do in the ground state of the half-filled Hubbard model. It follows from the results of Ref. [157] that the total number of such states is 2^L. We call these states *Heisenberg sector states*.

3.3.2 Macro states

At the level of macro states the Heisenberg sector corresponds to the requirement

$$\rho^h(k) = 0 = \sigma'^p_n(\Lambda) \ , \ n = 1, 2, \ldots \tag{3.26}$$

We note that the correspondence between (3.26) and the microscopic definition of 3.3.1 is to be understood in a thermodynamic fashion. There clearly will be eigenstates that are captured by (3.26), but go beyond the narrow specification we used in 3.3.1. For example, adding a finite number of k-Λ strings will not change the macro state (3.26), as this affect the densities only to order $\mathcal{O}(L^{-1})$.

Importantly, the "freezing" of the charge degrees of freedom that characterises the Heisenberg sector implies that the thermodynamic entropy density for these macro states depends only on the spin degrees of freedom

$$s = \sum_{n=1}^{\infty} \int_{-\infty}^{\infty} d\Lambda \ \mathcal{S}\left[\sigma^p_n(\Lambda), \sigma^h_n(\Lambda)\right]. \tag{3.27}$$

3.3.2.1 Maximal entropy states in the Heisenberg sector

The next question we want to address is which macro states in the Heisenberg sector maximise the entropy at a given energy density. These states would be selected with probability one if one randomly picked an eigenstate at a given energy density in an asymptotically large system. We start from the thermodynamic limit of the Takahashi equations (3.5) for Heisenberg sector states

$$\begin{aligned}\rho^p(k) &= \frac{1}{2\pi} + \cos k \sum_{n=1}^{\infty} \int_{-\infty}^{\infty} \mathrm{d}\Lambda\, a_n(\Lambda - \sin k)\sigma_n^p(\Lambda)\ , \\ \sigma_n^h(\Lambda) &= -\sum_{m=1}^{\infty} \int_{-\infty}^{\infty} \mathrm{d}\Lambda'\, A_{nm}(\Lambda - \Lambda')\ \sigma_m^p(\Lambda') + \int_{-\pi}^{\pi} \mathrm{d}k\, a_n(\sin k - \Lambda)\, \rho^p(k)\ .\end{aligned} \tag{3.28}$$

We then define an analogue of the free energy density by

$$f = e - \mathcal{T} s\ , \tag{3.29}$$

where e and s are the energy and entropy densities of Heisenberg sector states and are given by (3.7) and (3.27) respectively. The "temperature" $\mathcal{T}$ is understood simply as a Lagrange parameter that allows us to fix the energy density. We now extremise the free energy with respect to the particle and hole densities, subject to (3.28). This fixes the ratios $\eta_n(\Lambda) = \frac{\sigma_n^h(\Lambda)}{\sigma_n^p(\Lambda)}$ to be solutions to the system of TBA-like equations

$$\ln\big(1 + \eta_n(\Lambda)\big) = \frac{g_1(\Lambda)}{\mathcal{T}} + \sum_{m=1}^{\infty} \int_{-\infty}^{\infty} d\Lambda'\ A_{nm}(\Lambda - \Lambda') \ln\left[1 + \frac{1}{\eta_n(\Lambda')}\right], \tag{3.30}$$

where $g_1(\Lambda) = -4\mathrm{Re}\sqrt{1 - (\Lambda - inu)^2} + 4nu$. The entropy density for these macro states is given by

$$s = \sum_{n=1}^{\infty} \int_{-\infty}^{\infty} d\Lambda \left[\frac{g_1(\Lambda)}{\mathcal{T}} \sigma_n^p(\Lambda) + g_2(\Lambda) \ln\big(1 + \eta_n^{-1}(\Lambda)\big)\right], \tag{3.31}$$

where $g_2(\Lambda) = \frac{1}{\pi}\mathrm{Re}\frac{1}{\sqrt{1-(\Lambda+inu)^2}}$.

3.4 Entanglement entropy of Heisenberg sector states

As we have seen above, the Bethe Ansatz solution of the Hubbard model provides us with a means to compute the thermodynamic entropy density for any macro state.

On the other hand, the notion of a QDL involves entanglement properties after a partial measurement. Implementing such partial measurements in the Bethe Ansatz framework is beyond currently available methods. However, some information about entanglement properties of energy eigenstates can be inferred as follows. For short-ranged Hamiltonians there is a relation between the thermodynamic and entanglement entropies: if we consider a large subsystem A of size $|A|$ in the thermodynamic limit, the volume term in the entanglement entropy of an eigenstate $|\Psi\rangle$ is given by

$$S_{\mathrm{vN,A}} = s|A| + o(|A|), \tag{3.32}$$

where s is the thermodynamic entropy density. As we have seen in (3.27), the thermodynamic entropy density of Heisenberg sector states depends only on the spin degrees of freedom. This then implies that the volume term in the entanglement entropy is independent of the charge degrees of freedom, and depends on the spin sector only. In particular, as (3.32) is based only on the properties of the macro state under consideration, we know that microscopic rearrangements in the charge sector, such as introducing k-Λ strings, will not affect (3.32). The emerging picture is consistent with expectations for a QDL state: the spin degrees of freedom exhibit a volume law entanglement entropy, while the charge degrees of freedom are only weakly entangled. The spin degrees of freedom will be "heavy" in the terminology of Ref. [86] at large values of U, because their bandwidth is proportional to t^2/U. The bandwidth of the charge degrees of freedom remains $\mathcal{O}(t)$ and they are therefore "light" in comparison. We stress that Heisenberg states obey (3.32) for any value of u, and the heavy vs light separation is not required. This is presumably a consequence of integrability.

Considerations based on the von Neumann entanglement entropy fall short of the full QDL diagnostic proposed in Ref. [86], which requires carrying out a partial measurement of the spin degrees of freedom. Evidence based on a strong coupling analysis that supports the view that Heisenberg sector states pass the full QDL diagnostic has been put forward in Ref. [91].

3.5 Thermal states in the large-U limit

We have constructed an exponential (in the system size) number of eigenstates, which exhibit QDL behaviour in the thermodynamic limit. However, these states are atypical in the sense introduced above: the most likely states at a given energy density are thermal. It is therefore instructive to contrast the entanglement properties of Heisenberg sector states to those of typical states. The latter are given as solutions of the systems (3.15) and (3.5) of coupled integral equations. While it is not possible to solve these analytically in general, in the limit of strong interactions analytic results can be obtained [158–160]. This is also the most interesting in the QDL context, as it provides a natural notion of light (charge) and heavy (spin) degrees of freedom. For simplicity we focus on the "spin-disordered regime"

$$\frac{4t^2}{U} \ll T \ll U \ . \tag{3.33}$$

This corresponds to temperatures that are small compared to the Mott gap, but large compared to the exchange energy. Here one has[160]

$$\rho^h(k) = \mathcal{O}\big(e^{-u/T}\big) \ , \quad \sigma'^{p,h}_n(\Lambda) = \mathcal{O}\big(e^{-u/T}\big). \tag{3.34}$$

Substituting this into the general expression (3.7) for the thermodynamic entropy density we obtain

$$s = \sum_{n=1}^{\infty} \int_{-\infty}^{\infty} d\Lambda \ \mathcal{S}\left[{\sigma_n}^p(\Lambda), {\sigma_n}^h(\Lambda)\right] + \mathcal{O}\Big(\frac{u}{T} e^{-u/T}\Big). \tag{3.35}$$

Finally, using the relation between thermodynamic and EE (3.32) we conclude that for thermal states in the spin-disordered regime the contribution of the charge degrees of freedom contribute to the volume term is

$$\begin{aligned} S_{\mathrm{vN,A}} &= \big(s_{\mathrm{spin}} + s_{\mathrm{charge}}\big)|A| + o\big(|A|\big) \ , \\ s_{\mathrm{spin}} &= \mathcal{O}(1) \ , \quad s_{\mathrm{charge}} = \mathcal{O}\Big(\frac{u}{T} e^{-u/T}\Big) \ . \end{aligned} \tag{3.36}$$

Here s_{charge} includes the contributions from pure charge degrees of freedom as well as bound states of spin and charge. Importantly, unlike Heisenberg sector states,

typical states have a contribution from the charge degrees of freedom to the volume term. However, this contribution is exponentially small in u/T and therefore only visible for extremely large subsystems. While we have focussed on the spin-disordered regime, the behaviour (3.36) extends to thermal states for all $0 < T \ll U$. In Ref. [91] behaviour of the kind (3.36) (for the entanglement entropy after a partial measurement) was proposed as a "weak" form of a QDL, which one may expect to occur quite generically in strong coupling limits.

3.6 t/U-Expansion

The analysis presented above provides a strong indication that the Heisenberg sector states realise the QDL concept. However, the exact solution does not presently allow one to examine the QDL diagnostic proposed in Ref. [86], which requires the calculation of the EE after a partial measurement. We therefore now turn to a complementary approach, namely a strong-coupling expansion in powers of t/U. This is most conveniently implemented by following Ref. [7]. At a given site j there are four possible states $|0\rangle_j$, $|\uparrow\rangle_j = c^\dagger_{j,\uparrow}|0\rangle_j$, $|\downarrow\rangle_j = c^\dagger_{j,\downarrow}|0\rangle_j$ and $|2\rangle_j = c^\dagger_{j,\uparrow}c^\dagger_{j,\downarrow}|0\rangle_j$. Defining Hubbard operators by $X^{ab}_j = |a\rangle_{jj}\langle b|$, the Hamiltonian (3.1) can be expressed in the form

$$H = UD + t\,(T_0 + T_1 + T_{-1})\,, \tag{3.37}$$

where $D = \frac{1}{4}\sum_j X^{22}_j + X^{00}_j - X^{\uparrow\uparrow}_j - X^{\downarrow\downarrow}_j$ and $T_a = \sum_j T_{a,j}$ are correlated hopping terms that change the number of doubly occupied sites by a

$$\begin{aligned} T_{0,j} &= -\sum_\sigma \left(X^{2\sigma}_j X^{\sigma 2}_{j+1} + X^{\sigma 0}_j X^{0\sigma}_{j+1} + \text{h.c.}\right), \\ T_{1,j} = T^\dagger_{-1,j} &= -\sum_\sigma \sigma \left[X^{2\bar\sigma}_j X^{0\sigma}_{j+1} + X^{0\bar\sigma}_j X^{2\sigma}_{j+1}\right] \ . \end{aligned}$$

The t/U-expansion is conveniently cast in the form of a unitary transformation [7]

$$H' = e^{iS} H e^{-iS} = H + [iS, H] + \frac{1}{2}[iS, [iS, H]] + \ldots, \tag{3.38}$$

where the generator iS is chosen as a power series in t/U $iS = \sum_{n=1}^\infty \left(\frac{t}{U}\right)^n iS^{[n]}$. The operators $S^{[1]}, \ldots, S^{[k]}$ can be chosen such that the first $k+1$ terms in the t/U-

expansion of H' will not change the number of doubly occupied sites. It follows from Ref. [7] that the unitary transformation can be written as

$$\begin{aligned} e^{-iS} &= \sum_{k\geq 0} \sum_{[m]} \left(\frac{t}{U}\right)^k \alpha^{(k)}[m] T^{(k)}[m], \\ T^{(k)}[m] &= T_{m_1} T_{m_2} \ldots T_{m_k} \ , \quad m_j \in \{-1, 0, 1\}, \end{aligned} \tag{3.39}$$

where $\alpha^{(k)}[m]$ are suitably chosen coefficients.

3.6.1 Heisenberg sector states in the t/U expansion

We now need to identify the Heisenberg sector states in the framework of the t/U-expansion. We propose that they are characterised by their property that, in the framework of the t/U-expansion, they are connected by our unitary transformation to states without any double occupancies

$$|\psi_H\rangle\Big|_{t/U} = |\psi\rangle = e^{-iS} \sum_{\alpha_j=\uparrow,\downarrow} f_{\alpha_1 \ldots \alpha_L} \Big[\prod_{j=1}^{L} X^{\alpha_j 0} \Big] |0\rangle. \tag{3.40}$$

Our identification is based on the fact that in the Bethe ansatz solution exact eigenstates are labelled by sets of (half-odd) integer quantum numbers, which makes it possible to follow a particular state when changing the interaction strength U. When sending U/t to infinity for a large but fixed system size one finds that in this limit the lowest energy eigenstates belong to the Heisenberg sector, which in turn leads to the identification (3.40). In the following we will use the eigenstate $|\psi_H\rangle$ and its t/U-expansion $|\psi\rangle$ interchangeably and leave a discussion of contributions not captured by the t/U-expansion for our concluding remarks. The ground state of the half-filled Hubbard model is a particular example of a Heisenberg state. Heisenberg sector states have the important property that they are singlets under the η-pairing SU(2) algebra. This follows from the easily established fact that

$$[\eta, T_m] = 0 = [\eta^\dagger, T_m] = [\eta^z, T_m] \ , \quad m = 0, \pm 1. \tag{3.41}$$

The commutation relations (3.41) imply that $T^{(k)}[m]$ commute with the η-pairing operators, and this in turn implies by virtue of (3.39) that

$$[\eta, e^{-iS}] = 0 = [\eta^\dagger, e^{-iS}] = [\eta^z, e^{-iS}]. \tag{3.42}$$

This, together with the fact that all states with only singly occupied sites are annihilated by both η and $\eta^\dagger$, establishes that all Heisenberg states are η-pairing singlets

$$\eta|\psi\rangle = \eta^\dagger|\psi\rangle = \eta^z|\psi\rangle = 0. \tag{3.43}$$

Note that the construction of [7] holds for different double-occupancy sectors, and H' reduces to a spin Hamiltonian only in the particular case we entertain from here. Generically, one obtains a t-J model[26]. Using the results of Refs [161, 162] we may construct a basis for the space of η-pairing singlets. Let us select a set $A = \{a_1, \ldots, a_{2q}\}$ of $2q$ lattice sites and denote the complementary set by $\bar{A}$. We take all $\bar{A}$ sites to be singly occupied by spin-σ_j fermions, while we form singlet η-pairing dimers $|S(a,b)\rangle = |2\rangle_a|0\rangle_b + (-1)^{a+b-1}|0\rangle_a|2\rangle_b$ on the A sites. This gives an overcomplete set of states

$$|\boldsymbol{k};\boldsymbol{\sigma}\rangle = \prod_{i=1}^{q} |S(k_{2i-1}, k_{2i})\rangle \prod_{j\in\bar{A}} |\sigma_j\rangle_j, \tag{3.44}$$

where $\boldsymbol{k} = k_1, \ldots, k_{2q}$ is a permutation of $\{a_1, \ldots, a_{2q}\}$. It is easily verified that the states (3.44) are η-pairing singlets. A linearly independent set of states (3.44) is formed by imposing a "non-crossing" constraint on the permitted values of $\boldsymbol{k}$ as follows. We first impose an ordering of sites $\{a_1, \ldots, a_{2q}\}$, e.g. $a_1 < a_2 < \cdots < a_{2q}$. In one dimension this is simply the natural order of the sites. We then connect the q pairs of sites $\{(k_{2i-1}, k_{2i})\}$ by lines, *cf.* Fig. 3.4. If no lines cross, the state corresponding to the pairing $\boldsymbol{k}$ is permitted. A basis $\mathfrak{B}$ of all η-pairing singlet states in the half-filled Hubbard model is obtained by taking into account all "sectors" $0 \leq 2q \leq L$ and all distinct sets $\{a_1, \ldots, a_{2q}\}$ of lattice sites in a given sector. All eigenstates in the

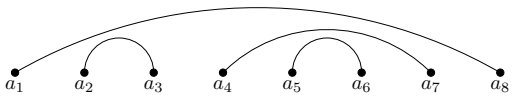

Figure 3.4: The pairing $\boldsymbol{k} = \{a_1, a_8, a_2, a_3, a_4, a_7, a_5, a_6\}$ does not involve crossed lines and fulfils the constraint.

Heisenberg sector can then be expressed in the form

$$|\psi\rangle = \sum_{|\boldsymbol{k};\boldsymbol{\sigma}\rangle \in \mathfrak{B}} A_{\boldsymbol{k};\boldsymbol{\sigma}} \, |\boldsymbol{k};\boldsymbol{\sigma}\rangle \ . \tag{3.45}$$

3.6.2 One spatial dimension

The t/U-expansion allows us to determine the dependence of the amplitudes $A_{\boldsymbol{k};\boldsymbol{\sigma}}$ on U. It is useful to define the "total bond length" by

$$\mathcal{D}\Big(\sum_{|\boldsymbol{k};\boldsymbol{\sigma}\rangle \in \mathfrak{B}} A_{\boldsymbol{k};\boldsymbol{\sigma}} \, |\boldsymbol{k};\boldsymbol{\sigma}\rangle \Big) = \max_{\substack{|\boldsymbol{k};\boldsymbol{\sigma}\rangle \in \mathfrak{B} \\ A_{\boldsymbol{k};\boldsymbol{\sigma}} \neq 0}} \mathcal{D}\left(|\boldsymbol{k};\boldsymbol{\sigma}\rangle\right), \tag{3.46}$$

where we take $\mathcal{D}\big(|\boldsymbol{k};\boldsymbol{\sigma}\rangle\big) = \sum_{i=1}^{q} (\|k_{2i-1} - k_{2i}\| + 1)$. It is a straightforward matter to show (see Appendix 3.B) that $\mathcal{D}\big(T_n|\psi\rangle\big) \leq \mathcal{D}\big(|\psi\rangle\big) + n + 1$ where $n = 0, \pm 1$ and $|\psi\rangle$ is any Heisenberg sector state (3.45). This in turn implies that $\mathcal{D}\left[T^{(k)}[m]|\psi_0\rangle\right] \leq k + q$, where $q = \sum_{i=1}^{k} m_i$ and $|\psi_0\rangle$ is any state with only singly occupied sites. Applying this to the expressions (3.40), (3.39) for Heisenberg states, we conclude that the expansion coefficients in (3.45) fulfil

$$A_{\boldsymbol{k};\boldsymbol{\sigma}} = \mathcal{O}\Big(\big(t/U\big)^{\sum_{i=1}^{q} \|k_{2i} - k_{2i-1}\|} \Big). \tag{3.47}$$

These results cannot be straightforwardly generalised to $D > 1$ because our definition of a total bond length hinges on $|\boldsymbol{k};\boldsymbol{\sigma}\rangle$ forming a basis of states, which imposes constraints on the allowed values of $\boldsymbol{k}$. In a typical Heisenberg sector state we have a finite density of doubly occupied sites and the coefficients (3.47) are of an extremely high order in t/U. In order to proceed we will assume that the t/U-expansion for the wave-function (3.45) has a finite radius of convergence. We know this to be the case for certain quantities such as the ground state energy [26].

3.6.3 Quantum disentangled diagnostic

To reiterate the problem: according to Refs [86, 88] a QDL can be diagnosed by preparing the system in a finite energy-density eigenstate with volume-law bipartite EE entropy, upon which we carry out a projective measurement of the z-component

of spin on each site of the lattice. If the resulting state is characterised by an area-law EE, the original state realises a QDL.

We now address this proposal in the framework of the t/U-expansion. As our initial state we choose a finite energy density eigenstate (3.40) in the Heisenberg sector. These generically have volume-law entanglement entropies as can be seen from the fact that the corresponding macro-states have finite thermodynamic entropy densities. As the 1D Hubbard model is integrable there also exist finite energy density eigenstates with area-law EE, but these are the exception rather than the rule. Let us assume that the outcome of our projective spin measurement is that we obtain spin zero at all sites in the set $A = \{a_1, a_2, \dots a_{2q}\}$ and spin $\sigma_j = \pm 1/2$ everywhere else. Then the state of the system after the projective measurement can be written as

$$\begin{aligned} |\psi_{\text{proj}}\rangle = \frac{1}{\sqrt{\mathcal{N}}} \prod_{j_1=1}^{a_1-1} X_{j_1}^{\sigma_{j_1}\sigma_{j_1}} \left(X_{a_1}^{00} + X_{a_1}^{22}\right) \\ \times \prod_{j_2=a_1+1}^{a_2-1} X_{j_2}^{\sigma_{j_2}\sigma_{j_2}} \left(X_{a_2}^{00} + X_{a_2}^{22}\right) \cdots |\psi\rangle, \end{aligned} \tag{3.48}$$

where $\mathcal{N}$ is a normalisation factor. Using our results (3.45) for the structure of Heisenberg states in the t/U expansion, we can rewrite this in the form

$$|\psi_{\text{proj}}\rangle = {\sum_{Q\in S_{2q}}}' W(Q) \prod_{i=1}^{q} |S(k_{Q_{2i-1}}, k_{Q_{2i}})\rangle |\boldsymbol{\sigma}\rangle. \tag{3.49}$$

Here $|\boldsymbol{\sigma}\rangle = \prod_{j\notin A} |\sigma_j\rangle$ is a product state fixed by the projective measurement, and the sum $\sum'_{Q\in S_{2q}}$ is restricted to the permutations Q such that $a_{Q_1}, a_{Q_2}, \dots a_{Q_{2q}}$ corresponds to singlet states that satisfy the non-crossing condition. As a result of (3.47) the amplitudes $W(Q)$ fulfil

$$W(Q) \sim \mathcal{O}\left(\left(t/U\right)^{\sum_{i=1}^{q} \|k_{Q_{2i}} - k_{Q_{2i-1}}\|}\right). \tag{3.50}$$

In the leading order in the t/U-expansion that is allowed to be non-zero by the above considerations there is only a single term in (3.49) and we are dealing with a spatially ordered product state of singlet dimers, *cf.* Fig. 3.5. In the following we will assume for simplicity that the numerical coefficient of this term is indeed

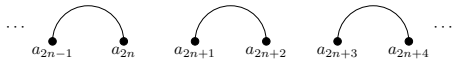

Figure 3.5: Structure of the singlet pairings in the leading non-vanishing term of the projected state in the t/U-expansion.

different from zero, which will be generically the case. Depending on the choice of the initial Heisenberg state and the outcome of the projective measurement it is possible that this coefficient vanishes. Such cases can be accommodated by relatively straightforward modifications of the following discussion.

3.6.4 Entanglement entropy.

At any finite order in the t/U-expansion the projected states (3.49) are only weakly entangled. Let us consider the generic case, in which the leading non-zero term in the projected state has the form shown in Fig. 3.5. In this case the leading term in von Neumann entropy of a sub-system A is simply given by $S_{\mathrm{vN},A} = \ln(2)$ if we cut one of the singlet dimers when we bipartition the system, and zero otherwise. At leading order it is not possible for the bipartition to cut more than one dimer. In order to describe the structure of the leading corrections to this result we take the subsystem A to be the interval $[1, \ell]$, where $a_{2n+1} < \ell < a_{2n+2}$. Here $\{a_j\}$ are the sites in the projected state that are either doubly occupied or empty. We then cast the projected state in the form

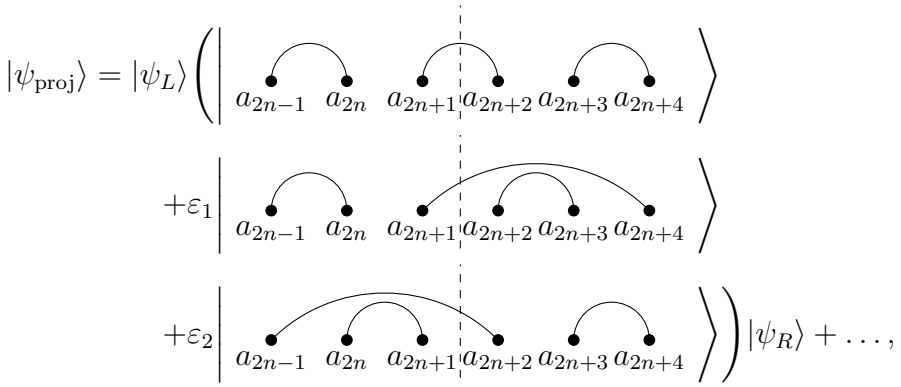

(3.51)

where $|\psi_L\rangle$ ($|\psi_R\rangle$) is the part of the leading term of the projected state that involves the sites $j < a_{2n-1}$ ($j > a_{2n+4}$). The coefficients $\epsilon_{1,2}$ are of order $(t/U)^{2(a_{2n+3}-a_{2n+2})}$ and $(t/U)^{2(a_{2n+1}-a_{2n})}$ respectively. The von Neumann entropy for our subsystem is

then

$$S_{\mathrm{vN},A} = \ln 2 + \frac{9}{16}\varepsilon_1^2\varepsilon_2^2\big(1 + 2\ln\left(\frac{4}{3}\right) - 2\ln(\varepsilon_1\varepsilon_2)\big) + \dots \tag{3.52}$$

We note that the correction is positive. The physical picture that emerges is very simple: for small t/U, the projected state is very close to being a product of Bell pairs and the bipartite EE takes the form shown in Fig. 3.6. The average double occupancy

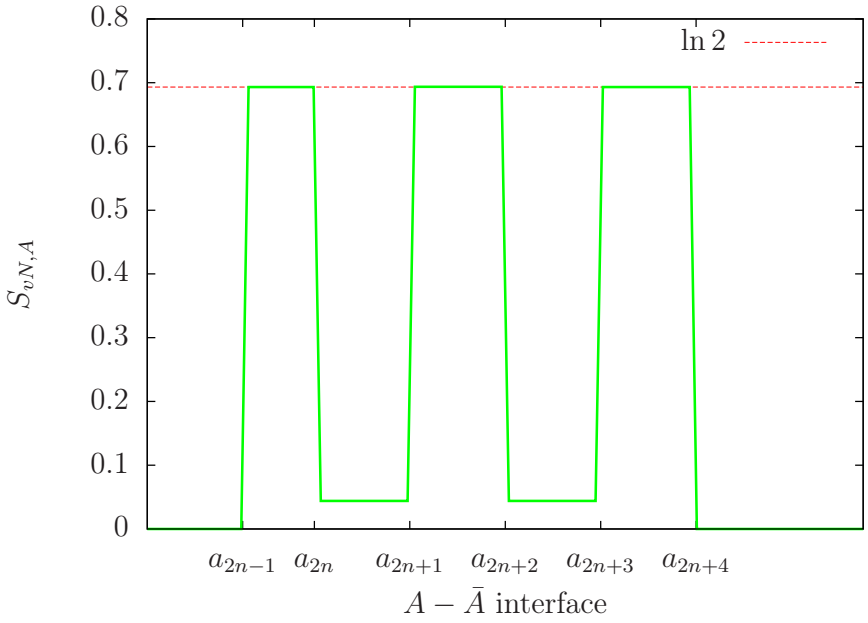

Figure 3.6: Form of the bipartite entanglement entropy after projective measurement of a general Heisenberg state. Deviations from $S(x) = \ln 2, 0$ arise from higher order terms, as seen in (3.51), (3.52).

in a Heisenberg state is $\mathcal{O}(t^2/U^2)$, which implies that the average distance between doubly occupied/unoccupied sites is very large $\sim U^2/t^2$. Hence, if the outcome of our spin measurement is close to its average, the sites $a_1, \dots, a_{2q}$ are well separated and the leading term (3.5) is expected to provide an excellent approximation as long as the t/U-expansion converges.

3.6.5 Higher dimensions $D > 1$

A key element of our analysis in the one dimensional case is the notion of a bond length, which fulfils $\mathcal{D}(|\psi_1\rangle) \leq \mathcal{D}(|\psi_1\rangle + |\psi_2\rangle)$ for arbitrary η-pairing singlet states

$|\psi_{1,2}\rangle$. Our definition of a bond length utilises the availability of a convenient basis of such states. It is this aspect which makes the $D = 1$ special. In $D > 1$ we proceed by again first fixing a set $A = \{a_i\}$ of $2q$ unoccupied or doubly occupied sites. We denote by E_{ij} a bond that joins sites a_i and a_j. We then define a dimer configuration $\mathfrak{C}$ as a set of q bonds C_{ij} connecting sites a_i and a_j such that all sites belong to precisely one bond. Each dimer configuration gives rise to η-pairing singlet states of the form

$$|\mathfrak{C};\boldsymbol{\sigma}\rangle = \prod_{C_{ij}\in\mathfrak{C}} |S(a_i,a_j)\rangle \prod_{j\notin A} |\sigma_j\rangle_j \ . \tag{3.53}$$

The states (3.53) form an overcomplete set. In order to select a set of linearly independent states we use the function $\overline{\mathcal{D}}$ defined by $\overline{\mathcal{D}}\left(|\mathfrak{C};\boldsymbol{\sigma}\rangle\right) = \sum_{C_{ij}\in\mathfrak{C}} \big(\|a_i - a_j\| + 1\big)$, where $\|a_i - a_j\|$ denotes the Manhattan distance between sites a_i and a_j. Among (3.53) we select the $\frac{(2q)!}{(q+1)!(q!)}$ states that have the lowest values under the map $\overline{\mathcal{D}}$. Repeating this construction for all values of $2q \leq L$ and all distinct sets A gives a basis $\mathcal{B}$ of η-pairing singlet states. We now define our total bond distance $\mathcal{D}$ in the same way as in (3.46) with the covering $\mathfrak{C}$ taking the place of the vector $\boldsymbol{k}$. With these definitions in place it is straightforward to show (see Appendix 3.B) that $\mathcal{D}\big(T_n|\psi\rangle\big) \leq \mathcal{D}\big(|\psi\rangle\big) + n + 1$ where $n = 0, \pm 1$ and $|\psi\rangle$ is any Heisenberg sector state

$$|\psi\rangle = \sum_{|\mathfrak{C};\boldsymbol{\sigma}\rangle\in\mathfrak{B}} A_{\mathfrak{C};\boldsymbol{\sigma}}\ |\mathfrak{C};\boldsymbol{\sigma}\rangle \ . \tag{3.54}$$

This in turn implies that $\mathcal{D}\left[T^{(k)}[m]|\psi_0\rangle\right] \leq k + q$, where $q = \sum_{i=1}^{k} m_i$ and $|\psi_0\rangle$ is any state with only singly occupied sites. It follows that the d-dimensional generalisation of (3.47) is

$$A_{\mathfrak{C};\boldsymbol{\sigma}} = \mathcal{O}\Big(\big(t/U\big)^{\sum_{C_{ij}\in\mathfrak{C}}\|a_i - a_j\|}\Big). \tag{3.55}$$

The main difference to $D = 1$ is that now there can be several basis states contributing to the leading order term in t/U. To see this we may consider a square lattice and focus on the situation where the sites in A completely fill an $m \times n$ rectangle (with at least one of m, n even). The leading-order term is that generated by $(T_1)^{mn/2}$ produces a superposition of all states in $\mathfrak{B}$ that correspond to nearest-neighbour dimer coverings of this rectangle. Nevertheless, it is apparent that to leading order

in the t/U-expansion the structure of the state is such that the entanglement entropy follows an area-law.

3.7 Conclusions

We have shown that there are particular "Heisenberg sector" eigenstates in the one dimensional half-filled Hubbard model that realise the quantum disentangled liquid state of matter proposed in Ref. [86]. These states are obtained by freezing the charge degrees of freedom in their ground state configuration in the framework of the Bethe ansatz solution of the Hubbard model. Using methods of integrability we have demonstrated that the charge degrees of freedom ("light particles") do not contribute to the volume term of the bipartite entanglement entropy. Employing strong-coupling expansion techniques we have shown (under the assumption that the expansion converges) that a measurement of the spin degrees of freedom at all sites ("heavy particles") leaves the system in a state that is area-law entangled, which is the defining characteristic of a QDL[86].

In contrast to Heisenberg sector states, the entanglement entropy for maximal entropy (thermal) states at a given energy density at large values of U/t does have a contribution that involves the charge degrees of freedom, but it is of the form (3.36), i.e.

$$\begin{aligned} S_{\mathrm{vN,A}} &= \big(s_{\mathrm{spin}} + s_{\mathrm{charge}}\big)|A| + o\big(|A|\big) \ , \\ s_{\mathrm{spin}} &= \mathcal{O}(1) \ , \quad s_{\mathrm{charge}} = \mathcal{O}\Big(\frac{u}{T}e^{-u/T}\Big) \ , \end{aligned} \tag{3.56}$$

We expect a similar volume law to occur in the entanglement entropy after a measurement of all spins. This suggests that there is an approximate variant of a QDL, which is characterised a volume term in the EE after measurement of the heavy degrees of freedom that is parametrically small in a way that makes it observable only in enormously large systems. In particular, it would be practically impossible to detect in any numerical simulation. We expect this scenario to be realised quite generally in strong coupling limits irrespective of whether the model one is dealing with is integrable or not. In particular, this scenario is compatible with our strong-coupling

analysis of the QDL diagnostic in $D = 2$.

An interesting question is how to access Heisenberg sector states in the one dimensional case. In principle this can be achieved by means of a quantum quench [74] from a suitably chosen initial state. Fixing the energy density to be small compared to the Mott gap is sufficient to obtain a non-equilibrium steady state that realises the weak form of a QDL characterised by (3.36). In order to remove the s_{charge} contribution, the expectation values of higher conservation laws in the initial state have to be chosen appropriately and it would be interesting to investigate this issue further.

3.A Thermodynamic Bethe Ansatz equations

The Thermodynamic Bethe Ansatz equations for the one dimensional Hubbard model in zero magnetic field are[26, 153]

$$\begin{aligned}
\ln\zeta(k) &= \frac{-2\cos k-\mu-2u}{T}+\sum_{n=1}^{\infty}\int_{-\infty}^{\infty}\mathrm{d}\Lambda\, a_n(\sin k-\Lambda)\ln\left(1+\frac{1}{\eta_n'(\Lambda)}\right)\\
&\quad-\sum_{n=1}^{\infty}\int_{-\infty}^{\infty}\mathrm{d}\Lambda\, a_n(\sin k-\Lambda)\ln\left(1+\frac{1}{\eta_n(\Lambda)}\right),\\
\ln\left(1+\eta_n(\Lambda)\right) &= -\int_{-\pi}^{\pi}\mathrm{d}k\ \cos(k)\ a_n(\sin k-\Lambda)\ln\left(1+\frac{1}{\zeta(k)}\right)+\sum_{m=1}^{\infty}A_{nm}*\ln\left(1+\frac{1}{\eta_m}\right)\Bigg|_{\Lambda},\\
\ln\left(1+\eta_n'(\Lambda)\right) &= \frac{4\mathrm{Re}\sqrt{1-(\Lambda-inu)^2}-2n\mu-4nu}{T}\\
&\quad-\int_{-\pi}^{\pi}\mathrm{d}k\ \cos(k)\ a_n(\sin k-\Lambda)\ln\left(1+\frac{1}{\zeta(k)}\right)+\sum_{m=1}^{\infty}A_{nm}*\ln\left(1+\frac{1}{\eta_m'}\right)\Bigg|_{\Lambda}.
\end{aligned}\tag{3.57}$$

3.B Some inequalities for the total bond length of Heisenberg states

Here we show that

$$\mathcal{D}\left(T_n|\psi\rangle\right)\leq\mathcal{D}\left(|\psi\rangle\right)+n+1,\qquad n=0,\pm1.\tag{3.58}$$

We consider the one and higher dimensional cases separately.

3.B.1 One Dimension

Any Heisenberg state can be written in the form (3.45)

$$|\psi\rangle = \sum_{|\boldsymbol{k};\boldsymbol{\sigma}\rangle \in \mathfrak{B}} A_{\boldsymbol{k};\boldsymbol{\sigma}} \; |\boldsymbol{k};\boldsymbol{\sigma}\rangle \; . \tag{3.59}$$

To establish (3.58) it therefore suffices to show that

$$\mathcal{D}\left(T_n|\mathbf{k};\boldsymbol{\sigma}\rangle\right) \leq \mathcal{D}\left(|\mathbf{k};\boldsymbol{\sigma}\rangle\right) + n + 1 \; . \tag{3.60}$$

We next consider the three cases $n = 0, \pm 1$ in turn.

3.B.1.1 a. Inequality for T_1:

Due to the definition of the bond distance, it is clear that

$$\mathcal{D}\left(\sum_j T_{m,j}|\mathbf{k};\boldsymbol{\sigma}\rangle\right) \leq \sup_j \mathcal{D}\left(T_{m,j}|\mathbf{k};\boldsymbol{\sigma}\rangle\right), \tag{3.61}$$

and therefore for $m = \pm 1, 0$, we simply need to find the case which yields the largest value in order to prove the inequality. $T_{1,j}$ creates an η-singlet on two adjacent sites and $\mathcal{D}$ counts the total number of sites spanned by the singlet bonds, applying $T_{1,j}$ increases this by at most that in the case of a system with no doubly occupied sites. We can view the result graphically

$$\begin{aligned} \mathcal{D}\left(T_{1,j}\left|\; a_{2n-2} \;\; a_{2n-1} \right\rangle\right) &\leq \mathcal{D}\left(\left|\; a_{2n-2} \;\; a_{2n-1} \quad j \;\; j+1 \right\rangle\right), \\ &\leq \mathcal{D}\left(\left|\; a_{2n-2} \;\; a_{2n-1} \right\rangle\right) + 2. \end{aligned} \tag{3.62}$$

3.B.1.2 b. Inequality for T_0:

$T_{0,j}$ neither creates nor destroys any η-singlet pairs. Instead, for a given singlet pair, it moves one of the doubly-occupied/empty sites in the pair either left or right one site i.e. it extends the bond distance of the pair by ± 1. The case where the distance *increases* i.e. saturates the inequality, can be represented graphically as

$$\begin{aligned} \mathcal{D}\left(T_{0,2n}\left|\; a_{2n-1} \;\; a_{2n} \right\rangle\right) &\leq \mathcal{D}\left(\left|\; a_{2n-1} \;\; a_{2n}+1 \right\rangle\right), \\ &\leq \mathcal{D}\left(\left|\; a_{2n-1} \;\; a_{2n} \right\rangle\right) + 1. \end{aligned} \tag{3.63}$$

3.B.1.3 c. Inequality for T_{-1}:

It is simple to show that $T_{-1,j}$ "fuses" the ends of singlet pairs together to create a new singlet pair between the unaffected sites. Using this, we can consider the two possible distinct cases graphically. Explicit calculation shows that this intuition holds. The cases are: (i) $a_{2n-1} = a_{2n} - 1$ i.e. they are adjacent

$$\begin{aligned} \mathcal{D}\left(T_{-1,a_{2n-1}}\left|\right.\right. &\overset{a_{2n-2}}{\bullet}\!\!\frown\!\!\overset{a_{2n-1}}{\bullet}\quad \overset{a_{2n}}{\bullet}\!\!\frown\!\!\overset{a_{2n+1}}{\bullet}\left.\left.\right\rangle\right) \leq \mathcal{D}\left(\left|\right.\right. \overset{a_{2n-2}}{\bullet}\!\!\frown\!\!\overset{a_{2n+1}}{\bullet}\left.\left.\right\rangle\right), \\ &\leq \mathcal{D}\left(\left|\right.\right. \overset{a_{2n-2}}{\bullet}\!\!\frown\!\!\overset{a_{2n-1}}{\bullet}\quad \overset{a_{2n}}{\bullet}\!\!\frown\!\!\overset{a_{2n+1}}{\bullet}\left.\left.\right\rangle\right), \end{aligned} \tag{3.64}$$

(ii) $a_{2n} = a_{2n+1} - 1$ i.e. two singlets are nested

$$\begin{aligned} \mathcal{D}\left(T_{-1,a_{2n}}\left|\right.\right. &\overset{a_{2n-2}}{\bullet}\!\!\frown\!\!\overset{a_{2n+1}}{\bullet}\quad \overset{a_{2n-1}}{\bullet}\!\!\frown\!\!\overset{a_{2n}}{\bullet}\left.\left.\right\rangle\right) \leq \mathcal{D}\left(\left|\right.\right. \overset{a_{2n-2}}{\bullet}\!\!\frown\!\!\overset{a_{2n-1}}{\bullet}\quad \overset{}{\bullet}\!\!\frown\!\!\overset{}{\bullet}\left.\left.\right\rangle\right), \\ &\leq \mathcal{D}\left(\left|\right.\right. \overset{a_{2n-2}}{\bullet}\!\!\frown\!\!\overset{a_{2n-1}}{\bullet}\quad \overset{a_{2n}}{\bullet}\!\!\frown\!\!\overset{a_{2n+1}}{\bullet}\left.\left.\right\rangle\right). \end{aligned} \tag{3.65}$$

3.B.2 Higher Dimensions

Any Heisenberg state can be written in the form (3.54)

$$|\psi\rangle = \sum_{|\mathfrak{C};\boldsymbol{\sigma}\rangle \in \mathfrak{B}} A_{\mathfrak{C};\boldsymbol{\sigma}} \, |\mathfrak{C};\boldsymbol{\sigma}\rangle \ , \tag{3.66}$$

so that in order to establish (3.58) it suffices to show that

$$\mathcal{D}\left(T_n|\mathfrak{C};\boldsymbol{\sigma}\rangle\right) \leq \mathcal{D}\left(|\mathfrak{C};\boldsymbol{\sigma}\rangle\right) + n + 1 \ . \tag{3.67}$$

for all basis states $|\mathfrak{C};\boldsymbol{\sigma}\rangle \in \mathfrak{B}$. We consider the three cases $n = 0, \pm 1$ in turn.

3.B.2.1 a. Inequality for T_0:

We note that by construction we have for all basis states

$$\mathcal{D}(|\mathfrak{C};\boldsymbol{\sigma}\rangle) = \overline{\mathcal{D}}(|\mathfrak{C};\boldsymbol{\sigma}\rangle) \ , \ |\mathfrak{C};\boldsymbol{\sigma}\rangle \in \mathfrak{B}. \tag{3.68}$$

Following through the same steps as in the one dimensional case we see that T_0 can increase the Manhattan distance between any pair in the configuration by at most 1

i.e.

$$\begin{aligned}\mathcal{D}\left(T_0|\mathfrak{C};\boldsymbol{\sigma}\rangle\right) &\leq \overline{\mathcal{D}}\left(T_0|\mathfrak{C};\boldsymbol{\sigma}\rangle\right), \\ &\leq \overline{\mathcal{D}}\left(|\mathfrak{C};\boldsymbol{\sigma}\rangle\right)+1=\mathcal{D}(|\mathfrak{C};\boldsymbol{\sigma}\rangle),\end{aligned} \tag{3.69}$$

where in the last step we used (3.68).

3.B.2.2 b. Inequality for T_1:

Similarly, acting with T_1 creates a new configuration with an additional edge

$$\begin{aligned}\mathcal{D}\left(T_1|\mathfrak{C};\boldsymbol{\sigma}\rangle\right) &\leq \overline{\mathcal{D}}\left(T_1|\mathfrak{C};\boldsymbol{\sigma}\rangle\right), \\ &\leq \overline{\mathcal{D}}\left(|\mathfrak{C};\boldsymbol{\sigma}\rangle\right)+2=\mathcal{D}\left(|\mathfrak{C};\boldsymbol{\sigma}\rangle\right)+2,\end{aligned} \tag{3.70}$$

where in the last step we used (3.68).

3.B.2.3 c. Inequality for T_{-1}:

Finally, acting with T_{-1} always removes a pair of "adjacent" unoccupied/doubly occupied sites. Thinking in terms of configurations, this then either removes a paired bond, or fuses two bonds into one. If we explicitly write the points defining the configuration $\mathfrak{C}$, the first case corresponds to

$$\begin{aligned}T_{-1}:\{\{k_1,k_2\},\{k_3,k_4\},\ldots,\{k_{2q-1},k_{2q}\}\} \\ \to\{\{k_3,k_4\},\ldots,\{k_{2q-1},k_{2q}\}\}.\end{aligned} \tag{3.71}$$

This implies that

$$\overline{\mathcal{D}}\left(T_{-1}|\mathfrak{C};\boldsymbol{\sigma}\rangle\right)\leq\overline{\mathcal{D}}\left(|\mathfrak{C};\boldsymbol{\sigma}\rangle\right)-\left(\|k_1-k_2\|+1\right). \tag{3.72}$$

The second case corresponds to

$$\begin{aligned}T_{-1}:\{\{k_1,k_2\},\{k_3,k_4\},\ldots,\{k_{2q-1},k_{2q}\}\} \\ \to\{\{k_1,k_4\},\ldots,\{k_{2q-1},k_{2q}\}\},\end{aligned} \tag{3.73}$$

which implies that

$$\begin{aligned}\overline{\mathcal{D}}\left(T_{-1}|\mathfrak{C};\boldsymbol{\sigma}\rangle\right)\leq\overline{\mathcal{D}}\left(|\mathfrak{C};\boldsymbol{\sigma}\rangle\right)+\left(\|k_1-k_4\|+1\right) \\ -\left(\|k_1-k_2\|+1\right)-\left(\|k_3-k_4\|+1\right).\end{aligned} \tag{3.74}$$

By construction k_2 and k_3 are "adjacent", so that

$$\left(\|k_1-k_4\|+1\right)-\left(\|k_1-k_2\|+1\right)-\left(\|k_3-k_4\|+1\right)\leq 0. \tag{3.75}$$

Putting everything together we have

$$\mathcal{D}\left(T_{-1}|\mathfrak{C};\boldsymbol{\sigma}\rangle\right)\leq\mathcal{D}\left(|\mathfrak{C};\boldsymbol{\sigma}\rangle\right),\qquad|\mathfrak{C};\boldsymbol{\sigma}\rangle\in\mathcal{B}. \tag{3.76}$$

Chapter 4

Concluding remarks

We close here by summarising the work of the previous chapters and noting some open questions.

In Chapter 2, we applied MIM methods to understand the onset of the optical conductivity away from asymptotically low energies. Here, the usual techniques of the Luttinger liquid are destined to fail. Using the exact solution of the Hubbard model, we identified which excitations contribute to the spectral weight in analogy to threshold singularities. We dealt with the problem of projecting operators onto the mobile impurity space of operators and calculated the onset behaviour accounting for the flat dispersion relation of the impurity. We also commented on the connection to the known singular behaviour at half-filling. Calculations of the detailed properties of response functions in the Hubbard model pose interesting problems in their own right, and away from the regime we studied it is difficult to see how to develop further analytic understanding. There are a number of open questions with regard to the theory of non-Linear Luttinger liquids. Firstly, in all of the calculations we have looked at, the non-Linear Luttinger liquid theory has no way to capture the non-universal amplitudes of correlation functions. When considering the optical conductivity these were left as fit parameters. In the case of the XXZ model, a tour-de-force in integrability[163, 164] has allowed the calculation of the prefactors, meaning that there are *no* free parameters in the answer. It would be interesting to understand these amplitudes in more detail in a wider range of models. Furthermore, as we have not been shy to point out: integrable models are special, the excitations we

consider are long-lived and we can use the finite-size spectrum to uniquely determine parameters in our theory. It would be interesting to develop a better understanding of how the picture changes upon the breaking of integrability.

In Chapter 3 we provided evidence supporting a "weak" version of QDL behaviour in the one-dimensional Hubbard model. One may object that the "weak" and "strong" notions are distinct, yet in numerical simulations of modest sizes this is a distinction without measurable difference. By way of example, in DMRG studies the volume/area-law entanglement coefficients are often determined by finite-size scaling studies and to successfully adopt such an approach here, the volume-law term we identify would only be realistically detectable for system sizes exponentially large in U/t, which itself is large by construction.

The current approach via integrability relies on the TBA to make general thermodynamic statements, or via the strong coupling expansion. The strong-coupling expansion does not hinge on integrability, but the convergence properties of such an expansion are currently not well understood in general. It would certainly be interesting to further investigate this phenomenon further in integrable and non-integrable systems.

With respect to the strong coupling expansion, the question of convergence is not a simple one to address. Some well-understood quantities are known to have a good strong coupling expansion. The energy density of the ground state at half-filling or of the special families of eigenstates constructed in Section 3.2.2 have exact expressions whose power series converge for all $u > 1$. However, such results do not currently exist for the more complicated quantities we examine i.e. at the level of the wavefunction.

To understand the wavefunction away from strong coupling requires detailed knowledge at finite energy density, with a volume-law EE by design. Such eigenstates are undoubtedly overwhelmingly complicated, particularly as they will be of Bethe Ansatz form and therefore contain $N!$ terms, where N is extensive in the system size. A small number of finite energy-density eigenstates are known in the case

of the Hubbard model[165, 166], but are not useful in the analysis of the QDL [1]. By their nature, non-integrable systems are difficult to deal with as there are far fewer analytic tools with which to approach them. The obvious direction in which to proceed is numerically. Exact diagonalisation is limited to small system sizes, and this is a particular constraint when the existence of multiple degrees of freedom per site increases the dimension of the local Hilbert space. Additionally, the efficient techniques such as DMRG typically rely on area-law entanglement of eigenstates. By construction we wish to consider scenarios where this is not the case, and this makes numerical study far more difficult.

[1]Their construction involves the η-pairing SU(2) symmetry, and are defined as $|\psi_n\rangle \propto (\eta^+)^n|0\rangle$, and this has two main consequences: firstly, there are only $\mathcal{O}(L)$ of these states, meaning that they will always have vanishing entropy density. Second, their construction always puts them at the "edge" of a block-diagonal part of the Hamiltonian and so they do not contain information about the "middle of the spectrum" in a meaningful sense.

Bibliography

[1] K. R. Popper, *Of Clouds and Clocks: An Approach to the Problem of Rationality and the Freedom of Man*, Washington University, (1966).

[2] P. W. Anderson, Science, New Series, Vol. 177, No. 4047. (Aug. 4, 1972), pp. 393-396.

[3] K. G. Wilson, Rev. Mod. Phys. **47**(4), 773 (1975).

[4] J. Cardy, *Scaling and Renormalization in Statistical Physics*, Cambridge (1996).

[5] J. Hubbard, Proc. R. Soc. Lond. A 1963 276 238-257.

[6] H. A. Kramers, Physica **1**, 182 (1934); P. W. Anderson, Phys. Rev. **79**, 350 (1950).

[7] A. H. MacDonald, S. M. Girvin, D. Yoshioka, Phys. Rev. B **37**, 9753 (1988).

[8] H. Bethe, *Zur theorie der metalle*, Zeitschrift für Physik, 71(3-4), 205-226 (1931).

[9] I. Affleck, B. I. Halperin, J. Phys. A 29:2627-2632 (1996).

[10] T. A. Hilker, G. Salomon, F. Grusdt, A. Omran, M. Boll, E. Demler, I. Bloch, C. Gross, arXiv:1702.00642.

[11] M. Boll, T. A. Hilker, G. Salomon, A. Omran, I. Bloch, C. Gross, arXiv:1605.05661.

[12] P. Bordia, H. Lüschen, S. Scherg, S. Gopalakrishnan, M. Knap, U. Schneider, I. Bloch, arXiv:1704.03063.

[13] H. P. Lüschen, P. Bordia, S. Scherg, F. Alet, E. Altman, U. Schneider, I. Bloch, arXiv:1612.07173.

[14] N. D. Mermin, H. Wagner, Phys. Rev. Lett. **17**, 1133 (1966); Erratum, ibid. **17**, 1307 (1966).

[15] P. C. Hohenberg, Phys. Rev. Lett. **158**, 383 (1967).

[16] 0. Penrose, Phil. Mag. **42**, 1373 (1951); 0. Penrose, L. Onsager, Phys. Rev. **104**, 576 (1956).

[17] J. S. Bell, *Speakable and unspeakable in quantum mechanics*, Cambridge University Press, Cambridge (2004).

[18] A. Altand, B. Simons, *Condensed matter field theory*, Cambridge (2010).

[19] R. Claessen, M. Sing, U. Schwingenschogl, P. Blaha, M. Dressel, C. S. Jacobsen, Phys. Rev. Lett. **88**, 096402 (2002).

[20] H. Benthien, F. Gebhard, E. Jeckelmann, Phys. Rev. Lett. **92**, 256401 (2004).

[21] P. Debray, V. N. Zverev, V. Gurevich, R. Klesse, R. S. Newrock, Semicond. Sci. Technol. 17, R21 (2002).

[22] D. Laroche, G. Gervais, M. P. Lilly, J. L. Reno, Nature Nanotechnology 6, 793 (2011).

[23] D. N. Aristov, Phys. Rev. B **76**, 085327 (2007).

[24] M. Pustilnik, E. G. Mishchenko, L. I. Glazman, A. V. Andreev, Phys. Rev. Lett. **91**, 126805 (2003)

[25] E. Jeckelmann, F. Gebhard, F. H. L. Essler, Phys. Rev. Lett. **85**, 3910 (2000).

[26] F. H. L. Essler, H. Frahm, F. Göhmann, A. Klümper, V. E. Korepin, *The One-Dimensional Hubbard Model*, Cambridge University Press, Cambridge (2005).

[27] V. E. Korepin , N. M. Bogoliubov, A. G. Izergin, *Quantum inverse scattering method and correlation functions*. Cambridge University Press, Cambridge (1997).

[28] B. Sutherland,*Beautiful Models*, World Scientific, Singapore, (2004).

[29] M. Gaudin, *La fonction d'onde de Bethe*, Masson, Paris, (1983).

[30] M. Takahashi, *Thermodynamics of One-Dimensional Solvable Models*, Cambridge University Press, Cambridge, (1999).

[31] J.-S. Caux, J. Mossel, J. Stat. Mech. P02023 (2011).

[32] J. M. Deutsch, Phys. Rev. A **43**, 2046 (1991).

[33] M. Rigol, V. Dunjko, V. Yurovsky M. Olshanii, Phys. Rev. Lett. **98**, 50405 (2007).

[34] S. Groha, F. H. L. Essler, arXiv:1702.06550

[35] L. D. Landau, E. M. Lifshitz, L. P. Pitaevskii, *Statistical physics, part I* (1980); L. D. Landau, E. M. Lifshitz. *Statistical physics, part II* (1980).

[36] P. W. Anderson, *Basic Notions of Condensed Matter Physics*, Chapter 3, Addison-Wesley, Reading, Mass., (1997).

[37] S. Tomonaga, Progress of Theoretical Physics **1**.2, 27-42 (1946).

[38] J. M. Luttinger, J. Math. Phys. **15**, 609 (1963).

[39] D. C. Mattis, E. H. Lieb, Journal of Mathematical Physics **6**.2, 304-312 (1965).

[40] T. Giamarchi, *Quantum physics in one dimension*, Clarendon Press, Oxford (2004).

[41] A. O. Gogolin, A. A. Nersesyan, A. M. Tsvelik, *Bosonization and strongly correlated systems*, Cambridge University Press (2004).

[42] P. Francesco, P. Mathieu, D. Sénéchal, *Conformal field theory*, Springer (2012).

[43] D. Sénéchal, arXiv:cond-mat/9908262.

[44] J. von Delft, H. Schoeller, Annalen Phys. **7** 225-305 (1998).

[45] M. Abramowitz, I. Stegun p. 825, 24.2.1 eq. I(B).

[46] F. D. M. Haldane, J. Phys. C: Solid State Phys. **14** 2585 (1981).

[47] D. M. Edwards, J. A. Hertz. Physica B: Condensed Matter **163**.1-3, 527-529 (1990).

[48] F. D. M. Haldane, Phys. Lett. A **81**, pp. 153-155 (1981).

[49] A. Imambekov, T. L. Schmidt, L. I. Glazman, Rev. Mod. Phys **84**, 1253 (2012).

[50] P. W. Anderson, Phys. Rev. Lett. **18**, 1049 (1967).

[51] P. Nozières, C. T. De Dominicis, Phys. Rev. **178**, 1097 (1969).

[52] K .D. Schotte, U. Schotte, Phys. Rev. **182**, 479 (1969).

[53] K. V. Samokhin, J. Phys. Condens. Matter **10**, L533 (1998).

[54] R. G. Pereira, J. Sirker, J.-S. Caux, R. Hagemans, J. M. Maillet, S. R. White, I. Affleck, Phys. Rev. Lett. **96**, 257202 (2006).

[55] R. G. Pereira, S. R. White, I. Affleck, Phys. Rev. B **79**, 165113 (2009).

[56] R. G. Pereira, S. R. White, I. Affleck, Phys. Rev. Lett. **100**, 027206 (2008).

[57] G. Müller, H. Beck, J. C. Bonner, Phys. Rev. Lett. **43**, 75 (1979); G. Müller, H. Thomas, H. Beck, J. C. Bonner, Phys. Rev. B **24**, 1429 (1981).

[58] I. Affleck, A. W. W. Ludwig, J. Phys. A **27**, 5375 (1994).

[59] F. H. L. Essler, R. G. Pereira, I. Schneider, Phys. Rev. B **91**, 245150 (2015).

[60] C. N. Yang, Phys. Rev. Lett. **19**, 1312 (1967).

[61] E. H. Lieb, F. Y. Wu, Phys. Rev. Lett. **20**, 1445 (1968); Erratum, ibid. **21**, 192 (1968).

[62] F. H. L. Essler, V. E. Korepin, K. Schoutens, Nucl. Phys. B **372**, 559 (1992).

[63] M. Takahashi, Prog. Theor. Phys. **46** 401 (1971),
M. Takahashi, Prog. Theor. Phys. **47** 69 (1972).

[64] A. M. Tsvelick, P. B. Wiegmann, Adv. Phys. **32**, 453 (1983).

[65] T. Deguchi, F. H. L. Essler, F. Göhmann, A. Klümper, V. E. Korepin, K. Kusakabe, Phys. Rep. **331** 197 (2000).

[66] F. H. L. Essler, V. E. Korepin, K. Schoutens, Phys. Rev. Lett. **67** 3848 (1991).
F. H. L. Essler, V. E. Korepin, K. Schoutens, Nucl. Phys. B **384** 431 (1992).

[67] N. J. Robinson, F. H. L. Essler, E. Jeckelmann, A. M. Tsvelik, Phys. Rev. B **85**, 195103 (2012).

[68] F. H. L. Essler, Phys. Rev. B **81**, 205120 (2010).

[69] L. Seabra, F. H. L. Essler, F. Pollmann, I. Schneider, T. Veness, Phys. Rev. B **90**, 245127 (2014).

[70] R. P. Feynman, *Statistical mechanics: a set of lectures*, Hachette UK, (1998).

[71] P. Calabrese, J. Cardy, J. Stat. Mech P04010 (2005).

[72] M. Srednicki, Phys. Rev. E **50**, 888 (1994).

[73] P. Calabrese, J. Cardy, J. Stat. Mech. P06008, (2007).

[74] F. H. L. Essler, M. Fagotti J. Stat. Mech. 064002 (2016).

[75] M. A. Cazalilla and M.-C. Chung, J. Stat. Mech. 064004 (2016).

[76] L. Vidmar and M. Rigol, J. Stat. Mech. 064007 (2016).

[77] E. Ilievski, J. De Nardis, B. Wouters, J.-S. Caux, F. H. L. Essler, T. Prosen, Phys. Rev. Lett. **115**, 157201 (2015).

[78] A. C. Cassidy, C. W. Clark, M. Rigol, Phys. Rev. Lett **106**, 140405 (2011).

[79] I. V. Gornyi, A. D. Mirlin, D. G. Polyakov, Phys. Rev. Lett. 95, 206603 (2005).

[80] D. M. Basko, I. L. Aleiner, B. L. Altshuler, Annals of Physics 321, 1126 (2006).

[81] V. Oganesyan, D. A. Huse, Phys. Rev. B 75, 155111 (2007).

[82] A. Pal, D. A. Huse, Phys. Rev. B 82, 174411 (2010).

[83] A. Chandran, A. Pal, C. R. Laumann, A. Scardicchio, Phys. Rev. B **94**, 144203 (2016).

[84] M. Serbyn, Z. Papic, D. A. Abanin, Phys. Rev. Lett. 111, 127201 (2013).

[85] D. A. Huse, R. Nandkishore, V. Oganesyan, Phys. Rev. B 90, 174202 (2014).

[86] T. Grover, M. P. A. Fisher, Journal of Statistical Mechanics: Theory and Experiment **10**, 10010 (2014).

[87] M. Srednicki, J. Phys. A **32**, 1163 (1998).

[88] J. R. Garrison, R. V. Mishmash, M. P. A. Fisher, Phys. Rev. B **95**, 054204 (2017).

[89] T. Veness, F. H. L. Essler, Phys. Rev. B **93**, 205101 (2016).

[90] A. C. Tiegel, T. Veness, P. E. Dargel, A. Honecker, T. Pruschke, I. P. McCulloch, F. H. L. Essler Phys. Rev. B **93**, 125108 (2016).

[91] T. Veness, F. H. L. Essler, M. P. A. Fisher, arXiv:1611.02075.

[92] J.-P. Farges, *Organic Conductors*, Marcel Dekker, New York (1994).

[93] F. Woynarovich, J. Phys. A **22**, 4243 (1989).

[94] H. Frahm, V. E. Korepin, Phys. Rev. B **42** 10553 (1990).

[95] A. Rozhkov, Eur. Phys. J. B **47**, 193 (2005).

[96] A. V. Rozhkov, Phys. Rev. B **74**, 245123 (2006).

[97] E. Bettelheim, A. G. Abanov, P. Wiegmann, Phys. Rev. Lett. **97**, 246401 (2006).

[98] M. Pustilnik, M. Khodas, A. Kamenev, L. I. Glazman, Phys. Rev. Lett. **96**, 196405 (2006).

[99] E. Bettelheim, A. G. Abanov, P. Wiegmann, J. Phys. A**41**, 392003 (2008).

[100] M. Khodas, M. Pustilnik, A. Kamenev, L. I. Glazman, Phys. Rev. Lett. **99**, 110405 (2007).

[101] M. Khodas, M. Pustilnik, A. Kamenev, L. I. Glazman, Phys. Rev. B **76**, 155402 (2007).

[102] A. Imambekov, L.I. Glazman, Phys. Rev. Lett. **100**, 206805 (2008).

[103] A. Imambekov, L. I. Glazman, Phys. Rev. Lett. **102**, 126405 (2009).

[104] A. Imambekov, L. I. Glazman, Science **323**, 228 (2009).

[105] A. G. Abanov, E. Bettelheim, P. Wiegmann, J. Phys. A42, 135201 (2009).

[106] R. G. Pereira, E. Sela, Phys. Rev. B **82**, 115324 (2010).

[107] T. L. Schmidt, A. Imambekov, L. I. Glazman, Phys. Rev. Lett. **104**, 116403 (2010).

[108] T. L. Schmidt, A. Imambekov, L. I. Glazman, Phys. Rev. B **82** 245104 (2010).

[109] R. G. Pereira, K. Penc, S. R. White, P. D. Sacramento, J. M. P. Carmelo, Phys. Rev. B **85**, 165132 (2012).

[110] A. V. Rozhkov, Phys. Rev. Lett. **112**, 106403 (2014).

[111] J. M. P. Carmelo, K. Penc, L. M. Martelo, P. D. Sacramento, J. M. B. Lopes Dos Santos, R. Claessen, M. Sing, U. Schwingenschlögl, Europhys. Lett. 67, 233 (2004).

[112] J. M. P. Carmelo, K. Penc, P. D. Sacramento, M. Sing, R. Claessen, J. Phys.: Condens. Matter 18, 5191 (2006).

[113] J. M. P. Carmelo, D. Bozi, K. Penc, J. Phys. Cond. Mat. 20, 415103 (2008).

[114] V. V. Cheianov, M. Pustilnik, Phys. Rev. Lett. **100**, 126403 (2008).

[115] T. Price, A. Lamacraft, Phys. Rev. B**90**, 241415 (2014).

[116] R. G. Pereira, Int. J. Mod. Phys. B **26**, 1244008 (2012).

[117] L. Balents, Phys. Rev. B **61**, 4429 (2000).

[118] D. Controzzi, F. H. L. Essler, A. M. Tsvelik, Phys. Rev. Lett. **86**, 680 (2001).

[119] D. Controzzi, F. H. L. Essler, A. M. Tsvelik, arXiv:cond-mat/0011439.

[120] E. Jeckelmann, Phys. Rev. B **66**, 045114 (2002).

[121] E. Jeckelmann, Phys. Rev. B **67**, 075106 (2003).

[122] H. J. Schulz, Phys. Rev. Lett. **64**, 2831 (1990).

[123] B. S. Shastry, B. Sutherland, Phys. Rev. Lett **65** 243 (1990).

[124] T. Giamarchi, Phys. Rev. B **44**, 2905 (1991).

[125] T. Giamarchi, A. J. Millis, Phys. Rev. B **46**, 9325 (1992).

[126] T. Giamarchi, Physica B: Cond. Matt. **230**, 975 (1997).

[127] J. M. P. Carmelo, N. M. R. Peres, P. D. Sacramento, Phys. Rev. Lett. **84**, 4673 (2000).

[128] F. H. L. Essler, V. E. Korepin, Phys. Rev. Lett. **72**, 908 (1994).

[129] F. H. L. Essler, V. E. Korepin, Nucl. Phys. B **426**, 505 (1994).

[130] F. H. L. Essler, H. Frahm, Phys. Rev. B**60**, 8540 (1999).

[131] O. J. Heilmann, E. H. Lieb, Ann. N.Y. Acad. Sci. **172** 584 (1971)

[132] C. N. Yang, Phys. Rev. Lett. **63**, 2144 (1989).

[133] W. Richardson, J. Opt. Soc. Am. **62**, 55 (1972).

[134] L. B. Lucy, Astronomical J. **79**, 745 (1974).

[135] J. von Neumann, Zeit. Phys. 57, 30 (1929); translation European Phys. J. H **35**, 201 (2010).

[136] M. Greiner, O. Mandel, T. W. Hänsch, I. Bloch, Nature **419**, 51-54 (2002).

[137] T. Kinoshita, T. Wenger, D. S. Weiss, Nature **440**, 900 (2006).

[138] S. Hofferberth, I. Lesanovsky, B. Fischer, T. Schumm, J. Schmiedmayer, Nature **449**, 324-327 (2007).

[139] L. Hackermuller, U. Schneider, M. Moreno-Cardoner, T. Kitagawa, S. Will, T. Best, E. Demler, E. Altman, I. Bloch, B. Paredes, Science **327**, 1621 (2010).

[140] S. Trotzky Y.-A. Chen, A. Flesch, I. P. McCulloch, U. Schollwöck, J. Eisert, I. Bloch, Nature Phys. **8**, 325 (2012).

[141] M. Gring, M. Kuhnert, T. Langen, T. Kitagawa, B. Rauer, M. Schreitl, I. Mazets, D. A. Smith, E. Demler, J. Schmiedmayer, Science **337**, 1318 (2012).

[142] M. Cheneau, P. Barmettler, D. Poletti, M. Endres, P. Schauss, T. Fukuhara, C. Gross, I. Bloch, C. Kollath, S. Kuhr, Nature **481**, 484 (2012).

[143] T. Langen, R. Geiger, M. Kuhnert, B. Rauer, J. Schmiedmayer, Nature Physics **9**, 640 (2013).

[144] F. Meinert, M. J. Mark, E. Kirilov, K. Lauber, P. Weinmann, A. J. Daley, H.-C. Nägerl, Phys. Rev. Lett. **111**, 053003 (2013).

[145] N. Navon, A. L. Gaunt, R. P. Smith, Z. Hadzibabic, Science **347**, 167 (2015).

[146] M. Schreiber, S. S. Hodgman, P. Bordia, H. P. Lüschen, M. H. Fischer, R. Vosk, E. Altman, U. Schneider, I. Bloch, Science **349**, 842 (2015).

[147] L. D'Alessio, Y. Kafri, A. Polkovnikov, M. Rigol, Adv. Phys. 65, 239 (2016).

[148] J.S. Caux and F.H.L. Essler, Phys. Rev. Lett. **110**, 257203 (2013).
2013

[149] B. Bauer, C. Nayak, Journal of Statistical Mechanics: Theory and Experiment 9, 09005 (2013).

[150] J. Z. Imbrie, Journal of Statistical Physics 163, 998 (2016).

[151] O. J. Heilmann, E. H. Lieb, Ann. N.Y. Acad. Sci. **172**, 584 (1971); C. N. Yang, Phys. Rev. Lett. **63**, 2144 (1989).

[152] V. Alba, M. Fagotti and P. Calabrese, J. Stat. Mech., P10020 (2009).

[153] M. Takahashi, Prog. Theor. Phys. **47**, 69 (1972).

[154] F.H.L. Essler, V.E. Korepin and K. Schoutens, Phys. Rev. Lett. **67**, 3848 (1991).

[155] F.H.L. Essler, V.E. Korepin, and K. Schoutens, Nucl. Phys. **B372**, 559 (1992).

[156] T. A. Hilker, G. Salomon, F. Grusdt, A. Omran, M. Boll, E. Demler, I. Bloch, C. Gross, arXiv:1702.00642.

[157] F.H.L. Essler, V.E. Korepin, and K. Schoutens, Nucl. Phys. **B384**, 431 (1992).

[158] M. Takahashi, Prog. Theor. Phys. **52**, 103 (1974).

[159] Z. N. C. Ha, Phys. Rev. B**46**, 12205 (1992).

[160] S. Ejima, F. H. L. Essler, F. Gebhard, J. Phys. **A39**, 4845 (2006).

[161] H. N. V. Temperley, E. H. Lieb, Proc. R. Soc. London A **322**, 251 (1971).

[162] R. Saito, J. Phys. Soc. Jpn. **59**, 482 (1990).

[163] A. Shashi, L. I. Glazman, J-S. Caux, A. Imambekov, Phys. Rev. B **84**, 045408 (2011).

[164] A. Shashi, M. Panfil, J-S. Caux, A. Imambekov, Phys. Rev. B **85**, 155136 (2012).

[165] O. Vafek, N. Regnault, B. A. Bernevig, arXiv:1608.06639

[166] C. N. Yang, Phys. Rev. Lett. **63**, 2144 (1989).